OPTIMIZATION OF A HIGH-EFFICIENCY JET EJECTOR BY COMPUTATIONAL FLUID DYNAMICS SOFTWARE

A Thesis

by

SOMSAK WATANAWANAVET

Submitted to the Office of Graduate Studies of
Texas A&M University
in partial fulfillment of the requirements for the degree of

MASTER OF SCIENCE

May 2005

Major Subject: Chemical Engineering

OPTIMIZATION OF A HIGH-EFFICIENCY JET EJECTOR BY COMPUTATIONAL FLUID DYNAMICS SOFTWARE

A Thesis

by

SOMSAK WATANAWANAVET

Submitted to Texas A&M University
in partial fulfillment of the requirements
for the degree of

MASTER OF SCIENCE

Approved as to style and content by:

Mark T. Holtzapple (Co-Chair of Committee)	Charles J. Glover (Co-Chair of Committee)
Othon K. Rediniotis (Member)	Kenneth R. Hall (Head of Department)

May 2005

Major Subject: Chemical Engineering

ABSTRACT

Optimization of a High-Efficiency Jet Ejector by

Computational Fluid Dynamics Software. (May 2005)

Somsak Watanawanavet, B.S., Chulalongkorn University

Co-Chairs of Advisory Committee: Dr. Mark T. Holtzapple
Dr. Charles J. Glover

Research was performed to optimize high-efficiency jet ejector geometry (Holtzapple, 2001) by varying nozzle diameter ratios from 0.03 to 0.21, and motive velocities from Mach 0.39 to 1.97. The high-efficiency jet ejector was simulated by Fluent Computational Fluid Dynamics (CFD) software. A conventional finite-volume scheme was utilized to solve two-dimensional transport equations with the standard k-ε turbulence model (Kim et. al., 1999). In this study of a constant-area jet ejector, all parameters were expressed in dimensionless terms. The objective of this study was to investigate the optimum length, throat diameter, nozzle position, and inlet curvature of the convergence section. Also, the optimum compression ratio and efficiency were determined.

By comparing simulation results to an experiment, CFD modeling has shown high-quality results. The overall deviation was 8.19%, thus confirming the model accuracy. Dimensionless analysis was performed to make the research results applicable to any fluid, operating pressure, and geometric scale. A multi-stage jet ejector system with a total 1.2 compression ratio was analyzed to present how the research results may be used to solve an actual design problem.

The results from the optimization study indicate that the jet ejector efficiency improves significantly compared to a conventional jet-ejector design. In cases with a subsonic motive velocity, the efficiency of the jet ejector is greater than 90%. A high compression ratio can be achieved with a large nozzle diameter ratio. Dimensionless group analysis reveals that the research results are valid for any fluid, operating pressure, and geometric scale for a given motive-stream Mach number and Reynolds ratio between the motive and propelled streams. For a given Reynolds ratio and motive-stream Mach number, the dimensionless outlet pressure and throat pressure are expressed as C_p and C_{pm}, respectively.

A multi-stage jet ejector system with a total 1.2 compression ratio was analyzed based on the optimization results. The result indicates that the system requires a lot of high-pressure motive steam, which is uneconomic. A high-efficiency jet ejector with mixing vanes is proposed to reduce the motive-steam consumption and is recommended for further study.

DEDICATION

To my parents, for their encouragement both physically and mentally,

ACKNOWLEDGEMENTS

I would like to thank the co-chair of my committee, Dr. Mark T, Holtzapple, for his intellect, time, and guidance. Because of these characteristics, I thoroughly enjoyed doing the research under his advisory.

I am very grateful to the other co-chair of my committee, Dr. Charles J. Glover, for his wonderful ideas and dedication. His idea for deriving the newly defined efficiency equation was applied.

I am very appreciative to my committee member, Dr. Othon Rediniotis, for his sincere commentary and contributions during the research process.

I am very thankful for Ganesh Mohan. He provided a great contribution in proving the dimensionless group analysis and came up with a wonderful result.

I would like to thank my friends for their wonderful help and support.

I would like to especially thank Lakkana Kittiratanawiwat. Her support helped me overcome the difficulties of this thesis.

Lastly, I want to thank the Shell company for financially supporting the project.

TABLE OF CONTENTS

Page

LIST OF FIGURES

FIGURE Page

FIGURE Page

LIST OF TABLES

INTRODUCTION

Jet ejectors are the simplest devices among all compressors and vacuum pumps. They do not contain any moving parts, lubricants or seals; therefore, they are considered as highly reliable devices with low capital and maintenance costs. Furthermore, most jet ejectors use steam or compressed air as the motive fluid, which is easily found in chemical plants. Due to their simplicity and high reliability, they are widely used in chemical industrial processes; however, jet ejectors have a low efficiency.

Many factors affect jet ejector performance, including the fluid molecular weight, feed temperature, mixing tube length, nozzle position, throat dimension, motive velocity, Reynolds number, pressure ratio, and specific heat ratio (DeFrate and Hoerl (1959); and Kim et al. (1999)).

Previous research by Riffat and Omer (2001) and Da-Wen and Eames (1995) attempted to study the effect of nozzle position on jet ejector performance. They found that the nozzle position had a great effect on the jet ejector performance, as it determines the distance over which the motive and propelled stream are completely mixed. ESDU (1986) suggested that the nozzle should be placed between 0.5 and 1.0 length of throat diameter before the entrance of the throat section. Holton (1951) studied the effect of fluid molecular weight, whereas Holton and Schultz (1951) studied the effect of fluid temperature.

This thesis follows the style of the *AIChE Journal*.

A number of researchers made an effort to understand the effect of jet ejector geometry on jet ejector performance. For example, Kroll (1947) investigated the effect of convergence, divergence, length, and diameter of the throat section, nozzle position, induced fluid entrance, and motive velocity. Croft and Lilley (1976) investigated the optimum length and diameter of the throat section, nozzle position, and angle of divergence.

A few literature researchers have studied the effect of nozzle diameter on jet ejector performance. This is a major focus of our proposal. The optimum length and diameter of the throat section, the nozzle position, and the radius of the inlet curvature before a convergence section in a constant-area jet ejector design are investigated for each individual nozzle diameter. The nozzle diameter ratio, defined by D_n/D_p, is varied from 0.03 to 0.23. The motive velocity at nozzle exit is varied from Mach 0.39 to 1.98. The back pressure of the ejector is maintained constant at 101.3 kPa. Steam is used as a working fluid.

In this research, the optimum jet-ejector geometry for each nozzle diameter ratio and motive velocity was investigated using Fluent computational fluid dynamic (CFD) software. CFD software has been proved by a number of researchers (Riffat and Everitt, 1999; Hoggarth, 1970; Riffat et al., 1996; Talpallikar et al., 1998; Neve, 1993) as a powerful tool for predicting flow fields inside jet ejectors. Fluent uses a mass-average segregated solver to solve the fundamental transport equations such as continuity, momentum conservation, and momentum conservation for incompressible, Newtonian fluid (the Navier-Stokes equation). The governing equations are discretized in space

using a finite volume differencing formulation, based upon an unstructured grid system. The standard k-ε turbulent method is employed to solve the governing equations. The reliability of CFD modeling is examined by comparing a simulation result with an experiment result, which was done by Manohar Vishwanathappa, a graduate chemical engineering student at Texas A&M University. The deviation between both results is 8.19%, thus confirms the model reliability.

Finally, a multi-stage jet ejector system with a total 1.2 compression ratio is analyzed to demonstrate the implementation of the research to solve an actual design problem.

OBJECTIVES

The main objective of this research is to optimize the geometry of a conventional constant-area jet ejector design using Fluent CFD software. The research varies motive velocity and nozzle diameter ratio.

There are four specific research goals in this optimization study:

1. Determine the optimum entrainment ratio.
2. Optimize the throat section, including the length and diameter, the nozzle position, and the radius of inlet curvature before the convergence section.
3. Evaluate the dimensionless pressure of the propelled stream and motive stream, and the efficiency of the optimum design.
4. Analyze a multi-stage jet ejector system with 1.2 compression ratio based on the research results.

The second objective is to verify the reliability of CFD modeling. There are three specific research goals:

1. Verify the accuracy of CFD modeling by comparing a simulation result with an experimental result, which was done by Manohar Vishwanathappa, a graduate chemical engineering student at Texas A&M University.
2. Determine the effect of grid size by comparing between a coarser and a finer grid-size model with various numbers of iterations.
3. Verify the CFD model consistency by studying the effect of potential boundary conditions on simulation results.

By working closely with Ganesh Mohan, a graduate mechanical engineering student at Texas A&M University, the third objective is to implement dimensionless group analysis in the research. The specific research goal follows

1. Investigate a fluid dimensionless variable to make the research result valid for any fluid, operating pressure condition, and geometric scale.

LITERATURE REVIEW

Design and Optimization

In the past, when engineers designed jet ejectors, either a "rule-of-thumb" or "trial-and-error" approach was used. Both approaches may provide unsatisfactory performance, and thus consume too much power, material, and labor.

Conventional jet ejectors are classified by the dimension of the convergence section. There are two types:

1. Constant-pressure jet ejector
2. Constant-area jet ejector

DeFrate and Hoerl (1959) and Kim et al. (1999) discovered that the constant-pressure configuration provides a better performance than the constant-area configuration, because turbulent mixing in the jet-ejector is achieved more actively under an adverse pressure gradient, which occurs in the constant-area jet ejector, rather than under constant pressure (Kim et al., 1999). Stronger turbulent mixing dissipates the ejector performance. DeFrate and Hoerl (1959) provided the mathematical functions, which are valid for both configurations. The mathematical functions are used to calculate:

1. Optimum motive- and propelled-stream velocity as a function of expansion ratio for an arbitrary molecular weight and temperature
2. Area ratio (D_n/D_t) as a function of entrainment ratio

The jet ejector is classified into two types depending on its convergence configuration:

1. Constant-pressure jet ejector
2. Constant-area jet ejector

The different between both types is shown in Figure 1.

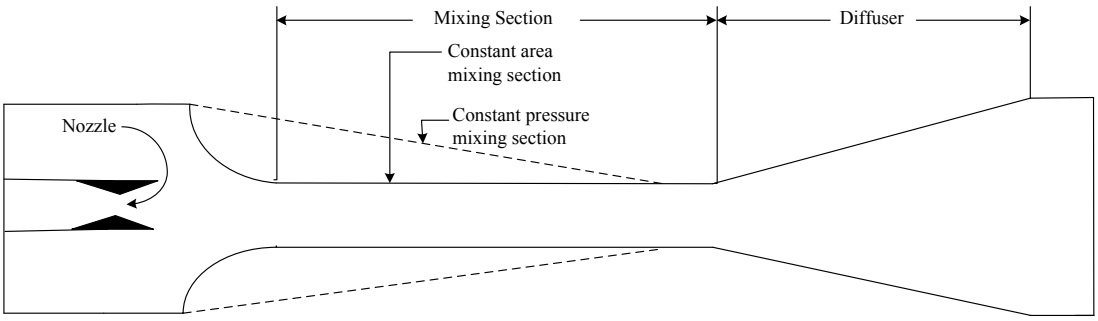

Figure 1. Jet ejector type.

The jet ejector performance is mainly affected by mixing, turbulence, friction, separation, and energy consumption in the suction of the propelled stream. To maximize jet ejector performance, enhancing turbulent mixing should be a major consideration. The literatures indicate that the nozzle geometry should be well-designed to boost the tangential shear interaction between the propelled and motive stream. Also both streams should blend completely inside the throat. The jet ejector should be designed properly to diminish turbulence effects.

Each part of a jet ejector is explained in the following section. Figure 2 indicates the geometric symbols used in the following section.

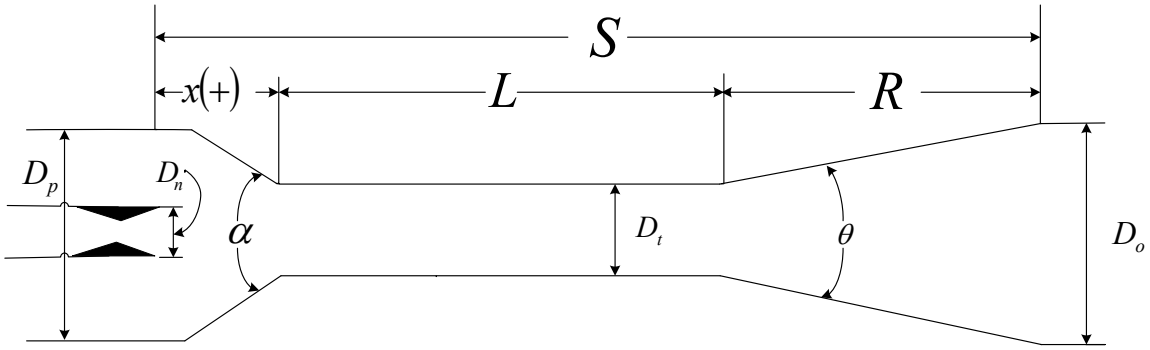

Figure 2. Symbols in jet ejector (Kroll, 1947).

Convergence Section

According to Kroll (1947), Engdahl and Holton (1943); Mellanby (1928); Watson (1933) found that the best design for the convergence section is a well-rounded, bell-mouthed entry. A conical or tapered entry is recommended to have an angle, α, greater than 20 degrees, because the nozzle jet, which has a general angle of about 20 degrees, will not create objectionable shock and eddy losses at the convergence inlet (Mellanby, 1928). Watson (1933) did an experiment and stated that 25 degrees is about the best convergence angle.

Regarding the well-rounded geometry, a conical entry reduces the flow 2%, whereas a coupling and sharp entry reduce the flow 4 and 11%, respectively (Bailey, Wood (1933); Engdahl, and Holton (1943); Stern (1932) (also cited in Kroll (1947)).

Throat Section

Kroll (1947) also discusses that Mellanby (1928) and Watson (1933) reported that diffusers with a throat section created a greater vacuum than diffusers without a

throat section. Mellanby (1928) also showed that a parallel throat throughout is inferior, but still much better than no parallel throat at all.

The length of the throat section must be designed properly. It should be sufficiently long to create a uniform velocity profile before the entrance of the divergence section. The uniform velocity decreases the total energy losses in the divergence section, thus obtaining better high-pressure recovery (Berge et al., 2000) (also cited in Kroll (1947)).

Two literature sources cited in Kroll (1947) (Duperow and Bossart, (1927); and Keenan and Neumann, (1942)) reported that an optimum throat length is about 7 times the throat diameter, whereas Engdahl (1943) came across with another optimum value of 7.5 times the throat diameter. Additionally, lengths of 5 to 10 times the throat diameter provided within 3% of optimum performance. Although the optimum length increased slightly with pressure and throat diameter, the increase was less than 1 diameter even when these factors were doubled (Keenan and Newmann, 1942). Engdahl (1943) reported that any length between 4 and 14 throat diameters will give within 4% of optimum performance. According to many literature sources, the length should be 7 to 9 times the throat diameter for the best performance.

The optimal throat diameter is sensitive to jet ejector parameters, especially the entrainment ratio. A small change in throat diameter creates a huge change in the entrainment ratio. If the throat area is too large, fluid leaks back into system; if it is too small, choking occurs. So, the throat diameter must be designed properly to obtain the best performance.

Divergence Section

Kroll (1947) indicated that the angle of the divergent section, θ, is usually 4 to 10 degrees. Too rapid a divergence immediately after the throat is not recommended (Kroll, 1947). The divergent length, say from 4 to 8 times the throat diameter, is desired for pressure recovery. The length, however, may be as short as twice the throat diameter if necessary. It was discovered that eliminating the divergence section reduced the entrainment ratio (M_m/M_p) by about 20%.

Nozzle

Two factors of the nozzle influence jet ejector performance:

1. Nozzle design
2. Nozzle position

Fewer researchers have studied the effect of nozzle design on jet ejector performance than nozzle position. Hill and Hedges (1974) studied the influence of nozzle design on jet ejector performance. In their experiment, two conically diverging nozzles were tested, but differing in the divergence angle. The exit and throat diameters of the nozzle were fixed in both cases. The experimental results show that the overall jet ejector performance was not influenced by the nozzle design. According to Kroll (1947), a study done by Engdahl and Holton (1943) confirms the above statement. They found that the nozzle, which was designed by conventional methods for a specific pressure, performed only slightly better than a simple straight-hole nozzle at pressure up to 170 psig. Also, a machined nozzle with a convergence section and a 10 degree angle of

divergence was only 3 to 6% better than a 100-psig small pipe-cap nozzle made by drilling a hole in a standard pipe cap. However, altering the nozzle design affects the motive-stream velocity. This was studied explicitly by Berkeley (1957). He also found that under normal circumstances, the expansion of motive stream in the ejector of a well-designed nozzle is almost always a fairy efficient part of the overall flow process. Therefore, very little energy is lost in the nozzle. But the task of efficiently converting velocity back into pressure is very difficult because energy is lost in this process. Additionally, Kroll (1947) reported that a poorly shaped nozzle causes unnecessary shock losses and useless lateral expansion, which decrease jet ejector efficiency tremendously.

The position of the nozzle has a greater effect on jet ejector performance than its design. A number of researchers investigated the optimum position of the nozzle in a jet ejector. Croft and Lilley (1976); and Kim et al. (1999) report that turbulence in the mixing tube decreases when the nozzle is placed right at the entrance of the throat section; however, Croft and Lilley (1976) also discovered that when the nozzle moves closer to the mixing tube, the entrainment ratio decreases. ESDU (1986) recommends placing the nozzle exit between 0.5 and 1.0 lengths of throat diameter upstream of the mixing chamber. Not only the jet ejector performance, but also the mixing distance of the motive and propelled streams is affected by the nozzle position. Kroll (1947) has suggested that nozzle position should be adjustable to obtain the best performance using field adjustments. Further, it is important to have the nozzle centered with the throat

tube. He also recommended that the nozzle should be cleaned as often as possible for best performance.

Entrainment Ratio

An experiment conducted by Mellanby (1928) concluded that for all practical purposes, the entrainment ratio is independent of the inlet position of the propelled stream. Holton (1951) discovered that the entrainment ration is a function of the molecular weight of the fluid, but independent of pressure, and jet ejector design. Figure 3 shows the correlation between the entrainment ratio and molecular weight. Furthermore, Holton and Schulz (1951) discovered that the entrainment ratio is a linear function of operating temperature, but independent of pressure and jet ejector design. Figure 4 displays the effect of the operating temperature on the entrainment ratio.

$$\text{Entrainment Ratio} = \frac{\text{mass flow rate of the propelled stream}}{\text{mass flow rate of the motive stream}} \qquad (1)$$

Kroll (1947) had summarized the results of optimized jet ejector geometry from a number of literature sources (see Table 1).

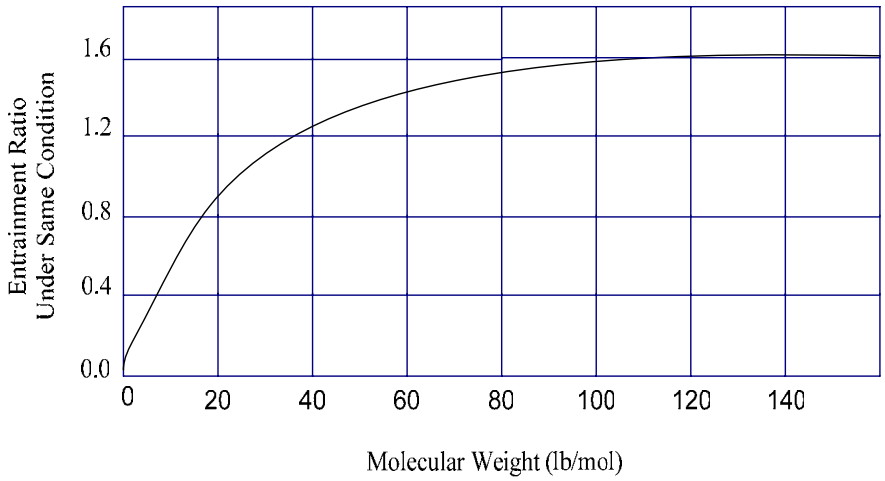

Figure 3. Entrainment ratio as a function of molecular weight (Holton, 1951).

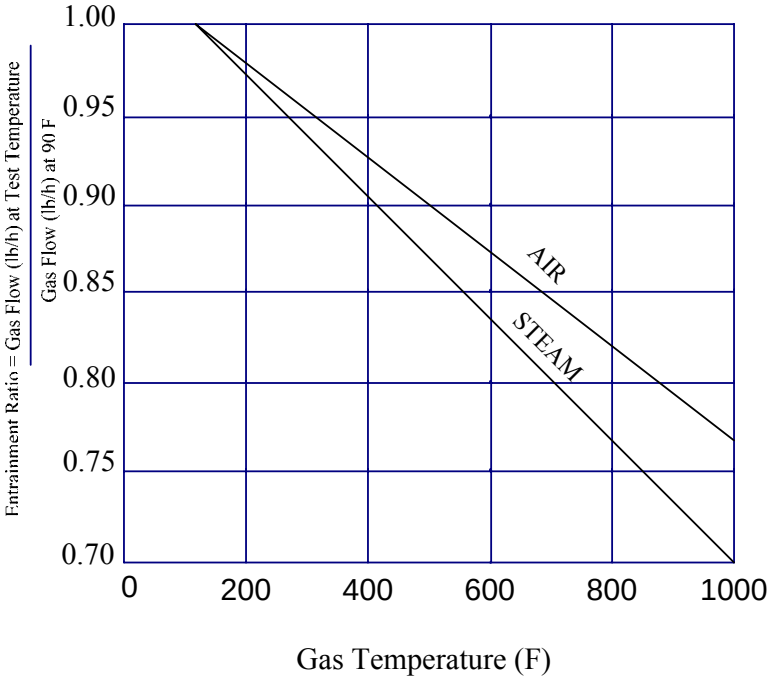

Figure 4. Entrainment ratio as a linear function of temperature for air and steam (Holton and Schultz, 1951).

Table 1. Summary of literature results about the optimization of the jet ejector (Kroll, 1947).

Reference	**Length of**				**Angle of Diffuser (degree)**	
Air-Jet Air Pumps	Throat	Divergence	Nozzle outlet to discharge	Nozzle outlet to throat	Convergence	Divergence
Symbol	***T***	***R***	***S***	***X***	***α***	***θ***
Keenan and Neumann (1942)	7 D_T	-	7.5 D_T	0.5 D_T	well rounded	-
Mellanby (1928)	4 D_T	10 D_T	-	variable	25	12
Kravath (1940)	1 D_T	12 D_T	15 D_T	2 D_T	28	5
Miller (1940)	-	-	-	5 D_T	-	16
SteamJet Air Pumps						
DuPerow and Bossart (1927)	-	-	6 D_T	1.2 D_T	-	7
Royds and Johnson (1941)	10 D_T	15 D_T	-	-	well rounded	-
Langhaar (1946)	3 D_T	4 D_T	10 D_T	3	24	10
Watson (1933)	2 D_T	6.7 D_T	12.3 D_T	3.6 D_T	28	8

Operating and Maintenance

A number of literature references state that pressure is the most critical variable when operating the jet ejector. The actual operating pressure should be evaluated closely during the operation. A jet ejector will not operate properly, causing a broken or unstable vacuum, if it is even a few hundred pascal below its design motive pressure (Knight, 1959). Due to that reason, a steam-pressure gage is highly recommended to be located on the steam chest of the ejectors to measure the inlet pressure of the propelled stream.

Three principles should always be followed for controlling steam jet ejectors (Knight, 1959):

1. Each jet ejector in a system operates along a fixed curve of suction pressure versus capacity for a given discharge pressure.
2. Each jet ejector has a fixed minimum suction pressure for a given discharge pressure, below which the jet ejector flow will be disrupted i.e., a pressure at which vapor flow in the diffuser will be reversed, operation below the break pressure is unstable, but if suction pressure increases above the break pressure, a greater pressure is attained at which stable operation returns, with normal flow in the diffuser.
3. Each jet ejector has a maximum discharge pressure for a given load, above which the jet ejector flow will be disrupted.

Knight (1959) also presented five ways for automatically controlling the pressure. The advantage and disadvantage of each approach were discussed in the literature.

Finally, Berkeley (1957) introduced six variables that should be considered when selecting a particular design of a steam jet ejector:

1. Suction pressure required
2. Amount of steam available
3. Amount of water available
4. Fluid to be evacuated
5. Equipment cost

6. Installation cost

Internal Flow Field

To enhance jet ejector performance, understanding the flow field mechanism inside the jet ejector is useful. Reinke et al. (2002) found that further away from the nozzle exit, the velocity profile is more uniform across the cross section. Because the viscous action of the jet fluid transfers its kinetic energy to the surroundings, fluid moves slower as the distance increases. The internal behavior of the jet ejector – particularly in the mixing section between the primary and secondary flows and also the effect of nozzle axial position – were studied by Croft and Lilley (1976). The energy contours, which are presented in the literature, reveal that at the mixing point, there is a high rate of thermal energy generation due to the high turbulence length scale in the mixing position. Also, the turbulent length scale decreases gradually through the throat section. This indicates that energy transfers from the motive stream to the propelled stream quickly. Turbulence length scale is a physical quantity related to the size of the large eddies containing energy in turbulent flows (Fluent, 2001). In fully developed flows in pipe, the turbulence length scale is restricted by the pipe diameter.

The flow velocity, temperature, and pressure inside the throat section – an effect of these parameters on the jet ejector performance inside the throat section – were studied by Djebedjian et al. (2000). The velocity distribution indicates the degree of mixing between motive and propelled streams and the quantity of entrained fluid. The length of the mixing tube creates a huge effect for producing a uniform velocity profile

at the entrance of the divergence section. The fluid velocity profile inside the throat section is presented in Figure 5A. The pressure increases significantly in the throat and the divergence section as shown in Figure 5B. The static temperature increases because heat is generated from kinetic energy losses in an energy-exchange process. As the fluid velocity decreases, the static temperature increases. The static temperature profile inside the throat section is presented in Figure 5C. The profiles of the fluid velocity and the static temperature are identical but opposite direction in magnitude.

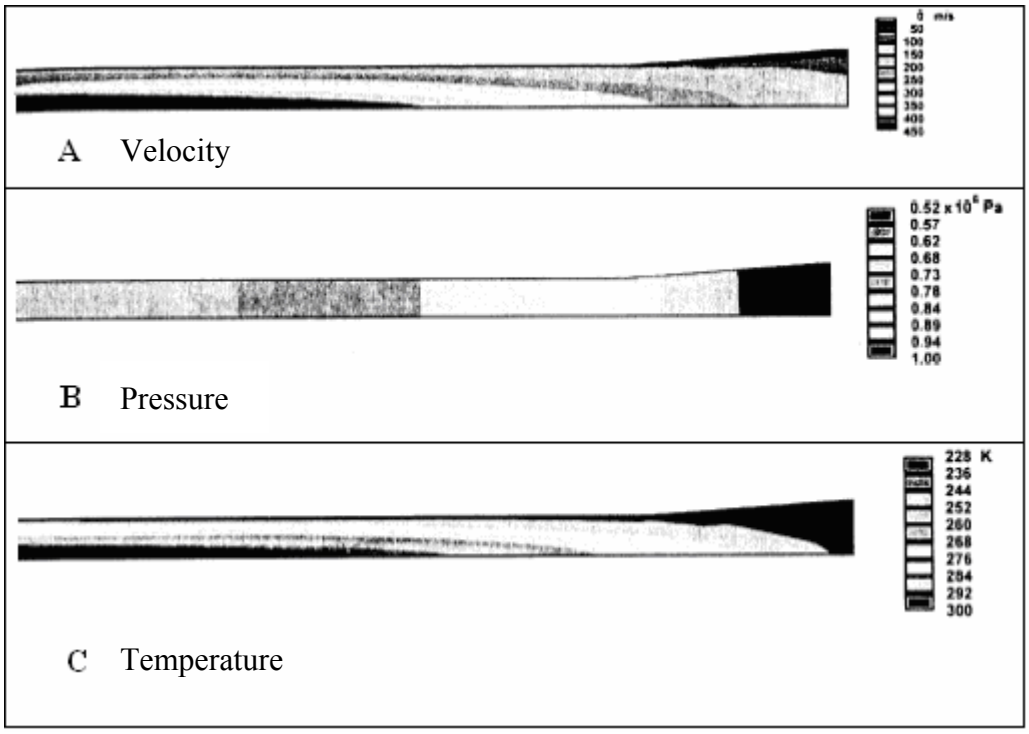

Figure 5. Flow variable profile inside the throat section, A) velocity, B) pressure, C) temperature (Djebedjian et al., 2000).

Shock Wave

When the motive-stream velocity exceeds the speed of sound, shock waves are unavoidable inside jet ejectors. Shock waves convert velocity back to pressure, but in an inefficient manner. Shock waves are more severe as the fluid velocity at the diffuser entrance increases. Generally, the motive stream is accelerated to a supersonic velocity through the convergent-divergent nozzle. Then, inside the throat section, the propelled stream is induced by a strong shear force with the motive stream leading to the resulting deceleration of the motive stream. The shock wave occurs in this step. The shock wave system interacts with the boundary layer along the jet ejector surface. The flow inside the ejector is exposed to a strong invicid-viscous interaction. The operating characteristics and performance of a supersonic ejector are difficult to predict using conventional gas dynamic theory. Consequently, the discharge pressure is limited to a certain value. DeFrate and Hoerl (1959) provided mathematical formulations to calculate pressure before and after the shock wave in the throat section, and the subsonic Mach number after the shock occurs. Kim et al. (1999) researched the shock wave inside jet ejectors explicitly. They studied the effect of throat area on the shock wave (see Figure 6). As the area of the throat section increases, a Mach stem reduces to an oblique shock wave. Reflections of the oblique shock result in a multiple oblique shock system (Kim et al., 1999). Mach stem is a shock front formed by the fusion of the incident and reflected shock fronts from an explosion. In an ideal case, the mach stem is perpendicular to the reflecting surface and slightly forward. They also found that the throat dimension strongly affects the shock system inside the mixing tube. Their result indicates that the

interaction between the shock system and the wall boundary layer in a constant-pressure jet ejector is noticeably stronger than a constant-area jet ejector. Therefore, it is expected that the flow would be subject to a stronger turbulence field in a constant-pressure (Figures 6A – D), rather than constant-area geometry (Figure 6E). This reduces the jet ejector performance significantly.

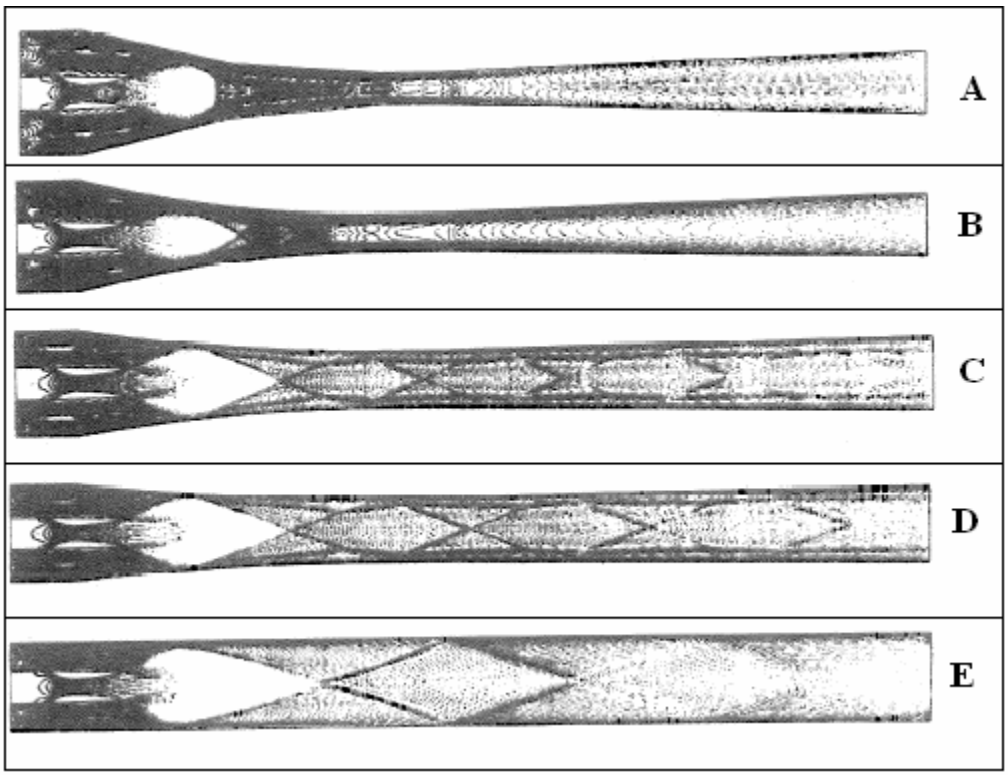

Figure 6. Iso-Mach contours for various ejector throat area ratios (Kim et al. 1999).

The shock wave occurs when the fluid velocity decreases to subsonic velocity. The pressure gradient changes suddenly in the shock wave area. Figure 7 illustrates the shock wave occurring inside the jet ejector.

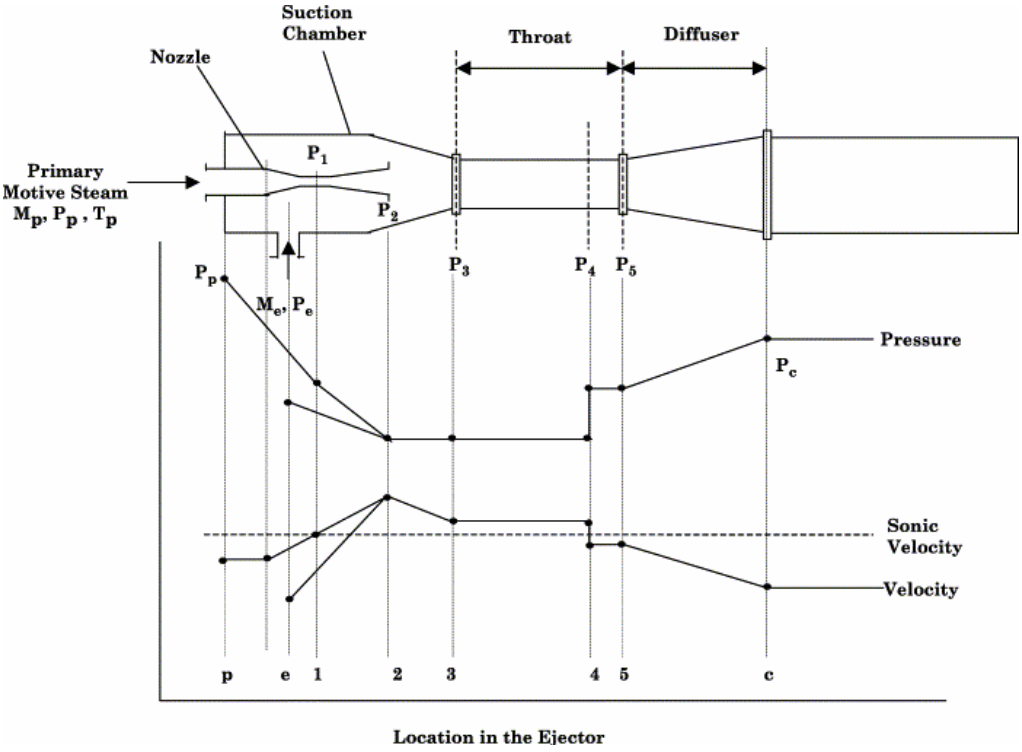

Figure 7. Variation in stream pressure and velocity as a function of location along the ejector (El-Dessouky et al., 2002).

Multi-Stage Jet Ejector System

A single jet ejector has a limiting capacity due to its shape, and also has practical limits on the overall compression ratio and throughput it can deliver. To enhance the compression ratio, two or more ejectors can be arranged in series. But for greater throughput capacity, two or more ejectors can be arranged in parallel. For these reasons, a multi-stage jet ejector system is considered.

The multi-stage jet ejector system contains:

1. Jet ejector
2. Condenser used for condensable fluid only
3. Interconnecting piping

A recent study indicates that five and six stages can produce almost any desired suction pressure. They have carved a unique and popular place in industry where large volumes of gases must be evacuated. Croll (1998) has suggested the capacities and operating ranges of the multi-stage jet ejector system, which are summarized in Table 2.

As the design pressure decreases, the number of ejector stages increases because the suction pressure of an ejector is further affected by the surrender of the energy from the motive stream to the propelled stream.

Table 2. Capacities and operating ranges of a multistage jet ejector (Croll, 1998).

System Type	Lowest Recommended Suction Pressure (kPa)
One-stage	10,000
Two-stage	1,600
Three-stage	130
Four-stage	25
Five-stage	2.5
Six-stage	0.4
Ejector and liquid-ring pump (Integrated pumping system)	20

In jet-ejector design and specification, it is convenient to divide sub-atmospheric pressure into four regions as shown in Table 3 (Croll, 1998).

Table 3. Sub-atmospheric pressure regions (Croll, 1998).

Region	Pressure range (Pa)
Rough vacuum	101,325 – 130
Medium vacuum	130 - 0.13
High vacuum	0.13 - 0.000013
Ultrahigh vacuum	below 0.000013

Most of the applications in chemical engineering are in the rough vacuum region. For example, the normal range of vacuum distillation, evaporation, drying, and filtration are covered in this range.

For selecting a multi-stage jet ejector system, five factors stated below must be satisfied. Many systems will be eliminated after the first two factors.

1. Suction pressure and capacity
2. Reliability and easy maintenance
3. Purchase, installation, and operating costs
4. Environmental restrictions
5. Air leakage

The reasons for these factors are explained explicitly in Croll (1998).

A diagram used for selecting a multi-stage jet ejector system is presented in Berkeley (1957). The diagram can be applied only to non-condensable gas loads. In case a portion of the load to the system is a condensable vapor, it is necessary to analyze the particular operating condition to determine the correct design for optimum economy. In

some cases, the gas load to the ejector is reduced considerably by using a pre-condenser to condense a large portion of the vapor before flowing into the system. Another advantage of using a condenser is that it increases the system reliability, because the system is protected against solid and liquid carryover, and also it reduces the concentration vapor in the load. Jet ejectors can be damaged permanently from excess moisture. Steam quality of less than 2% liquid is tolerable in most systems (Croll, 1998). Often the absolute pressure is too small to use a pre-condenser and it is necessary to compress or boost the vapor to a pressure where a large portion of the condensing can be done in an inter-condenser (Berkeley, 1957). Small secondary ejectors are utilized to compress the non-condensable vapor.

For a multi-stage jet ejector system handling air or other non-condensable gases, the best design is evaluated by the minimum steam and water requirement for its operation, which can be calculated from the diagram in Berkeley (1957). In cases where a large portion of the load is a condensable vapor, the cost of steam and water consumption will determine the best design. The equipment cost will usually change within the range of steam and water cost. Therefore, the operating cost has more influence than the initial cost in selecting the finest system.

THEORY

Conventional Jet Ejector

Jet ejectors are popular in the chemical process industries because of their simplicity and high reliability. In most cases, they provide the greatest option to generate a vacuum in processes. Their capacity ranges from very small to enormous. Due to their simplicity, conventional jet ejectors that are properly designed for a given situation are very forgiving of errors in estimated quantities and of operational upsets. Additionally, they are easily changed to give the exact results required (Mains and Richenberg, 1967).

Jet ejectors provide numerous advantages, which are summarized below:

1. Jet ejectors do not require extensive maintenance, because there are no moving parts to break or wear.
2. Jet ejectors have lower capital cost comparing to the other devices, due to their simple design.
3. Jet ejectors are easily installed, so they may be placed in inaccessible places without any constant deliberation.

On the other hand, the major disadvantages of jet ejector follow:

1. Jet ejectors are designed to perform at a particular optimum point. Deviation from this optimum point can dramatically reduce ejector efficiency.
2. Jet ejectors have very low thermal efficiency.

Jet Ejector Application

Due to their simplicity, jet ejectors have been used for various purposes. A number of the principle applications are listed below (Schmitt, 1975).

1. *Extraction*: suction of the induced fluid.
2. *Compression*: compression of the induced fluid discharged at the expansion pressure of the driving fluid.
3. *Ventilation and air conditioning*: extraction and discharge of gas with small differences in compression near atmospheric pressure.
4. *Propulsion or lifting:* intermediate compression of the fluid discharged at a certain adaptation velocity.
5. *Uniform mixing of two streams*: providing a uniform concentration or temperature in a chemical reaction
6. *Conveyance*: pneumatic or hydraulic transport of products in powder form or fractions.

Operating Principle

As shown in Figure 8, the conventional jet ejector design has four major sections:

1. nozzle
2. suction chamber
3. throat
4. diffuser

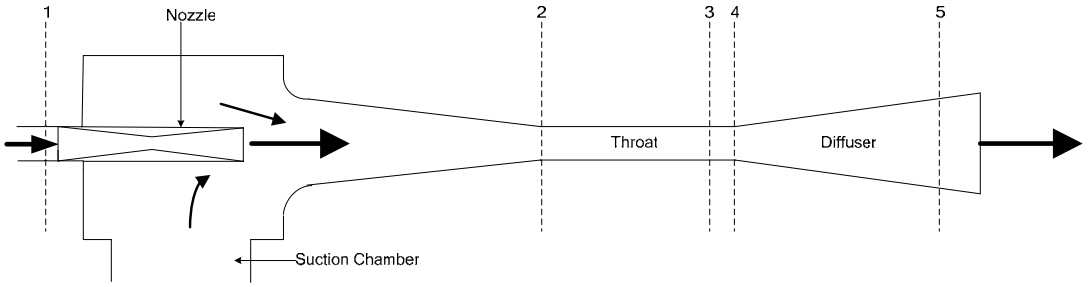

Figure 8. Conventional jet ejector design.

The operating principle of ejectors is described below:

1. A subsonic motive stream enters the nozzle at Point 1. The stream flows in the converging section of the nozzle, its velocity increases and its pressure decreases. At the nozzle throat, the stream reaches sonic velocity. In the diverging section of the nozzle, the increase in cross sectional area decreases the shock wave pressure and its velocity increases to supersonic velocity.
2. The entrained fluid enters the ejector, flowing to Point 2. Its velocity increases and its pressure decreases.
3. The motive stream and entrained stream mix within the suction chamber and the converging section of the diffuser, or they flow as two separate streams and mix together in the throat section.
4. In either case, there is a shock wave inside the throat section. The shock results from the reduced mixture velocity to a subsonic condition and the back pressure resistance of the condenser at Point 3.

5. The mixture flows into the diverging section of the diffuser. The kinetic energy of the mixture is transformed into pressure energy. The pressure of the emerging fluid is slightly higher than the condenser pressure, Point 5 (El-Dessouky et al., 2002).

All jet ejectors, no matter how many stages and whether they are condensing or not condensing, operate on this principle, each stage being another compressor (Mains and Richenberg, 1967).

High-Efficiency Jet Ejector

A high-efficiency jet ejector is proposed to increase the efficiency of conventional jet ejectors. In a conventional jet ejector, the high-velocity motive stream is fed to the jet ejector in a horizontal direction, whereas the propelled stream flows into the jet ejector in a vertical direction; thus, the horizontal momentum of both streams is extremely different at the mixing point. This causes turbulence resulting in a lot of energy losses inside the conventional jet ejector, which decreases its performance. A conventional jet ejector is displayed in Figure 9A.

To enhance the jet ejector performance, the momentum difference of both streams at the mixing position should be minimized. Following this concept, a high-efficiency jet ejector is generated by placing the nozzle right at the entrance of the throat section rather than the jet ejector inlet. From this modification, the propelled stream is accelerated through the converging section before mixing with the high-velocity motive stream. Consequently, two streams with nearly identical velocities are mixed, which is

inherently efficient (Holtzapple, 2001). Because it is a high-efficiency device, when built in multiple stages or a cascade, the overall efficiency can be high (Holtzapple, 2001). A high-efficiency jet ejector is displayed in Figure 9B.

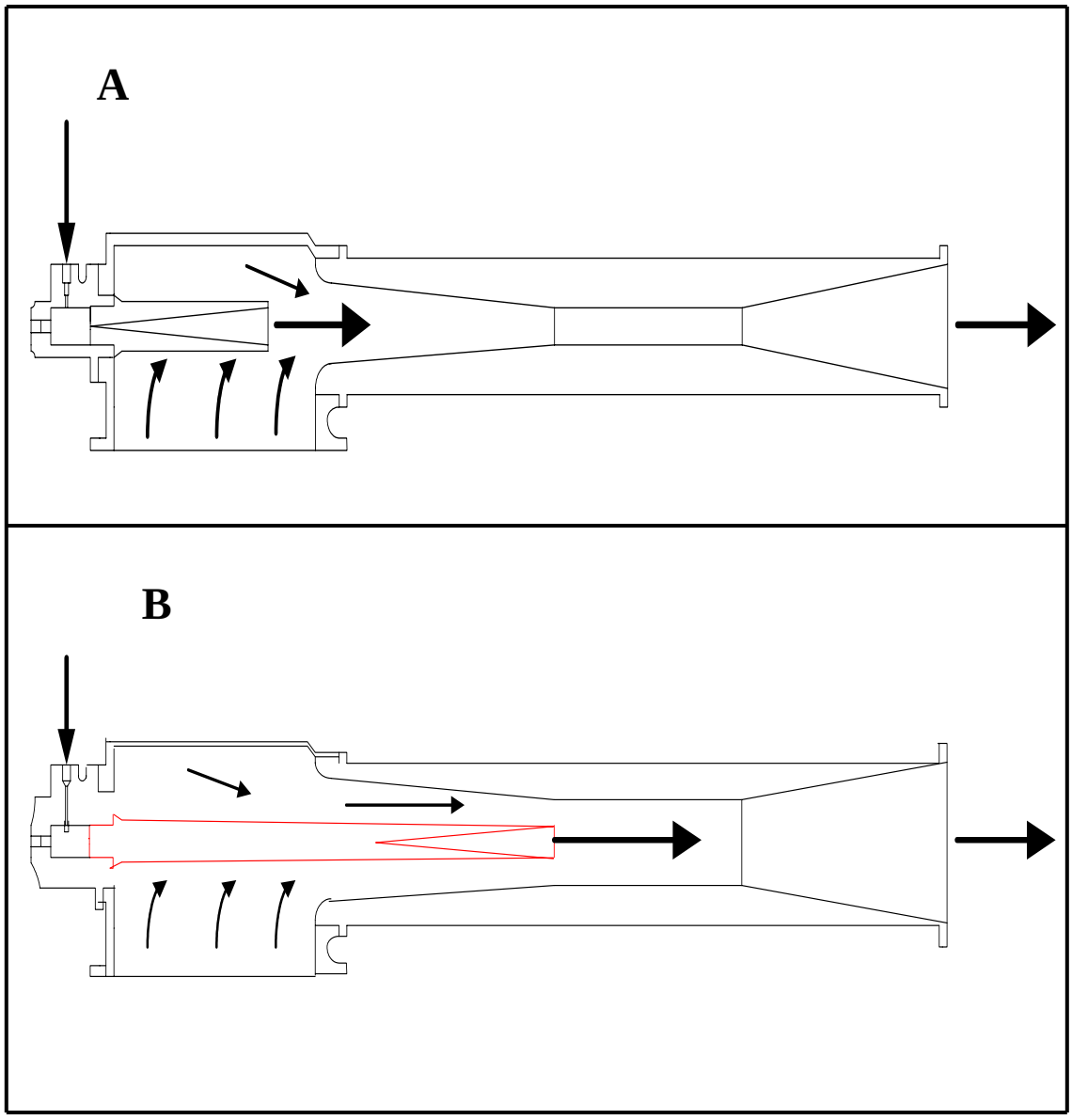

Figure 9. Jet ejector design. A) conventional design, B) high-efficiency design.

The primary concept to improve jet ejector performance is to minimize momentum differences between the motive and propelled streams. Verification of the concept is presented in the following section. A mathematical calculation compares small and large momentum differences between the motive and propelled streams.

First, the large momentum difference is demonstrated (see Figure 10).

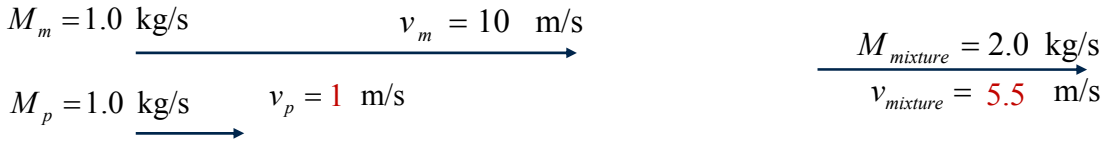

Figure 10. Diagram of large momentum different condition.

The total kinetic energy before mixing is the sum of the kinetic energy between the motive and propelled stream. The kinetic energy of motive stream is

$$E_{km} = \frac{1}{2} M_m v_m^2 = \frac{1}{2} \cdot (1 \text{ kg/s}) \cdot (10 \text{ m/s})^2 = 50 \text{ J/s} \quad (1)$$

where,

E_{km} = kinetic energy of the motive stream (J)

M_m = mass flow rate of the motive stream (kg/s)

v_m = velocity of the motive stream (m/s)

The kinetic energy of the propelled stream is:

$$E_{kp} = \frac{1}{2} M_p v_p^2 = \frac{1}{2} \cdot (1 \text{ kg/s}) \cdot (1 \text{ m/s})^2 = 0.5 \text{ J/s} \quad (2)$$

where,

E_{kp} = kinetic energy of the propelled stream (J)

M_p = mass flow rate of the propelled stream $(\mathrm{kg/s})$

v_p = velocity of the propelled stream $(\mathrm{m/s})$

From mass conservation, the mass flow rate of the mixture stream is the sum of the motive and propelled streams.

$$M_{mixture} = M_m + M_p = 1 + 1 = 2 \ \mathrm{kg/s} \tag{3}$$

where,

$M_{mixture}$ = mass flow rate of the mixture stream $(\mathrm{kg/s})$

The velocity of the mixture stream is computed by momentum conservation, as shown in the next step.

$$p_{mixture} = p_{motive} + p_{propelled} \tag{4}$$

where,

$p_{mixture}$ = momentum of the mixture stream $((\mathrm{kg \cdot m})/\mathrm{s})$

p_{motive} = momentum of the motive stream $((\mathrm{kg \cdot m})/\mathrm{s})$

$p_{propelled}$ = momentum of the propelled stream $((\mathrm{kg \cdot m})/\mathrm{s})$

So

$$M_{mixture} v_{mixture} = M_{motive} v_{motive} + M_{propelled} v_{propelled} \tag{5}$$

where,

$M_{mixture}$ = mass flow rate of the mixture stream $(\mathrm{kg/s})$

$v_{mixture}$ = velocity of the mixture stream $(\mathrm{m/s})$

Thus

$$v_{mixture} = \frac{M_{motive} v_{motive} + M_{propelled} v_{propelled}}{M_{mixture}} = \frac{(1\ \text{kg/s} \cdot 10\ \text{m/s}) + (1\ \text{kg/s} \cdot 1\ \text{m/s})}{2\ \text{kg/s}} = 5.5\ \text{m/s} \tag{6}$$

The kinetic energy of the mixture stream is

$$E_{kmix} = \frac{1}{2} M_{mix} v_{mix}^2 = \frac{1}{2} \cdot (2\ \text{kg/s}) \cdot (5.5\ \text{m/s})^2 = 27.5\ \text{J/s} \tag{7}$$

where,

E_{kmix} = kinetic energy of the mixture stream (J)

Energy efficiency is calculated by:

$$\eta = \frac{E_{kmix}}{E_{km} + E_{kp}} = \frac{27.5\ \text{J}}{50\ \text{J} + 0.5\ \text{J}} = 0.545 \tag{8}$$

where,

η = efficiency

In the small momentum different case, the velocity of the propelled stream is increased from 1 to 6 m/s (see Figure 11).

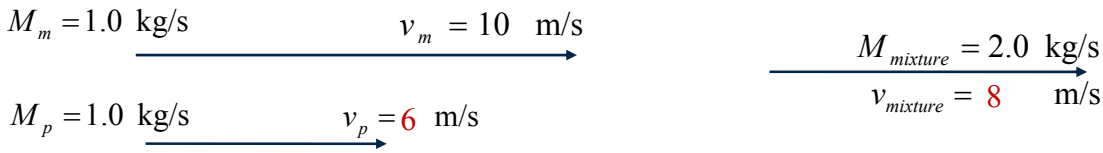

Figure 11. Diagram of small momentum different condition.

Following the above calculation, the kinetic energy of the motive stream is

$$E_{km} = \frac{1}{2} M_m v_m^2 = \frac{1}{2} \cdot (1 \text{ kg/s}) \cdot (10 \text{ m/s})^2 = 50 \text{ J/s} \quad (9)$$

The kinetic energy of the propelled stream is:

$$E_{kp} = \frac{1}{2} M_p v_p^2 = \frac{1}{2} \cdot (1 \text{ kg/s}) \cdot (6 \text{ m/s})^2 = 18 \text{ J/s} \quad (10)$$

The kinetic energy of the mixture stream is:

$$E_{kmix} = \frac{1}{2} M_{mix} v_{mix}^2 = \frac{1}{2} \cdot (2 \text{ kg/s}) \cdot (8 \text{ m/s})^2 = 64 \text{ J/s} \quad (11)$$

The resulting efficiency is:

$$\eta = \frac{E_{kmix}}{E_{km} + E_{kp}} = \frac{64 \text{ J}}{50 \text{ J} + 18 \text{ J}} = 0.941 \quad (12)$$

The calculation shows that efficiency increases substantially when the momentum difference between the motive and propelled streams decreases. This confirms that jet ejector performance improves by minimizing the momentum difference between the motive and propelled streams.

Computational Fluid Dynamics

Computational Fluid Dynamics (CFD) has been emerging since the 1950s due to improvements in the speed of computers and their memory size. CFD is primarily established as a tool for flow-based physical simulation, process evaluation, and component design. CFD, when implemented properly, is a low-cost, rapid, non-intrusive, parametric test method. As a design tool, it permits developments with greater reliability and repeatability, at a fraction of the cost and time of traditional design

approaches that involve empiricism, followed by prototyping and testing (Habashi, 1995).

According to Chapman et al. (1975); Chapman (1979, 1981); Green (1982); Rubbert (1986) and Jameson (1989) CFD has five major advantages compared with experimental fluid dynamics:

1. Significantly reduce lead time in design and development
2. Simulate flow conditions not reproducible in experimental model tests
3. More detailed and comprehensive information
4. More cost-effective than wind-tunnel testing
5. Lower energy consumption

Because of computer developments, CFD can solve more complex problems, which require more details, and ask for more precision.

Fluent Software

Fluent is a state-of-the-art computer program for modeling fluid flow and heat transfer in complex geometries (Fluent, 2001). In Fluent, the process to obtain the computational solution involves of two stages, as shown schematically in Figure 12.

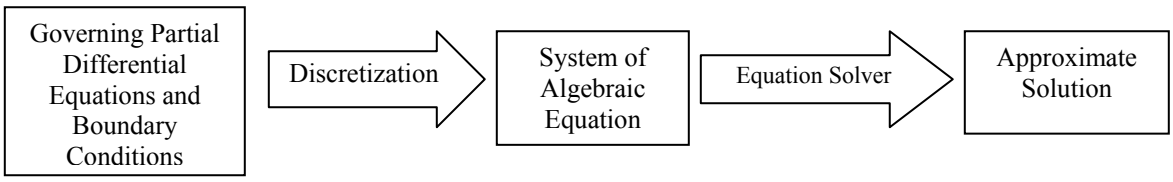

Figure 12. Overview of the computational solution procedure (Fletcher, 1987).

The first stage is called discretization. The continuous partial differential equations are converted into a discrete system of algebraic equations in this stage. The detail of discretization is explained in the following section. In the second stage, a numerical solver is selected to solve a discrete system obtaining from the first stage. The solution of the system of algebraic equations is obtained as a consequence.

Discretization

Discretization is a process that converts the governing partial differential equations to a system of algebraic equations. Several techniques are available in CFD software. The most common are finite difference, finite element, finite volume, and spectral methods (Fletcher, 1987).

The finite-volume technique is used in this study. Discretization of the governing equations is demonstrated easily by considering transport of a scalar quantity (ϕ) in the steady-state conservation equation. The steady-state conservation equation written in integral form for an arbitrary control volume (V) is expressed in Equation 13.

$$\oint \rho\phi\vec{v} \cdot d\vec{A} = \oint \Gamma_\phi \nabla\phi \cdot d\vec{A} + \int_V S_\phi dV \tag{13}$$

where,

ρ = density $\left(\text{kg/m}^3\right)$

$\vec{v}$ = velocity vector $\left(u\hat{i} + v\hat{j}\right)$ $\left(\text{m/s}\right)$

$\vec{A}$ = surface area vector $\left(\text{m}^2\right)$

Γ_ϕ = diffusion coefficient for ϕ $\left(\text{kg/}\left(\text{m} \cdot \text{s}\right)\right)$

$$(\nabla\phi) = \text{gradient of } \phi \left(\left(\frac{\partial\phi}{\partial x}\right)\hat{i} + \left(\frac{\partial\phi}{\partial y}\right)\hat{j}\right) \left(\text{m}^{-1}\right)$$

$$S_\phi = \text{source of } \phi \text{ per unit volume } \left(\text{kg}/\left(\text{m}^3 \cdot \text{s}\right)\right)$$

Equation 13 is applied to each control volume, or cell, in the computational domain (Fluent, 2001). Discretization of Equation 13 gives rise to Equation 14.

$$\sum_f^{N_{faces}} \rho_f \vec{v}_f \phi_f \cdot \vec{A}_f = \sum_f^{N_{faces}} \Gamma_\phi (\nabla\phi)_n \cdot \vec{A}_f + S_\phi V \tag{14}$$

where,

N_{faces} = number of faces enclosing cell

ϕ_f = value of ϕ convected through face f

$\rho_f \vec{v}_f \cdot \vec{A}_f$ = mass flux through the face $\left(\text{kg/s}\right)$

$\vec{A}_f$ = area of face f $\left(|A| = |A_x|\hat{i} + |A_y|\hat{j}\right)$ $\left(\text{m}^2\right)$

$(\nabla\phi)_n$ = magnitude of $\nabla\phi$ normal to face f $\left(\text{m}^{-1}\right)$

V = cell volume $\left(\text{m}^3\right)$

Figure 13 illustrates the discretization of a scalar transport equation by a finite-volume technique.

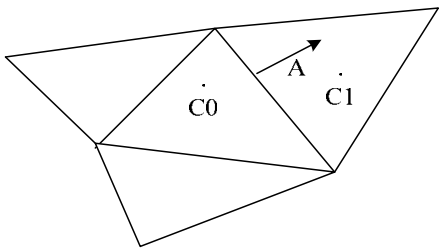

Figure 13. Control volume used to illustrate discretisation of a scalar transport equation (Fluent, 2001).

Discrete values of the scalar ϕ are stored at the cell center (C_o and C_1) in Figure 13. The connection terms in Equation 14 requires face value (ϕ_f). The face value is calculated by using an upwind scheme, whereas the diffusion terms in Equation 2 are central-differenced and second-order accurate.

Upwinding means that the face value (ϕ_f) is calculated from the cell-center value (ϕ) of the cell upstream relative to the direction of the velocity ($\vec{v}_n$) in Equation 14.

There are four upwind schemes available in Fluent:

1. First-Order Upwind
2. Second-Order Upwind
3. Power Law
4. Quick

First-Order Upwind Scheme

The face value (ϕ_f) is set equal to the cell-center value (ϕ) of the upstream cell.

Second-Order Upwind Scheme

The face value (ϕ_f) is calculated by the following equation:

$$\phi_f = \phi + \nabla\phi \cdot \nabla\vec{S} \tag{15}$$

where,

$\nabla\phi$ = gradient of the upstream cell $\left(\mathrm{m}^{-1}\right)$

$\nabla\vec{S}$ = displacement vector from centroid of the upstream cell to its face $\left(\mathrm{m}\right)$

The gradient is evaluated by the divergence theorem, which is written in discrete form as

$$\nabla\phi = \frac{1}{\mathrm{V}}\sum_{f}^{\mathrm{N_{faces}}}\tilde{\phi}_{\mathrm{f}}\vec{A} \tag{16}$$

where,

$\tilde{\phi}_f$ = converge face values

The face values ($\tilde{\phi}_f$) are computed by averaging the cell-center value (ϕ) from two cells adjacent to the face.

Power Law Scheme

The face value (ϕ_f) is interpolated by using the exact solution of a one-dimensional convection diffusion equation

$$\frac{\partial}{\partial x}\left(\rho u\phi\right) = \frac{\partial}{\partial x}\Gamma\frac{\partial\phi}{\partial x} \tag{17}$$

where Γ and ρu are constant across the interval ∂x.

Equation 17 is integrated giving rise Equation 18. Equation 18 explains how the cell-center value (ϕ) varies with *x*:

$$\frac{\phi(x)-\phi_o}{\phi_L-\phi_o}=\frac{\exp\left(\mathrm{Pe}\frac{x}{L}\right)-1}{\exp(\mathrm{Pe})-1} \tag{18}$$

where,

ϕ_o = ϕ at the first point

ϕ_L = ϕ at final point

Pe = Peclet number = $\frac{\rho u L}{\Gamma}$

The variation of $\phi(x)$ between x=0 and x=L is demonstrated in Figure 14 for a variety of Peclet numbers.

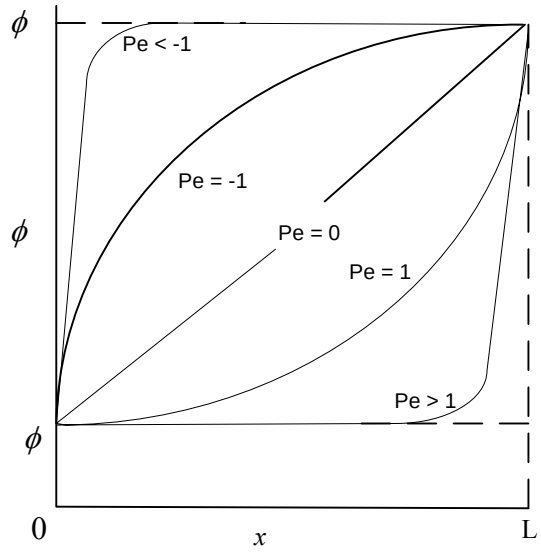

Figure 14. Variation of a variable ϕ between x=0 *and* x=L (Fluent, 2001).

Equation 18 is used as an equivalent "Power Law" format in Fluent, as its interpolation scheme.

Quick Scheme

Quick scheme is based on a weight average of second-order-upwind and central interpolations of the variable. A one-dimensional control volume is displayed in Figure 15.

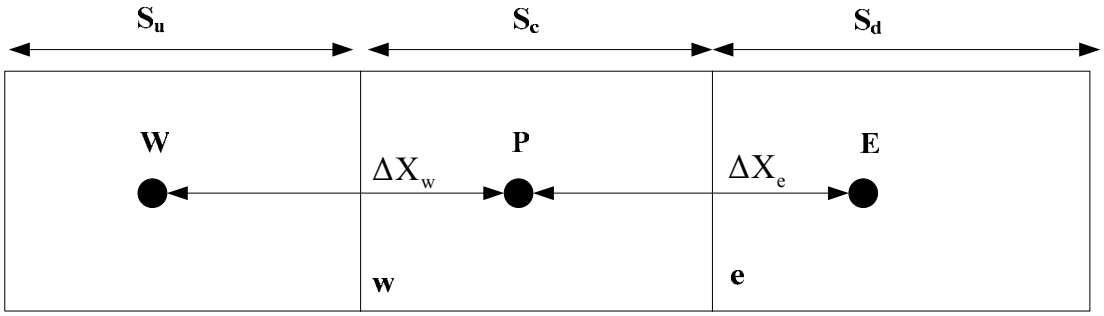

Figure 15. One-dimensional control volume (Fluent, 2001).

For the face *e* in Figure 15, if the fluid flows from left to right, such a value can be written as (Fluent, 2001).

$$\phi_e = \theta\left[\frac{S_d}{S_c + S_d}\phi_P + \frac{S_c}{S_c + S_d}\phi_E\right] + (1-\theta)\left[\frac{S_u + 2S_c}{S_u + S_c}\phi_P - \frac{S_c}{S_u + S_c}\phi_W\right] \qquad (19)$$

Seta (θ) is set at $\frac{1}{8}$ in a conventional quick scheme.

Pressure-Velocity Coupling

In Fluent, there are three options available for the pressure-velocity coupling algorithms, which are

1. SIMPLE; Semi-Implicit Method for Pressure-Linked Equations
2. SIMPLEC; SIMPLE-Consistence

3. PISO; Pressure-Implicit with Splitting of Operators

Because the SIMPLE algorithm is applied in this study, the SIMPLE algorithm is presented further in detail.

SIMPLE

The SIMPLE algorithm uses a relationship between velocity and pressure corrections to enforce mass conservation and to obtain the pressure field. The steady-state continuity and momentum equations in integral form are considered as the first step as shown in Equations 20 and 21, respectively.

$$\oint \rho \vec{v} \cdot d\vec{A} = 0 \tag{20}$$

$$\oint \rho \vec{v} \vec{v} \cdot d\vec{A} = -\oint \rho \phi \vec{I} \cdot d\vec{A} + \oint \bar{\bar{\tau}} \cdot d\vec{A} + \int_V \vec{F} dV \tag{21}$$

where,

$\vec{I}$ = identity matrix

$\bar{\bar{\tau}}$ = stress tensor $\left(\text{kg}/\left(\text{m} \cdot \text{s}^2\right)\right)$

$\vec{F}$ = force vector $\left(\text{N}\right)$

The continuity equation is integrated over the control volume in Figure 13. Equation 9 transforms to Equation 22.

$$\sum_f^{N_{faces}} J_f A_f = 0 \tag{22}$$

where,

J_f = mass flux through face f $\left(\text{kg}/\left(\text{m}^2 \cdot \text{s}\right)\right)$

The mass flux (J_f) is computed by

$$J_f = \hat{J}_f + d_f\left(P_{c0} - P_{c1}\right) \tag{23}$$

where,

$\hat{J}_f$ = mass flux containing the influence of velocities $\left(\text{kg}/\left(\text{m}^2 \cdot \text{s}\right)\right)$

d_f = a function of momentum equation on either side of f $\left(\text{s}/\text{m}\right)$

P_{c0} = pressure in cell C_0 on either side of the face $\left(\text{kg}/\left(\text{m} \cdot \text{s}^2\right)\right)$

P_{c1} = pressure in cell C_1 on either side of the face $\left(\text{kg}/\left(\text{m} \cdot \text{s}^2\right)\right)$

If the momentum equation is solved by using a guessed pressure field (P^*), Equation 23 will be modified to Equation 24.

$$J_f^* = \hat{J}_f^* + d_f\left(P_{c0}^* - P_{c1}^*\right) \tag{24}$$

However, the resulting face flux (J_f^*) does not satisfy the continuity equation. Therefore, a correction $J_f^{'}$ is added to the resulting face flux to satisfy the continuity equation as shown in Equation 25.

$$J_f = J_f^* + J_f^{'} \tag{25}$$

The SIMPLE algorithm postulates that the correction ($J_f^{'}$) can be written as (Fluent, 2001).

$$J_f^{'} = d_f\left(P_{c0}^{'} - P_{c1}^{'}\right) \tag{26}$$

where,

$P^{'}$ = the cell pressure correction $\left(\text{kg}/\left(\text{m} \cdot \text{s}^2\right)\right)$

When a solution is obtained, the face flux and the cell pressure are interpolated using Equation 27 and 28 respectively.

$$J_f = J_f^* + d_f\left(P_{c0}^{'} - P_{c1}^{'}\right) \tag{27}$$

$$P = P^* + \alpha_P P^{'} \tag{28}$$

where,

α_P = the under-relaxation factor for pressure

Ultimately, the corrected face flux (J_f) satisfies the discrete continuity equation. Equation 27 presents the corrected face flux which satisfies the discrete continuity equation during iteration.

Equation Solver

Equation solver is applied in the step of solving the system of algebraic equations to obtain an approximate solution as shown in Figure 12.

Fluent provides two different equation solvers:

1. Segregated solver
2. Coupled solver

These two alternatives are used to solve the continuity, momentum, energy, and species equation. The segregated solver solves these equations segregated from one another. But the coupled solver solves them coupled together. Regardless of the types of solvers, the control-volume technique is always applied. The procedure is explained below:

1. Divide the domain into discrete control volumes by using a computational grid
2. Integrate the governing equations on the individual control volumes to generate algebraic equations for the dependent variable such as velocities, pressure, temperature, and conserved scalar quantities.
3. Linearize the discretized equations and the resultant linear equation system to updated values of the dependent variables.

Segregated Solver

The segregated solver solves the governing equation separately. Each iteration step is presented in Figure 16 and is explained below.

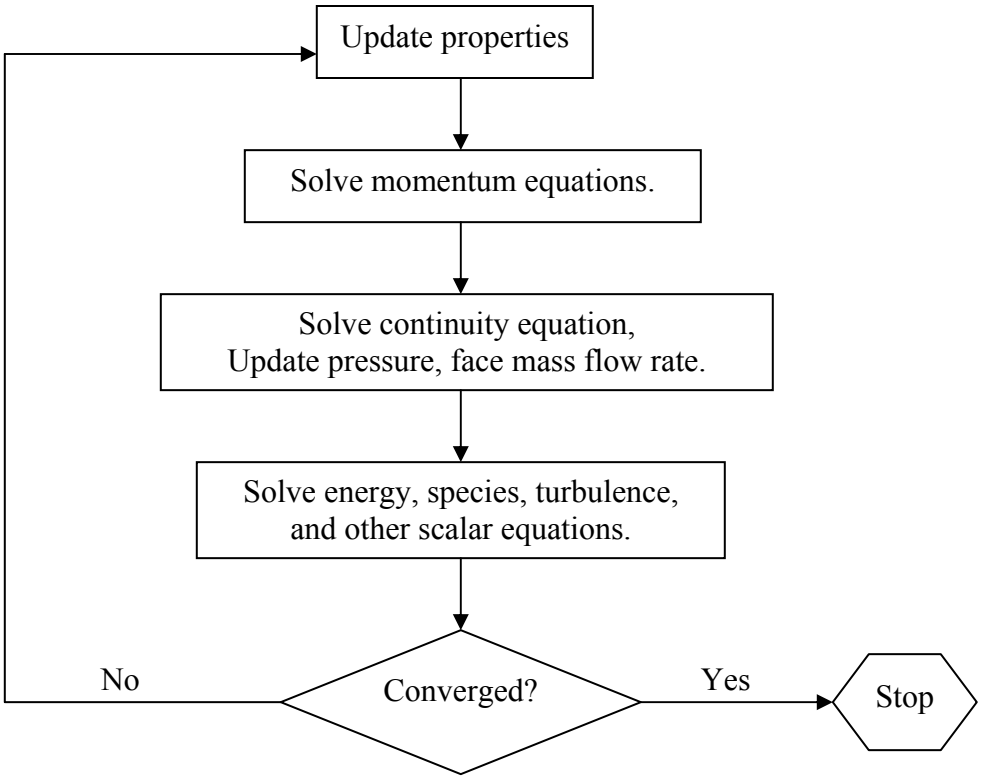

Figure 16. Procedure of the segregated solver.

1. Update fluid properties, based on the current solution. For the first iteration, the fluid properties will be updated from an initialized solution.
2. Solve momentum equations by using current values for pressure and face mass fluxes for updating the velocity field.
3. Solve the continuity equation to update, pressure, velocity fields and the face mass fluxes.
4. Solve equations for scalar quantities, such as turbulence, energy, species, and radiation by using the previously updated values of the other variables.

5. (Optional) Update the source terms in the appropriate continuous phase equations with a discrete phase trajectory calculation.
6. Check for convergence condition.

Coupled Solver

The governing equations of continuity, momentum, energy, and species transport are solved simultaneously in the coupled solver; whereas, the governing equations for additional scalars will be solved segregated from one another. Each iteration step is shown in Figure 17 and explained below.

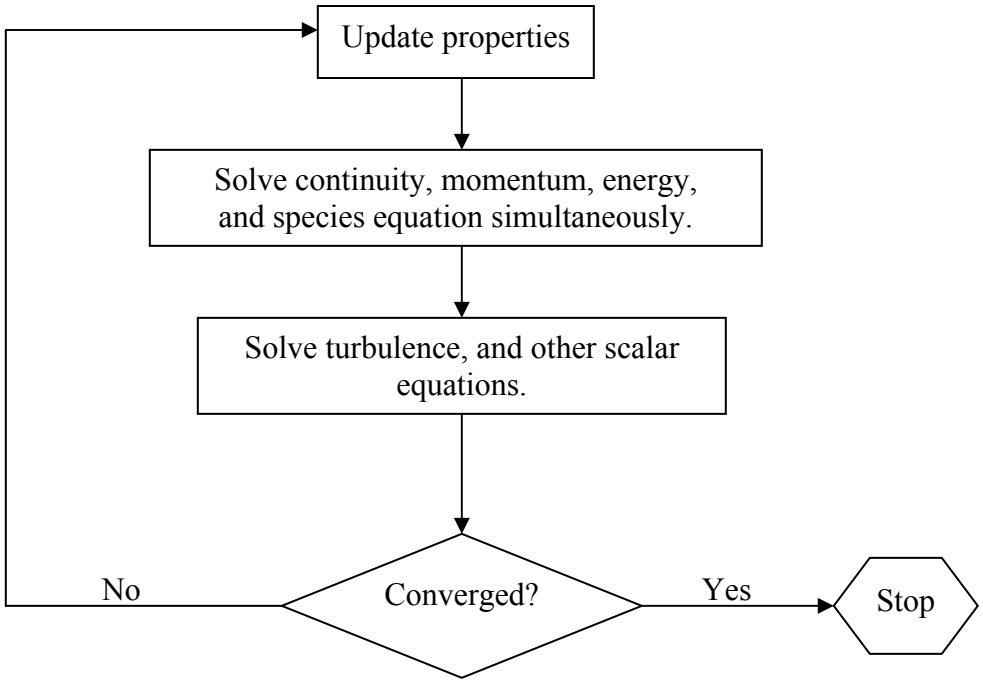

Figure 17. Procedure of the coupled solver.

1. Update fluid properties, based on the current solution. For the first iterations, the fluid properties will be updated based on an initialized solution.
2. Solve the continuity, momentum, energy, and species equations simultaneously.
3. Solve equations for scalars, such as turbulence and radiation by using the previously updated values of the other variables.
4. (Optional) Update the source terms in the appropriate continuous phase equations with a discrete phase trajectory calculation.
5. Check for convergence condition.

Turbulence Modeling

Fluid flow with a very high velocity and high Reynolds number is called turbulent flow. Because the jet ejector motive stream is turbulent, a turbulence model must be considered for calculating fluid properties in Fluent.

In turbulent flow, velocity fields fluctuate. These fluctuations mix with transport quantities such as momentum, energy, and species concentration; consequently, the transport quantities fluctuate as well. The exact governing equation; however, can be time-averaged or ensemble-averaged to cancel the small fluctuations. A modified set of equations is created from this operation. Unknown variables are generated in the modified equations, and these variables are determined as known quantities by using the turbulence model.

In Fluent, there are five turbulence models available:

1. Spalart-Allmaras model

2. k-ε models
    - Standard k-ε model
    - Renormalization-group (RNG) k-ε model
    - Realizable k-ε model
3. k-ω models
    - Standard k-ω model
    - Shear-stress transport (SST) k-ω model
4. Reynolds stress model (RSM)
5. Large eddy simulation (LES) model

The advantages and disadvantages of each model are described in the following section. Also, the reasons for selecting the standard k-ε model are addressed. Finally, the mathematical algorithm of standard k-ε is presented.

Because there is no single model that is universally accepted for all classes of problems, the choice of turbulence model depends on considerations such as the physics encompassed in the flow, the established practice for a specific class of problem, the level of accuracy required, the available computational resources, and the amount of time available for the simulation.

Spalart-Allmaras Model

Spalart-Allmaras model is mainly applied to aerospace applications. The model involves wall-bounded flows and gives good results for boundary layers subjected to adverse pressure gradients. It is popular in turbo-machinery applications. Because the

near-wall gradients of the transported variables in the model are much smaller than the ones in *k-ε* or *k-ω* models, the model is less sensitive to numerical error.

Standard k-ε Model

Standard *k-ε* model is considered the simplest "complete model" of turbulence. This model is widely used in industrial flow simulation due to robustness, economy, and reasonable accuracy for a wide range of turbulent flows. It is the workhorse of practical engineering flow calculations.

Renormalization-Group (RNG) k-ε Model

The RNG model is improved from the standard *k-ε* model by using a rigorous statistical technique. It is similar to the standard *k-ε* model, but includes the following refinements:

1. An additional term in its *ε* equation is added that significantly improves the accuracy for rapidly strained flows.
2. The effect of swirl on turbulence is included, enhancing accuracy for swirling flows.
3. An analytical formula for turbulent Prandtl numbers is provided
4. An analytically derived differential formula for effective viscosity is provided, so low-Reynolds-number is accounted for.

These features produce more reliability and accuracy in the model than the standard *k-ε* model. However, these additional features are not required in this study.

Realizable k-ε Model

The realizable *k-ε* model is different from the standard *k-ε* model in two important ways:

1. It contains a new formula for turbulent viscosity.
2. The transport of the mean-square vorticity fluctuation is included in this model.

This model provides superior performance for flow involving rotation, boundary layers under strong adverse pressure gradients, separation, and recirculation. Because the fluid flow in a jet ejector does not require any above additional features, this model is not applied.

Standard k-ω Model

Standard *k-ω* model is derived for low-Reynolds-number flow, compressibility, and shear flow spreading. In our problem, the Reynolds number is very high especially at the nozzle, so this model is not selected.

Shear-Stress Transport (SST) k-ω Model

SST *k-ω* model is created to blend the robust and accurate formulation of the *k-ω* model in the near-wall region effectively with the free-stream independence of the *k-ε* model in the far field.

The SST *k-ω* model is close to the standard *k-ω* model, but includes the following additional refinements:

1. A blending function is formulated by multiplying both the standard k-ω model and the transformed k-ε model. The blending function is designed to be one in the near-wall region, and zero away from the surface.
2. A damped cross-diffusion derivative term in the ω equation is accounted in the SST k-ω model.
3. The transport of the turbulent shear stress is accounted by modifying the definite of the turbulent viscosity.

The SST k-ω model is more accurate and reliable than the standard k-ω model due to these features, and it is applied for low-Reynolds-number flow only.

Reynolds Stress Model (RSM)

RSM is designed for the effects of streamline curvature, swirl, rotation, and rapid changes in strain rate. The examples relating to these flow characteristics are cyclone flow, highly swirling flow in combustor, rotating flow passage, and the stress-induced secondary flows in duct.

Large Eddy Simulation Model (LES)

The LES model is used for unsteady-state, high-Reynolds-number turbulent flow in complex geometries. The strength of this model is that an error included by the turbulence model is small; however, it requires the large computational resources to resolve the energy-containing turbulent eddies.

CPU Time and Solution Behavior

The relative CPU time required for each model is summarized in Table 4.

Table 4. Comparison of CPU time consuming of each turbulence model.

Turbulence Model	CPU Time Requirement
S-A	1 (least)
Standard k-ε	2
Standard k-ω	2
Realizable k-ε	3
RNG k-ε	4
SST	4
RSM	5
LES	6 (most)

Due to an additional transport equation, the standard k-ε model requires more computational effort than the Spalart-Allmaras model. The realizable k-ε model requires slightly higher CPU resource than the standard k-ε model. The RNG k-ε model needs 10 – 15% more computational effort than the standard k-ε model. The k-ω models require almost the same CPU resource as the k-ε models. On average, RSM requires 50 – 60% more computational effort compared to the k-ε and k-ω models and 15 – 20% more memory is required.

Because of finite computational resources and the flow behavior in jet ejectors, the standard k-ε model is the best compared to other schemes, so the standard k-ε model is applied throughout the study.

Mathematical Algorithm of the Standard k-ε Model

The standard *k-ε* model is a semi-empirical model for turbulent kinetic energy, *k*, and its dissipation rate, *ε*. The model assumes that the effects of molecular viscosity are negligible and the flow is fully turbulent.

The turbulence kinetic energy, *k*, and its dissipation rate, *ε*, are calculated from

$$\frac{\partial}{\partial t}(\rho k)+\frac{\partial}{\partial x_i}(\rho k u_i)=\frac{\partial}{\partial x_j}\left[\left(\mu+\frac{\mu_t}{\sigma_k}\right)\frac{\partial k}{\partial x_j}\right]+G_k+G_b-\rho\varepsilon-Y_M+S_k \qquad (29)$$

and

$$\frac{\partial}{\partial t}(\rho\varepsilon)+\frac{\partial}{\partial x_i}(\rho\varepsilon u_i)=\frac{\partial}{\partial x_j}\left[\left(\mu+\frac{\mu_t}{\sigma_\varepsilon}\right)\frac{\partial \varepsilon}{\partial x_j}\right]+C_{1\varepsilon}G_k\frac{\varepsilon}{k}-C_{2\varepsilon}\rho\frac{\varepsilon^2}{k}+S_\varepsilon \qquad (30)$$

where,

t = time (s)

ρ = density $(\mathrm{kg/m^3})$

k = turbulence kinetic energy $((\mathrm{J\cdot m^3})/\mathrm{kg})$

u = velocity $(\mathrm{m/s})$

x = distance (m)

μ = viscosity $(\mathrm{kg/(m\cdot s)})$

μ_t = turbulence viscosity $(\mathrm{kg/(m\cdot s)})$

G_k = generation of turbulence kinetic energy due to the mean velocity gradients (J)

G_b = generation of turbulence kinetic energy due to buoyancy force (J)

ε = rate of dissipation rate $\left((\mathrm{J}\cdot\mathrm{m}^3)/(\mathrm{kg}\cdot\mathrm{s})\right)$

Y_M = contribution of the fluctuating dilation in compressible turbulence to the overall dissipation (J)

$C_{1\varepsilon}$ = model constant = 1.44

$C_{2\varepsilon}$ = model constant = 1.92

σ_k = turbulent Prandtl number for k = 1.0

σ_ε = turbulent Prandtl number for ε = 1.3

S_k = user-defined source term for k (J)

S_ε = user-defined source term for ε (J)

μ_t = turbulent viscosity $(\mathrm{kg}/(\mathrm{m}\cdot\mathrm{s}))$

Turbulent viscosity is calculated by Equation 19.

$$\mu_t = \rho C_\mu \frac{k^2}{\varepsilon} \tag{31}$$

where,

C_μ = model constant = 0.09

Dimensionless Forms of Fluid Transport Equations

Dimensionless quantities are universal, and independent of operating variables, such as fluid, geometric scale, operating pressure, etc. Therefore, all parameters in the

research are converted to the dimensionless terms. The objective of this section is to demonstrate that the fluid transport equations can be transformed into dimensionless forms. This confirms that the dimensionless principle can relate to the research. The fluid transport equations such as the mass (continuity), momentum, and energy conservation equations are demonstrated in this section.

The mass conservation equation, or continuity equation, for the compressible flow is:

$$\frac{\partial \rho}{\partial t} + \overline{\nabla} \cdot \left(\rho \ \bar{v} \right) = 0 \tag{32}$$

where,

ρ = fluid density $\left(\text{kg/m}^3 \right)$

t = time $\left(\text{s} \right)$

$\bar{v}$ = fluid velocity in a vector notation $\left(\text{m/s} \right)$

$\overline{\nabla}$ = gradient operator

Momentum conservation for compressible flow in vector notation is (Happel and Brenner, 1965).

$$\rho \frac{Dv}{Dt} = -\overline{\nabla} P_{static} + \mu \nabla^2 \bar{v} + 2 \overline{\nabla} \mu \cdot \overline{\nabla} \bar{v} + \overline{\nabla} \mu \times \left(\overline{\nabla} \times \bar{v} \right) + \frac{1}{3} \mu \overline{\nabla} \left(\overline{\nabla} \cdot \bar{v} \right)$$

$$- \frac{2}{3} \left(\overline{\nabla} \cdot \bar{v} \right) \overline{\nabla} \mu + K \overline{\nabla} \left(\overline{\nabla} \cdot \bar{v} \right) + \left(\overline{\nabla} \cdot \bar{v} \right) \overline{\nabla} K + \rho \ g + j \times \bar{B} \tag{33}$$

where,

$\frac{D}{Dt}$ = material derivation

P_{static} = static pressure (Pa)

μ = fluid viscosity $(\mathrm{N \cdot m})$

∇^2 = LaPlacian operator

K = bulk viscosity $(\mathrm{N \cdot m})$

g = acceleration due to gravity $(\mathrm{m/s^2})$

j = current

$\overline{B}$ = magnetic field

The effects of K on fluid dynamics are difficult to detect and usually ignored (Deen W. M., 1998). Also, there is no magnetic field in our system, so the final term is negligible. To simplify Equation 33, the dynamic pressure term is introduced to replace the static pressure and the gravity force term in the equation. The relationship of the dynamic pressure can be written as (Deen, 1998):

$$\overline{\nabla} P_{dynamic} = \overline{\nabla} P_{static} - \rho\ \overline{g} \tag{34}$$

where,

$P_{dynamic}$ = dynamic pressure (Pa)

So Equation 33 converts to Equation 35.

$$\rho\frac{Dv}{Dt} = -\overline{\nabla}P_{dynamic} + \mu\nabla^2\overline{v} + 2\overline{\nabla}\mu\cdot\overline{\nabla}\overline{v} + \overline{\nabla}\mu\times\left(\overline{\nabla}\times\overline{v}\right)$$

$$+\frac{1}{3}\mu\overline{\nabla}\left(\overline{\nabla}\cdot\overline{v}\right) - \frac{2}{3}\left(\overline{\nabla}\cdot\overline{v}\right)\overline{\nabla}\mu \qquad (35)$$

The material derivation on the left-hand side is equivalent to Equation 36.

$$\rho\frac{Dv}{Dt} = \frac{\partial}{\partial t}\left(\rho\ \overline{v}\right) + \overline{\nabla}\cdot\left(\rho\ \overline{v}\overline{v}\right) \qquad (36)$$

Equation 35 is substituted by Equation 36 and becomes Equation 37, which is the dimensionless form of the continuity equation.

$$\frac{\partial}{\partial t}\left(\rho\ \overline{v}\right) + \overline{\nabla}\cdot\left(\rho\ \overline{v}\overline{v}\right) = -\overline{\nabla}P_{dynamic} + \mu\nabla^2\overline{v} + 2\overline{\nabla}\mu\cdot\overline{\nabla}\overline{v} + \overline{\nabla}\mu\times\left(\overline{\nabla}\times\overline{v}\right)$$

$$+\frac{1}{3}\mu\overline{\nabla}\left(\overline{\nabla}\cdot\overline{v}\right) - \frac{2}{3}\left(\overline{\nabla}\cdot\overline{v}\right)\overline{\nabla}\mu \qquad (37)$$

The Mass Conservation Equation (Continuity Equation)

A general form of the mass conservation equation in case of without any external force is

$$\frac{\partial\rho}{\partial t} + \overline{\nabla}\cdot\left(\rho\ \overline{v}\right) = 0$$

The characteristic density and velocity are introduced to transform Equation 32 to the dimensionless form.

Define:

ρ_c = characteristic density = an inlet density of the fluid $\left(\text{kg/m}^3\right)$

U = characteristic velocity = an inlet velocity of the fluid $\left(\text{m/s}\right)$

t_c = characteristic time (s)

With dimensionless variables and differential operators defined as (Deen, 1998):

$$\widetilde{\rho}=\frac{\rho}{\rho_c},\quad \widetilde{v}=\frac{\bar{v}}{\overline{U}},\quad \widetilde{t}=\frac{t}{t_c},\quad \widetilde{\nabla}=\overline{\nabla}L \tag{38}$$

where,

L = characteristic length = an inlet diameter of ejector (m)

For Equation 38, each term is converted to dimensionless form by multiplying and dividing each term by their characteristic parameters, and then rearranging the equation to the dimensionless parameters. Consequently, the dimensionless form of Equation 37 is presented in Equation 39.

$$\frac{\partial\widetilde{\rho}}{\partial\widetilde{t}}+\widetilde{\nabla}\left(\widetilde{\rho}\ \widetilde{v}\right)=\ 0 \tag{39}$$

The Momentum Conservation Equation

The general form of the momentum conservation equation is presented in Equation 40, which is

$$\frac{\partial}{\partial t}\left(\rho\ \bar{v}\right)+\overline{\nabla}\cdot\left(\rho\ \bar{v}\bar{v}\right)=-\overline{\nabla}P_{dynamic}+\mu\nabla^2\bar{v}+2\overline{\nabla}\mu\cdot\overline{\nabla}\bar{v}+\overline{\nabla}\mu\times\left(\overline{\nabla}\times\bar{v}\right)$$

$$+\frac{1}{3}\mu\overline{\nabla}\left(\overline{\nabla}\cdot\bar{v}\right)-\frac{2}{3}\left(\overline{\nabla}\cdot\bar{v}\right)\overline{\nabla}\mu \tag{40}$$

The characteristic dynamic pressure and viscosity are additionally defined from the continuity equation in this case.

Define:

$$\prod = \text{characteristic dynamic pressure} = \frac{1}{2}\rho_c U^2 \ \left(\text{Pa}\right)$$

$$\mu_c = \text{characteristic viscosity} = \text{inlet viscosity of the fluid} \ \left(\text{N}\cdot\text{m}\right)$$

Consequently, additional dimensionless variables and differential operators from Equation 37 are specified, which are

$$\widetilde{P} = \frac{P_{dynamic}}{\prod}, \quad \widetilde{\mu} = \frac{\mu}{\mu_c}, \quad \widetilde{\nabla}^2 = L^2\overline{\nabla}^2 \tag{41}$$

The same procedure as the continuity equation is applied at this stage to transform Equation 40. The dimensionless form of the momentum conservation equation is Equation 42.

$$\left(\frac{\rho_c U}{t_c}\right)\frac{\partial}{\partial\widetilde{t}}\left(\widetilde{\rho}\ \widetilde{v}\right)+\left(\frac{\rho_c U^2}{L}\right)\widetilde{\nabla}\left(\widetilde{\rho}\ \widetilde{v}\widetilde{v}\right)$$

$$= -\frac{\prod}{L}\widetilde{\nabla}\widetilde{P}+\left(\frac{\mu_C U}{L^2}\right)\left[\begin{array}{r}\widetilde{\mu}\widetilde{\nabla}^2\widetilde{v}+2\widetilde{\nabla}\widetilde{\mu}\cdot\widetilde{\nabla}\widetilde{v}+\widetilde{\nabla}\widetilde{\mu}\times\left(\widetilde{\nabla}\times\widetilde{v}\right)\\ +\frac{1}{3}\widetilde{\mu}\widetilde{\nabla}\left(\widetilde{\nabla}\cdot\widetilde{v}\right)-\frac{2}{3}\left(\widetilde{\nabla}\cdot\widetilde{v}\right)\widetilde{\nabla}\widetilde{\mu}\end{array}\right] \tag{42}$$

Equation 42 was multiplied by $\left(\frac{L^2}{\mu_c U}\right)$ and gave rise to Equation 43.

$$\left(\frac{\rho_c U}{t_c}\right)\times\left(\frac{L^2}{\mu_c U}\right)\frac{\partial}{\partial\widetilde{t}}\left(\widetilde{\rho}\ \widetilde{v}\right)+\left(\frac{\rho_c U^2}{L}\right)\times\left(\frac{L^2}{\mu_c U}\right)\widetilde{\nabla}\left(\widetilde{\rho}\ \widetilde{v}\widetilde{v}\right)\cdot$$

$$= -\frac{\prod}{L}\times\left(\frac{L^2}{\mu_c U}\right)\widetilde{\nabla}\widetilde{P}+\left[\begin{array}{r}\widetilde{\mu}\widetilde{\nabla}^2\widetilde{v}+2\widetilde{\nabla}\widetilde{\mu}\cdot\widetilde{\nabla}\widetilde{v}+\widetilde{\nabla}\widetilde{\mu}\times\left(\widetilde{\nabla}\times\widetilde{v}\right)\\ +\frac{1}{3}\widetilde{\mu}\widetilde{\nabla}\left(\widetilde{\nabla}\cdot\widetilde{v}\right)-\frac{2}{3}\left(\widetilde{\nabla}\cdot\widetilde{v}\right)\widetilde{\nabla}\widetilde{\mu}\end{array}\right] \tag{43}$$

Each dimensionless term in Equation 43 is replaced by the dimensionless parameters presented below.

$$Re = \frac{\rho\, UL}{\mu_c}, \quad Sr = \frac{t_c U}{L}$$

where,

Re = Reynolds number

Sr = Strouhal number

Therefore, the dimensionless term of the momentum conservation energy is presented in Equation 44.

$$Re\left[\frac{1}{Sr}\frac{\partial}{\partial \tilde{t}}\left(\tilde{\rho}\ \tilde{v}\right) + \tilde{\nabla}\left(\tilde{\rho}\ \tilde{v}\tilde{v}\right)\cdot\right] = -\left(\frac{\prod L}{\mu_c U}\right)\tilde{\nabla}\tilde{P} + \left[\begin{array}{r} \tilde{\mu}\tilde{\nabla}^2\tilde{v} + 2\tilde{\nabla}\tilde{\mu}\cdot\tilde{\nabla}\tilde{v} + \tilde{\nabla}\tilde{\mu}\times\left(\tilde{\nabla}\times\tilde{v}\right) \\ +\frac{1}{3}\tilde{\mu}\tilde{\nabla}\left(\tilde{\nabla}\cdot\tilde{v}\right) - \frac{2}{3}\left(\tilde{\nabla}\cdot\tilde{v}\right)\tilde{\nabla}\tilde{\mu} \end{array}\right] \quad (44)$$

The dimensionless form of the continuity and momentum conservation equations including the derivation are demonstrated. That means the dimensionless principle can be applied to explain the fluid flow field.

Compressible Flow

Compressible flow occurs when the flow velocity is over Mach 0.3. In compressible flow, the pressure gradient is large; the variation of the gas density with

pressure has a significant impact on the flow velocity, pressure, and temperature (Fluent, 2001).

In the research, the motive stream has the same behavior as compressible flow, because the motive stream flows out from the nozzle exit at supersonic velocity. The basic equation in compressible flow and the fluid transport equations are summarized in this section.

Basic Equations for Compressible Flows

The equations to calculate pressure and temperature in compressible flow are demonstrated, respectively. Both of them are expressed as a function of Mach number. The isentropic condition is applied in the equation.

$$\frac{P_o}{P} = \left(1 + \frac{\gamma - 1}{2} M^2\right)^{\frac{\gamma}{\gamma - 1}} \tag{45}$$

and

$$\frac{T_o}{T} = \left(1 + \frac{\gamma - 1}{2} M^2\right)^{\frac{\gamma}{\gamma - 1}} \tag{46}$$

where,

P_o = total pressure (Pa)

P = static pressure (Pa)

T_0 = total temperature (K)

T = static temperature (K)

γ = specific heat capacity ratio

M = Mach number

In compressible flow, fluid density changes as a function of pressure and temperature. For an ideal gas law, the fluid density can be calculated by Equation 47.

$$\rho = \frac{\left(P_{op} + P\right)}{\frac{R}{M_w}T} \tag{47}$$

where,

ρ = fluid density $\left(\text{kg/m}^3\right)$

P_{op} = operating pressure $\left(\text{Pa}\right)$

P = local static pressure $\left(\text{Pa}\right)$

R = universal gas constant = 8.314 $\text{J/}\left(\text{gmol}\cdot\text{K}\right)$

T = temperature $\left(\text{K}\right)$

MW = molecular weight $\left(\text{g/gmol}\right)$

The Mass Conservation Equation (The Continuity Equation)

According to Deen's (1998), a general conservation equation is

$$\frac{\partial b}{\partial t} + \overline{\nabla}\cdot\left(bv\right) = -\overline{\nabla}\cdot f + B_V \tag{48}$$

where,

b = concentration of some quantity (per unit volume)

t = time $\left(\text{s}\right)$

$\overline{\nabla}$ = gradient operator

v = fluid velocity (m/s)

f = diffusive part of the flux of that quantity

B_V = rate of formation of the quantity per unit volume

In the continuity equation, the concentration variable is the total mass density, so b is replaced by fluid density. Because there is no net flow relative to the mass-average velocity, the diffusive flux for total mass is canceled $(f = 0)$ (Deen, 1998). Additionally, there are no mass sources or sinks in the jet ejector, so B_V is negligible.

Thus, Equation 1 reduces to Equation 49.

$$\frac{\partial \rho}{\partial t} + \overline{\nabla} \cdot (\rho\, v) = 0 \tag{49}$$

The local mass conservation equation is called the mass continuity equation. In 2-D axi-symmetric geometry, the continuity equation is:

$$\frac{\partial \rho}{\partial t} + \frac{\partial}{\partial x}(\rho\ \overline{v}_x) + \frac{\partial}{\partial r}(\rho\ \overline{v}_r) + \frac{\rho\ \overline{v}_r}{r} = 0 \tag{50}$$

In Equation 50, x is the axial coordinate, r is the radial coordinate, $\overline{v}$ is the fluid velocity.

The Momentum Conservation Equation

From the governing conservation equation, the governing momentum conservation equation can be derived by the following step. Initially, b is substituted by momentum term ($\rho \overline{v}$) whereas the diffusive flux term (f) is replaced by the static pressure, the stress tensor and gravitational body force. In the jet ejector, there is no

external body force, so the rate of formation, B_v is negligible. Consequently, the governing momentum conservation equation is presented in Equation 51.

$$\frac{\partial}{\partial t}\left(\rho\ \overline{v}\right)+\overline{\nabla}\cdot\left(\rho\ \overline{v}\overline{v}\right)=-\overline{\nabla}P+\overline{\nabla}\cdot\left(\overline{\overline{\tau}}\right)+\rho\ \overline{g} \tag{51}$$

where,

P = static pressure $\left(\text{Pa}\right)$

$\overline{\overline{\tau}}$ = stress tensor $\left(\text{J}\right)$

g = local acceleration from gravity $\left(\text{m/s}^2\right)$

The stress tensor ($\overline{\overline{\tau}}$) for the compressible flows is presented in Equation 52.

$$\overline{\overline{\tau}}=\mu\left[\left(\overline{\nabla}\dot{v}+\overline{\nabla}\overline{v}^{T}\right)-\frac{2}{3}\overline{\nabla}\cdot\overline{v}I\right] \tag{52}$$

where,

μ = fluid viscosity $\left(\left(\text{kg}\cdot\text{m}^2\right)/\text{s}^2\right)$

I = unit tensor

For 2-D axi-symmetric geometry, the momentum conservation equations in axial and radial coordinates are presented in Equations 53 and 54, respectively (Deen, 1998).

In axial coordinate:

$$\frac{\partial}{\partial t}\left(\rho\overline{v}_x\right)+\frac{1}{r}\frac{\partial}{\partial x}\left(r\rho\overline{v}_x\overline{v}_x\right)+\frac{1}{r}\frac{\partial}{\partial r}\left(r\rho\overline{v}_r\overline{v}_x\right)=-\frac{\partial P}{\partial x}$$

$$+\frac{1}{r}\frac{\partial}{\partial x}\left[r\mu\left(2\frac{\partial\overline{v}_x}{\partial x}-\frac{2}{3}\left(\overline{\nabla}\cdot\overline{v}\right)\right)\right]$$

$$+\frac{1}{r}\frac{\partial}{\partial r}\left[r\mu\left(\frac{\partial \bar{v}_x}{\partial r}+\frac{\partial \bar{v}_r}{\partial x}\right)\right] \tag{53}$$

In radial coordinate:

$$\frac{\partial}{\partial t}\left(\rho \bar{v}_r\right)+\frac{1}{r}\frac{\partial}{\partial x}\left(r\rho \bar{v}_x \bar{v}_r\right)+\frac{1}{r}\frac{\partial}{\partial r}\left(r\rho \bar{v}_r \bar{v}_r\right)=-\frac{\partial P}{\partial r}$$

$$+\frac{1}{r}\frac{\partial}{\partial}\left[r\mu\left(\frac{\partial \bar{v}_x}{\partial r}+\frac{\partial \bar{v}_r}{\partial x}\right)\right]$$

$$+\frac{1}{r}\frac{\partial}{\partial r}\left[r\mu\left(2\frac{\partial \bar{v}_r}{\partial r}-\frac{2}{3}\left(\overline{\nabla}\cdot\bar{v}\right)\right)\right]$$

$$-2\mu\frac{\bar{v}_r}{r^2}+\frac{2}{3}\frac{\mu}{r}\left(\overline{\nabla}\cdot\bar{v}\right)+\rho\frac{\bar{v}_z^2}{r} \tag{54}$$

where,

$$\overline{\nabla}\cdot\bar{v}=\frac{\partial \bar{v}_x}{\partial x}+\frac{\partial \bar{v}_r}{\partial r}+\frac{\bar{v}_r}{r} \tag{55}$$

The Energy Equation

In compressible fluid, the energy equation is used corporately with the transported equations to calculate fluid properties. The governing energy equation is presented in Equation 56 (Fluent, 2001).

$$\frac{\partial}{\partial t}\left(\rho\ E\right)+\overline{\nabla}\cdot\left(\bar{v}\left(\rho\ E+p\right)\right)=\overline{\nabla}\cdot\left(k_{eff}\overline{\nabla}T-\sum_j h_j\bar{J}_j+\left(\overline{\overline{\tau}}_{eff}\bar{v}\right)\right)+S_h \tag{56}$$

where,

$$E = \text{internal energy}\ \left(\text{J}\right)$$

k_{eff} = effective conductivity $(\mathrm{J/K})$

∇T = total temperature difference (K)

h_i = sensible enthalpy of species j (J)

$\bar{J}_j$ = diffusion flux of species j (J)

$\bar{\bar{\tau}}_{eff}$ = effective viscous dissipation $((\mathrm{J \cdot s})/\mathrm{m})$

S_h = volumetric heat sources (J)

The effective conductivity (k_{eff}) is a combination of the turbulent thermal conductivity and the conventional heat conductivity, whereas the internal energy is evaluated by

$$E = h - \frac{p}{\rho} + \frac{v^2}{2} \tag{57}$$

where,

h = sensible enthalpy (J)

The sensible enthalpy is defined for ideal gases as

$$h = \sum_j Y_j h_j \tag{58}$$

where,

Y_j = mass fraction of species j

h_j = sensible enthalpy of species j (J)

The sensible enthalpy of species j can be calculated by

$$h_j = \int_{T_{ref}}^{T} c_{P,j} dT \tag{59}$$

where T_{ref} is 298.15 K.

The viscous dissipation term is energy created by viscous shear force in the flow field, whereas the energy source term is negligible in the system.

All the equations stated above are used to calculate fluid properties in Fluent.

MATERIALS AND METHODS

To optimize a high-efficiency jet ejector and design a multi-stage jet ejector system, many experiments were conducted to obtain high-quality research results. Each procedure in the Methodology section is explained in full detail with step-by-step instructions.

CFD Modeling

A number of researchers (Riffat and Everitt, 1999; Hoggarth, 1970; Riffat et al., 1996; Talpallikar et al., 1992; Neve, 1993) have certified CFD as a useful tool for predicting flow fields within a jet ejector (Riffat and Omer, 2001).

In this research, CFD software (Fluent) is used to simulate flow fields in the jet ejector. Steady-state 2-D compressible flow using the standard k-ε turbulent model is utilized to solve the problem. Because the jet ejector has symmetric geometry around a horizontal axis, and to minimize the amount of cells required, the geometry is drawn in an axi-symmetric mode around a symmetric axis.

In the research, the jet ejector geometry is drawn following the design in High-Efficiency Jet Ejector, an invention disclosure by Holtzapple (see Appendix F; 2001). Once the geometry of the jet ejector is created, a grid can be mapped to it. This step is completed by grid-generating software (GAMBIT). The grid size must be optimized so it is large enough to ensure that the flow is virtually independent of its size, but it should be minimized as much as possible to enable the model to run efficiently at an acceptable

speed (Riffat and Everitt, 1999). A non-uniform grid was selected because it provided the greatest control of the number of cells and their localized density. For optimal meshing, the grid density clusters near the wall and in the areas where gradients of flow variables differ tremendously. This is accomplished by applying weighting factors to increase the grid density at these areas. The model grid size is shown in Figure 18.

The calculation procedure uses conventional equations (Fluent, 2001), i.e., those are modified from two-dimensional mass conservation and momentum conservation for compressible, Newtonian fluid (the Navier-Stokes equation). To account for turbulent behavior, the standard k-ε model is selected. The ideal gas law is applied to calculate flow variables in the turbulent model. The wall boundary conditions are assumed to be adiabatic with no heat flux (Riffat, and Omer, 2001).

The calculation procedure used for CFD is to divide the geometry into segments, called a grid. Then, using the initial boundary and inlet conditions, the flow variables within each segment can be calculated in an iterative manner (Riffat and Everitt, 1999). Among several alternatives, the first-order interpolation scheme is applied to update the flow variables. In higher-order schemes, which provide more numerical accuracy, they are somewhat more sensitive and generate unstable numerical behavior.

A number of experiments were conducted to verify the reliability of CFD modeling. The discretization scheme, numerical solver, turbulence model, grid size, and boundary conditions affect the model reliability and must be examined. Each experimental procedure is explained in the following section.

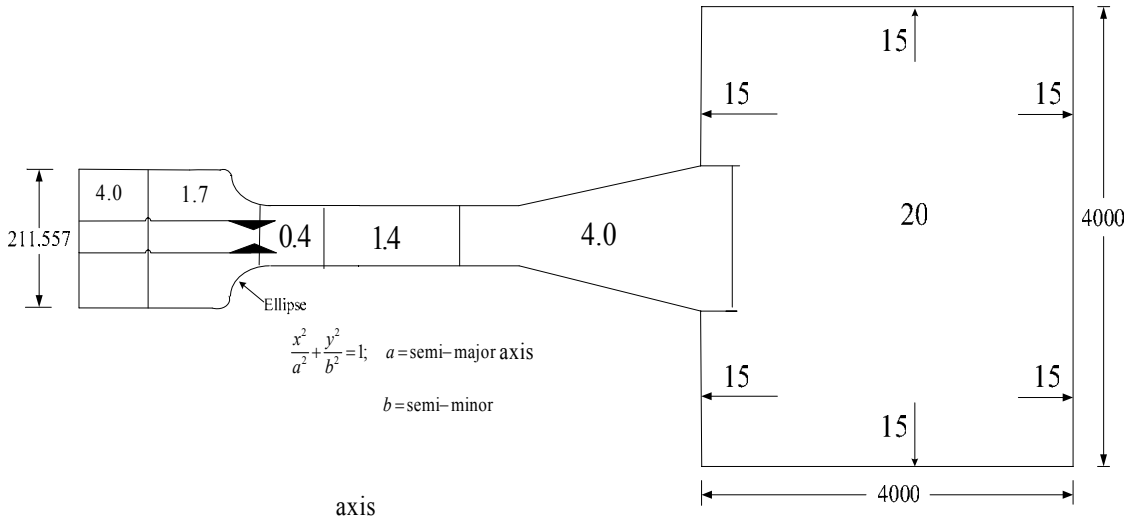

Figure 18. Grid size of an entire computational domain (unit: millimeter).

Model Reliability

The reliability of CFD modeling is considered as the most critical issue, which has to be examined before proceeding to other stages. The optimization result will be useless or even dangerous if the modeling cannot provide high-reliability results. For model reliability, three issues must be investigated: the accuracy of CFD software, the discretation process, and the CFD model boundary conditions. Three experiments were run to verify each issue individually. The procedure for each experiment is described as follows.

Model Accuracy

The accuracy of CFD modeling is investigated by comparing simulation results with experimental results done by Manohar Vishwanathappa, a graduate chemical engineering student at Texas A&M University. The simple jet-ejector geometry without mixing vanes is applied in this test. The motive-stream velocity in the model is identically specified with the experiment value. A number of cases with different propelled-stream mass flow rates are simulated. The static pressure difference between inlet and outlet of the jet ejector is reported and plotted as a function of propelled mass flow rate. The graph between the simulation and experiment results are compared to determine the deviation between both results. From this experiment, the discretization scheme, numerical solver, and turbulence model are examined.

Discretation

Discretation involves specifying the grid size and number of iterations. The grid size is examined by creating two different grid-size models (coarser and finer). Both models are simulated with various numbers of iterations (2,500, 4,500, and 6,000 iterations). The results from the finer grid-size and 6,000 iterations model is considered to be the most reliable. Because it consumes the most computational time and memory, it is inefficient to apply in the research. The best simulation model is defined as the one taking the least computational time and providing the result close to the most reliable case. When it is found, it will be employed throughout the research. In this experiment, the effects of grid-size and number of iterations are studied.

Model Boundary Conditions

The consistency of CFD modeling is verified by comparing a simulation result from all applicable boundary conditions in the model. Three points in the model, as shown in Figure 19, require a boundary condition. In Fluent, two boundary conditions (mass flow rate and total pressure) are available. At the motive stream, the motive-stream velocity is controlled in the optimization research. Because the mass flow rate boundary condition provides better control of the velocity than the total pressure boundary condition, the mass flow rate boundary condition is selected for the motive stream. At the wall surface, the back pressure is maintained constant at 101.3 kPa. Because the total pressure can control the back pressure better than the mass flow rate boundary condition, the total pressure boundary condition is selected for the wall surface. Therefore only the propelled stream boundary condition has to be verified. The experimental procedure is described as follows:

1. The mass flow rate boundary condition is first simulated under the best simulation, which is obtained from the previous experiment. An arbitrary propelled-stream mass flow rate is chosen to start the experiment.
2. Total pressure is reported from the mass flow rate boundary condition case run in Step 1. This total pressure is then used as a new boundary condition. Other variables (e.g., the numerical solver, the discretization scheme) remain the same as Step 1.

3. Iterations on the total pressure boundary condition model from Step 2 are continued until the propelled-stream mass flow rate equals the arbitrary value specified in Step 1. The number of iterations is reported.
4. The results (e.g., number of iteration, inlet and outlet static pressure, efficiency) of the two models (mass flow and total pressure boundary conditions) are compared.

The number of iterations affects the computational time. Because both the total pressure and mass flow rate boundary condition provide the same result, but require different numbers of iterations, the boundary condition that requires the fewest iterations would be applied in the research.

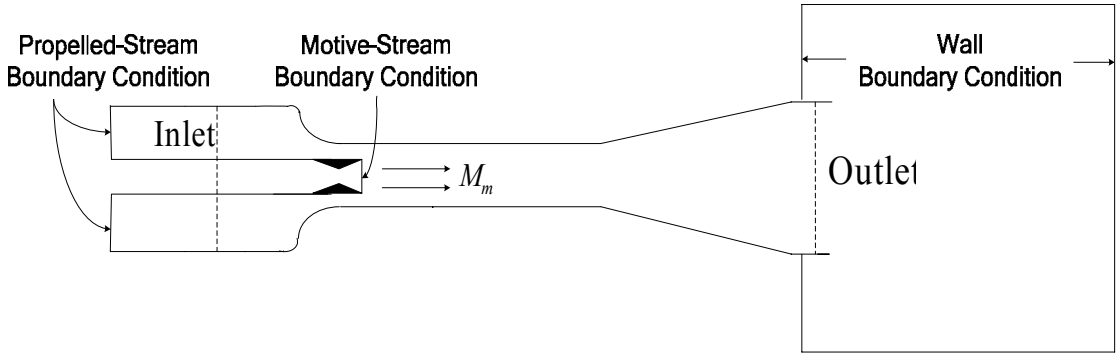

Figure 19. Boundary condition of CFD model.

Conclusion

The objective of this section is to summarize all the specified parameters in the CFD model (see Table 5), and present the grid-size in the computational domain.

Table 5. Summarize parameter specification in CFD modeling.

Type	Selection
CFD Modeling	
Numerical Solver	Conventional equation (Segregated Solver)
Turbulence Model	Standard k-ε model
Discretization Technique	Finite volume
Discretization Scheme	
Pressure	Standard scheme
Pressure-Velocity coupling	SIMPLE
Density	First-Order scheme
Energy	First-Order scheme
Momentum	First-Order scheme
Turbulence kinetic energy	First-Order scheme
Boundary Condition	
Propelled-Stream inlet	Inlet mass flow rate
Motive-Stream inlet	Inlet mass flow rate
Inlet and outlet of the box	Total pressure

Dimensionless Group Analysis

The main objective of this study is to prove that when all parameters are expressed in dimensionless terms, the results are valid for any fluid, geometric scale, and operating pressure. If the dimensionless group analysis produces a good agreement among all variables, the number of cases to be examined is reduced enormously. First, the definition of all dimensionless parameters, both the geometric parameters and fluid variables, are described. And then the procedure relating with the dimensionless group analysis is explained.

Geometric Parameters

The geometric parameters are displayed in Figure 20 and defined in Table 6.

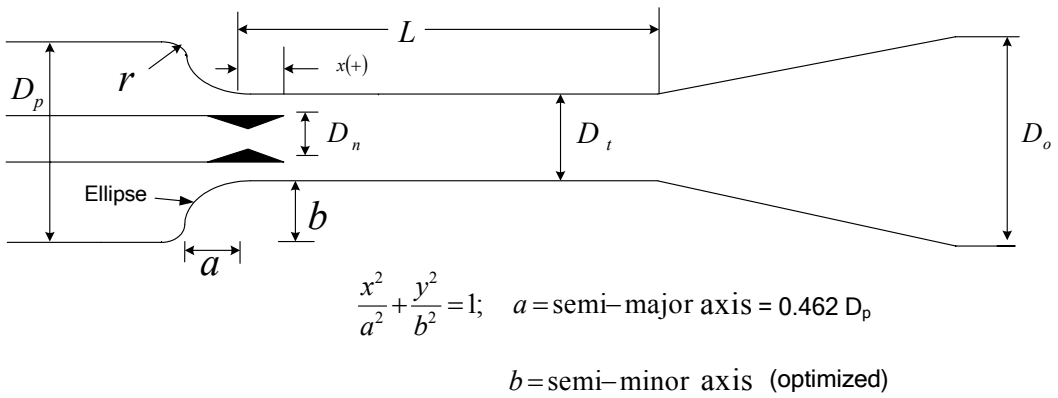

Figure 20. Geometric parameters in a jet ejector.

All geometric parameters are converted to dimensionless term by dividing by the jet-ejector inlet diameter (D_p). The dimensionless parameters are described in Table 7. The outlet diameter of the jet ejector is specified to equal the inlet diameter.

Table 6. Definition of geometric parameters.

Parameter	Definition
L	Length of the throat section
D_p	Inlet diameter
D_n	Nozzle diameter
D_t	Throat diameter
D_o	Outlet diameter
x	Distance from nozzle exit to beginning of the throat section
r	Radius of a curvature at the beginning of convergent section

Table 7. Geometric parameters in dimensionless term.

Parameter	Definition	Dimensionless Formation
L	Length ratio	$\frac{L}{D_p}$
D_n	Nozzle diameter ratio	$\frac{D_n}{D_p}$
D_t	Throat diameter ratio	$\frac{D_t}{D_p}$
x	Nozzle position ratio	$\frac{x}{D_p}$
r	Inlet curvature ratio	$\frac{r}{D_p}$

Fluid Variables

The fluid variables in the research are displayed in Figure 21 and defined in Table 8. They are converted to dimensionless terms, which are summarized in Table 9.

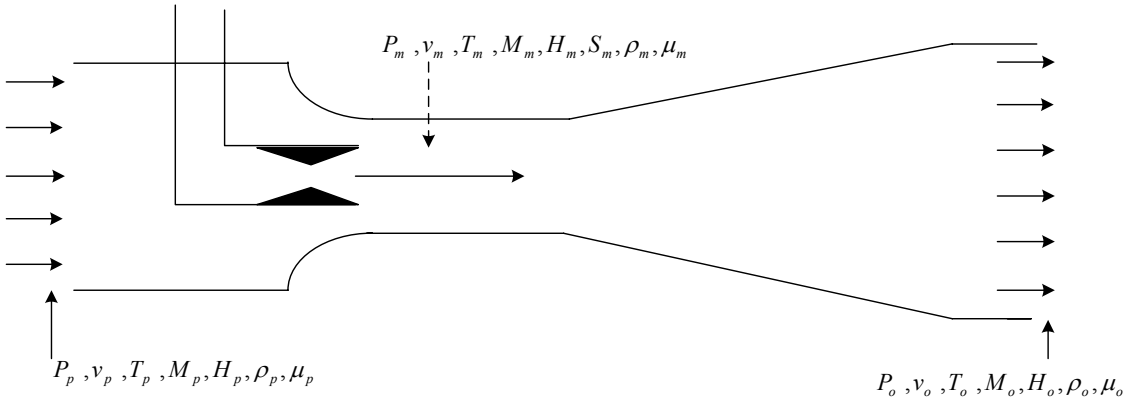

Figure 21. Flow variables in a jet ejector.

Table 8. Definition of fluid variables.

Parameter	Definition
P_p	Static pressure of the propelled stream
v_p	Fluid velocity of the propelled stream
T_p	Stagnation temperature of the propelled stream
M_p	Mass flow rate of the propelled stream
H_p	Enthalpy of the propelled stream
ρ_p	Density of the propelled stream
μ_p	Viscosity of the propelled stream
P_m	Static pressure of the motive stream
v_m	Fluid velocity of the motive stream
T_m	Stagnation temperature of the motive stream
M_m	Mass flow rate of the motive stream
H_m	Enthalpy of the motive stream
S_m	Entropy of the motive stream
ρ_m	Density of the motive stream
μ_m	Viscosity of the motive stream
P_o	Static pressure of the outlet stream
v_o	Fluid velocity of the outlet stream
T_o	Stagnation temperature of the outlet stream
M_o	Mass flow rate of the outlet stream
H_o	Enthalpy of the outlet stream
ρ_o	Density of the outlet stream
μ_o	Viscosity of the outlet stream

Table 9. Fluid variables in dimensionless formation.

Fluid Variables	Dimensionless Formation
Static pressure of inlet propelled stream, C_p	$\frac{P_o - P_p}{\frac{1}{2}\rho_p v_p^2}$
Static pressure of the motive stream at the nozzle outlet, C_{pm}	$\frac{P_o - P_m}{\frac{1}{2}\rho_p v_p^2}$
Velocity of inlet motive stream	$\frac{v_m}{\text{Speed of Sound}}$
Mass flow rate ratio	$\frac{M_m}{M_p}$
Reynolds ratio	$\left(\frac{\rho_m v_m D_n}{\mu_m}\right)\left(\frac{\mu_p}{\rho_p v_p D_p}\right)$

Many dimensionless groups (e.g., mass flow rate ratio, density ratio, velocity ratio, kinetic energy per volume ratio, Reynolds ratio, etc.) are verified in the analysis. Because the dimensionless pressure term of propelled (C_p) and motive (C_{pm}) streams are calculated based on the optimum design, the objective of this analysis is to identify which dimensionless groups provide the same C_p, and C_{pm} regardless of fluid type, geometric scale, and operating pressure. Reynolds number is primarily applied in the analysis because it is recognized as the standard dimensionless group of fluid flow in pipes. Two approaches are conducted to study the effect of the motive stream velocity, which are:

1. Maintaining Mach number of the motive stream and C_p constant
2. Maintaining the velocity magnitude of the motive stream and C_p constant

An optimum design of the jet ejector with 0.11 nozzle ratio is employed in the experiment. Initially, air and steam are used as two different fluid types. The geometric scale of the jet ejector is compared between 4× and 8× scale based on the dimension in Appendix F. Operating pressure is varied from 0.1 to 10.0 atm in the first-stage investigation, but intensively in the vacuum region. The specific conditions of each experimental method are summarized in Table 10.

Table 10. Experimental conditions of each approach.

Experimental Approach	Experimental Conditions	
1	The velocity of the motive stream maintained at Mach 1.1838	C_p value maintained constant at 31.99
2	The velocity magnitude of the motive stream maintained at 406.89 m/s	C_p value maintained constant at 31.99

With these three experimental methods, the best dimensionless groups are found. In the second stage, the most proper experimental method among three alternatives is selected for further investigation. Other different fluid types and geometric scales are applied in this investigation. The experiment condition is summarized in Table 11.

Table 11. Experimental conditions of the further investigation.

Experimental Set	Operating Pressure (atm)	Geometric Scale	Fluid Type
1	1.0	2×	Steam
2			Air
3			Hydrogen
4		4×	Carbon dioxide
5			Nitrogen

Because the operating pressure will be explored in the third-stage investigation, an atmospheric pressure is applied in the second-stage investigation. The second-stage investigation shows that the dimensionless groups are applicable to any fluid type, and geometric scale.

The operating pressure is fully investigated in the third-stage simulation. In this stage, steam and 2× scale with 0.11 nozzle-diameter ratio are applied as fluid, and geometric parameters, respectively. The motive-stream velocity is varied from Mach 0.78 to 1.98, which covers an optimization domain, but the propelled-stream velocity is maintained constant. As a consequence, C_p is changed from 4.30 to 101.12, which covers the optimization domain also. The operating pressure is ranged from 0.01 to 10.0 atm.

The procedure of the dimensionless group analysis is summarized in Figure 22.

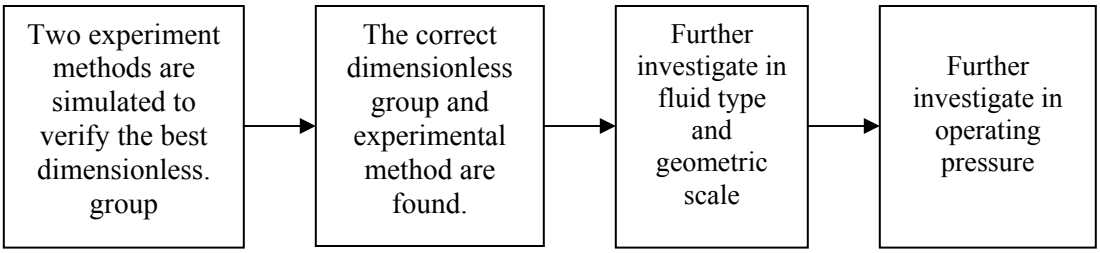

Figure 22. Procedure diagram of the dimensionless group analysis.

Jet Ejector Optimization

The main objective is to optimize the jet ejector geometry according to the particular nozzle diameter ratios and motive-stream velocities. The optimum parameters – which are the value of propelled mass flow rate ratio (M_m/M_p), length (L/D_p), and diameter ratio (D_t/D_p) of the throat section, nozzle position ratio (x/D_p), and radius ratio of inlet curvature of the convergence section (r/D_p) – are investigated in the research. The velocity of the motive stream in Mach number and the nozzle diameter ratio (D_n/D_p) are set as the independent parameters. The independent parameter domain included in the study that did not have divergence problems are illustrated in Table 12. The geometric parameters and flow variables are demonstrated in Figures 20 and 21, respectively.

Table 12. Study domain.

<table>
<tr><td rowspan="2">v_m
(Mach number)</td><td colspan="4">Nozzle diameter ratio (D_n/D_p)</td></tr>
<tr><td>0.3</td><td>0.6</td><td>0.11</td><td>0.23</td></tr>
<tr><td>0.39</td><td colspan="3" rowspan="5">Convergence Area</td><td rowspan="2"></td></tr>
<tr><td>0.79</td></tr>
<tr><td>1.18</td><td rowspan="3">Divergence Area</td></tr>
<tr><td>1.58</td></tr>
<tr><td>1.97</td></tr>
</table>

With the largest throat diameter ratio (0.23), the motive steam velocity is limited to Mach 0.79 because the CFD result is unstable when the velocity is beyond this point.

Optimization Procedure

The optimization procedure is demonstrated in Figure 23.

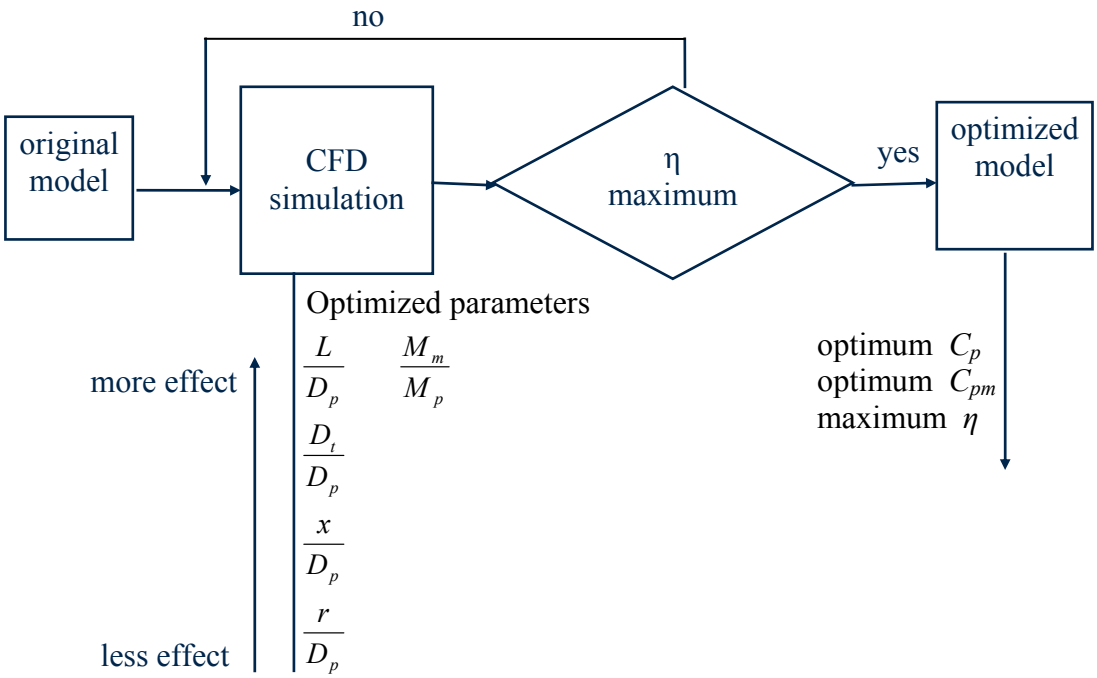

Figure 23. Optimization procedure.

The priority of optimized parameters is ranked by their effect on jet ejector performance. From Figure 23, the propelled mass flow rate and length ratio produce the greatest impact on jet ejector performance, whereas the radius inlet curvature of the convergence section does not produce much effect. The optimization procedure is described below:

1. From an original design in the High-Efficiency jet ejector disclosure of Holtzapple (see Appendix F; 2001), the optimized parameters are studied in ascending order of their effect (see Figure 23).
2. Fluid variables (e.g., pressure, velocity, density) are reported to calculate the jet ejector efficiency. The flow and geometric parameters are varied until the

optimal efficiency is obtained. The maximum efficiency is verified when there is no efficiency deviation from the previous round.

3. C_p and C_{pm} are calculated.

In the final step, all parameters (the optimized parameters, dimensionless pressure term of propelled and motive streams, and efficiency) are plotted as a function of nozzle diameter ratio and motive velocity by using curve-generating software (TableCurve 3D). The graph from TableCurve 3D shows the correlation among each parameter, nozzle diameter ratio, and motive velocity.

Multi-Stage Jet Ejector System

One of the objectives of the research is to analyze a multi-stage jet ejector system. The goal of analyzing the system is to exemplify how to implement the research results to solve a design problem. A system with 1.2 compression ratio is analyzed from information from the optimization study. The dimensionless pressure term of the propelled stream (C_p) and motive stream (C_{pm}), Reynolds ratio, and efficiency are used in the analysis. The flow arrangement of each jet ejector is illustrated in Figure 24. A sample section of the cascade diagram is presented in Figure 25. The outlet streams of lower-stage jet ejectors are used as the propelled streams of upper-stage jet ejectors. The outlet streams are pressurized by the upper-stage jet ejectors. They are injected as the motive streams of the lower-stage jet ejectors (see Figure 25). Because of this concept, an amount of the high-pressure stream consumption is reduced substantially. The calculation of fluid properties of each stream is explained in the following section.

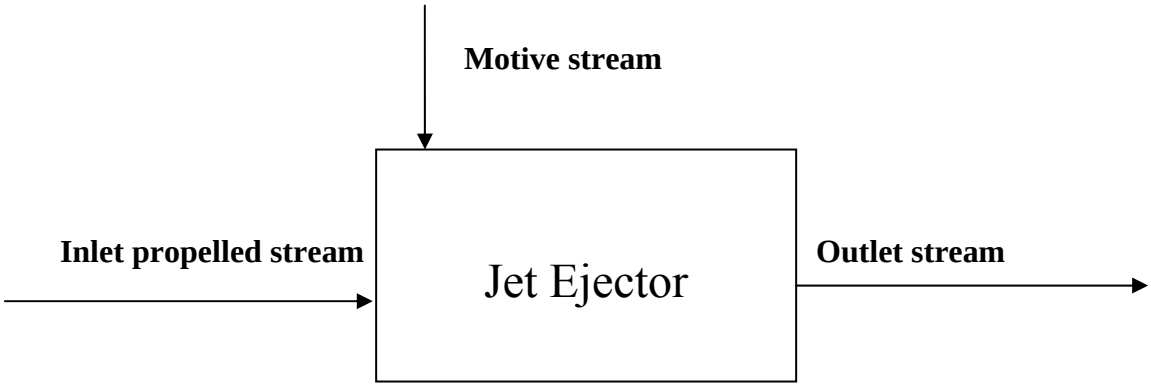

Figure 24. Flow composition in a single-stage jet ejector.

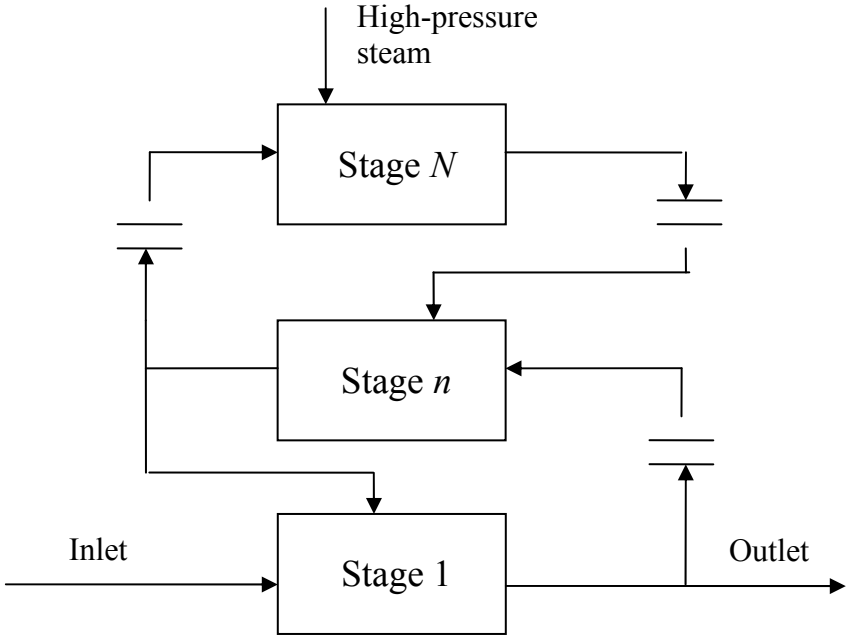

Figure 25. Sample set of a cascade diagram.

where,

n = intermediate stage

N = final stage

Stream Properties Evaluation

The calculation procedure evaluates the fluid properties of each stream in the jet ejector. Steam was used as the fluid. The fluid properties (pressure, temperature, density, inlet velocity, enthalpy, and entropy) are considered in the analysis. Because steam is applied in the system, a steam table (ALLPROPS) is used in the calculation. Fluid variables used in the calculation are displayed in Figure 21 and defined in Table 13.

Inlet Propelled Stream

The values of pressure, temperature, and density are obtained from the outlet stream of an earlier stage. For the first stage, the pressure of the inlet propelled stream is specified as saturated 1-atm, with temperature (373.15 K) and density (0.5975 kg/m^3) obtained from the steam table. The velocity of the inlet propelled stream, which is an optimum velocity for each particular design, is obtained from the research results.

Table 13. Definition of fluid variables used in the cascade design.

Steam	Fluid Variable	Definition
Propelled	P_p	Static pressure of the propelled stream
	v_p	Velocity of the propelled stream
	T_p	Temperature of the propelled stream
	ρ_p	Density of the propelled stream
Inlet Motive	$P_{m,in}$	Static pressure at the inlet of the motive stream
	$T_{m,in}$	Temperature at the inlet of the motive stream
	$v_{m,in}$	Velocity at the inlet of the motive stream
	$H_{m,in}$	Enthalpy at the inlet of the motive stream
	$S_{m,in}$	Entropy at the inlet of the motive stream
Outlet Motive	$P_{m,out}$	Static pressure at the outlet of the motive stream
	$T_{m,out}$	Temperature at the outlet of the motive stream
	$v_{m,out}$	Velocity at the outlet of the motive stream
	$H_{m,out}$	Enthalpy at the outlet of the motive stream
	$S_{m,out}$	Entropy at the outlet of the motive stream
Outlet	P_o	Static pressure of the outlet stream
	T_o	Temperature of the outlet stream
	ρ_o	Density of the outlet stream

Outlet Stream

The static pressure of the outlet stream is calculated from C_p, which is shown in Equation 1.

$$C_p = \frac{P_o - P_p}{\frac{1}{2}\rho_p v_p^2} \longrightarrow P_o = P_p + C_p\left(\frac{1}{2}\rho_p v_p^2\right) \qquad (1)$$

Temperature of the outlet stream is calculated by assuming isentropic compression, which is shown in Equation 2.

$$\frac{T_o}{T_p} = \left(\frac{P_o}{P_p}\right)^{\left(\frac{\gamma}{\gamma-1}\right)} \longrightarrow T_o = T_p\left(\frac{P_o}{P_p}\right)^{\left(\frac{\gamma}{\gamma-1}\right)} \quad (2)$$

where,

γ = ratio of heat capacity = 1.3 for steam

Once pressure and temperature are found, density can obtain from the steam table.

Motive-Stream Outlet

The pressure at the outlet of the motive stream is calculated from C_{pm}, which is shown in Equation 3:

$$C_{pm} = \frac{P_o - P_m}{\frac{1}{2}\rho_p v_p^2} \longrightarrow P_m = P_o - C_{pm}\left(\frac{1}{2}\rho_p v_p^2\right) \quad (3)$$

Temperature is calculated by assuming isentropic conditions, which is shown in Equation 4:

$$\frac{T_m}{T_o} = \left(\frac{P_m}{P_o}\right)^{\left(\frac{\gamma}{\gamma-1}\right)} \longrightarrow T_m = T_o\left(\frac{P_m}{P_o}\right)^{\left(\frac{\gamma}{\gamma-1}\right)} \quad (4)$$

Once pressure and temperature are specified, enthalpy and entropy can obtained from the steam table. The velocity at the outlet of the motive stream is a function of the compression ratio. The required velocity is obtained from the research results.

Motive-Stream Inlet

The entropy at the inlet of the motive stream equals the outlet of the motive stream because the nozzle is assumed to operate at isentropic conditions. Enthalpy can be calculated from the energy balance equation around the nozzle, which is shown in Equation 5 (Smith and Van Ness, 1975).

$$\frac{v_{m,in}^2 - v_{m,out}^{\ 2}}{2} = \eta\left(H_{m,in} - H_{m,out}\right) \tag{5}$$

where,

$v_{m,in}$ = velocity at the inlet of the motive stream $\left(\text{m/s}\right)$

$v_{m,out}$ = velocity at the outlet of the motive stream $\left(\text{m/s}\right)$

η = nozzle efficiency

$H_{m,in}$ = enthalpy at the inlet of the motive stream $\left(\text{J}\right)$

$H_{m,out}$ = enthalpy at the outlet of the motive stream $\left(\text{J}\right)$

To enhance the jet ejector efficiency, all velocities at the outlet of the motive stream in the cascade should be kept below Mach 1.0. CFD simulations show that in cases of subsonic motive velocity, the nozzle is 99% efficient (see the convergent nozzle study in Appendix E). The inlet velocity of the motive stream is specified at 24 m/s. By the inlet velocity of the motive stream, the convergent nozzle study indicates that the outlet velocity of the motive stream at Mach 1.0 is achievable by using a particular

nozzle geometry. Equation 5 gives rise to Equation 6 to calculate the enthalpy of the inlet of the motive stream ($H_{m,in}$) which is:

$$H_{m,in} = H_{m,out} + \frac{v_{m,in}^2 - v_{m,out}^2}{2 \cdot \eta} \tag{6}$$

Once the enthalpy and entropy are specified, pressure and temperature are obtained from the steam table.

Splitting an Outlet Stream

To minimize the amount of high-pressure steam used in the system, the outlet stream is separated into two parts (see Figure 25). The first part is used as the inlet propelled stream for the next stage. The second part is used as the motive stream for the lower stage. The major consideration of the stream separation is pressure. The static pressure of the outlet stream must be greater than the static pressure at the inlet of the motive stream of the lower stage; otherwise, the pressure from the outlet stream is insufficient to produce the velocity of the motive stream at the nozzle exit.

Material Balance

This section shows how to produce the material balance equations for the system. All situations, which are confronted in the system, are presented in the following section. All symbols used in the presentation are summarized in Figure 26.

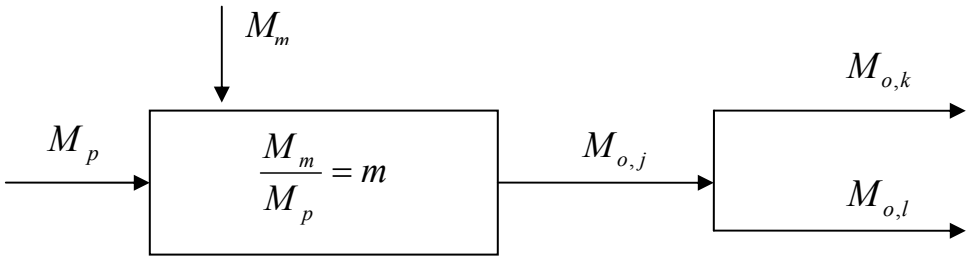

Figure 26. A flow diagram of single stage jet-ejector.

where,

m = optimum mass flow rate ratio

M_p = mass flow rate of the propelled stream (kg/s)

M_m = mass flow rate of the motive stream (kg/s)

$M_{o,j}$ = mass flow rate of the outlet stream before splitting (kg/s)

$M_{o,k}$ = mass flow rate of the outlet stream fed as the propelled stream of the next stage (kg/s)

$M_{o,l}$ = mass flow rate of the outlet stream fed as the motive stream of the lower stage (kg/s)

1. Optimum mass flow rate ratio

Based on the optimization study, the optimal mass flow rate ratio is recommended for each jet ejector configuration to achieve the maximum efficiency. The material balance equation of each jet ejector is

$$m = \frac{M_m}{M_p} \tag{7}$$

2. Balance around the jet ejector.

The outlet stream is the sum of the propelled and motive streams, so the material balance equation is

$$M_{o,j} - M_p - M_m = 0 \tag{8}$$

3. Outlet stream

Typically, the outlet stream divides into two parts. The first part is fed as the propelled stream of the next stage. The second part is fed as the motive stream of the lower stage or as the outlet stream of the system. If it is fed as the motive stream of the lower stage, the pressure between both stages must be consistent. The material balance equation due to this condition is

$$M_{o,j} - M_{o,k} - M_{o,l} = 0 \tag{9}$$

4. Mass flow rate of the motive stream of the most upper stage

To complete the material balance equations, the mass flow rate of the motive stream of the most upper stage is set to 1.0 kg/s as an initial condition.

Following the above instructions, the mass flow rate of every stream in the system will be verified.

RESULTS AND DISCUSSION

Model Development

A good model will provide a high-accuracy result and consumes the least computational resource. The model accuracy is verified in the next section. All the created models are displayed in Figure 27. The jet-ejector dimensions in the model are exactly the same as in the experimental apparatus (as shown in Appendix F).

The first model is displayed in Figure 27A. The pinch valve at the downstream pipe is used to adjust back pressure. The dash line in the model is the point for measuring the fluid properties of the inlet and outlet stream of the jet ejector. The boundary specification is summarized in Table 14.

Table 14. Boundary condition specification of the first model.

Position	Applied Boundary Condition	
	Case 1	Case 2
Propelled-stream boundary condition	Mass flow rate	Total pressure
Motive-stream boundary condition	Mass flow rate	Mass flow rate
Outlet-stream boundary condition	Total pressure	Total pressure

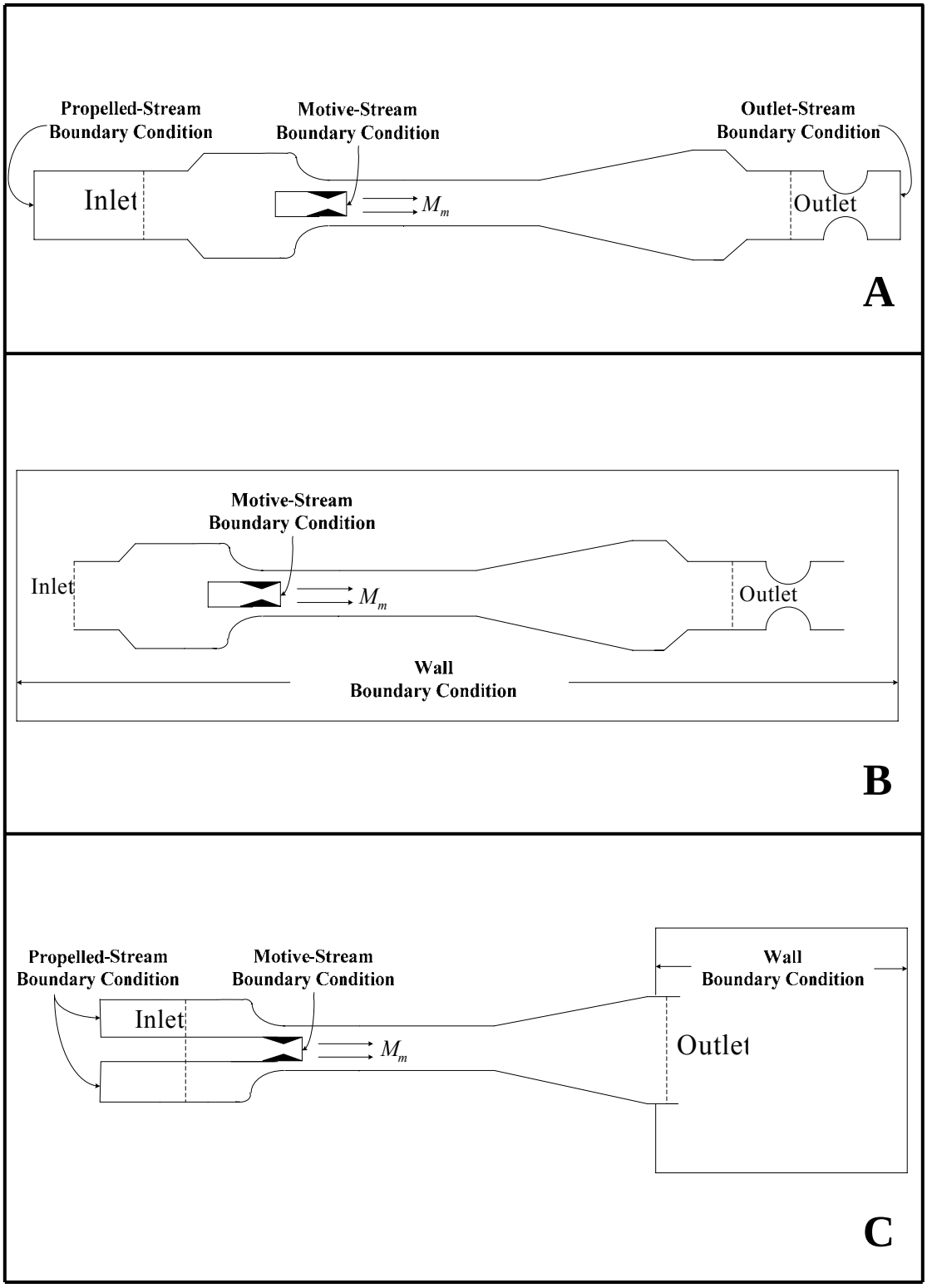

Figure 27. Various stages of model development. A) the first model, B) the second model, C) the final model.

In the first model, the back pressure is controlled by a pinch valve, so an additional parameter must be employed in the study, which makes the problem more complicated. Furthermore, the simulation result in the first boundary condition case was unstable due to over-specification. For the second boundary condition, the model prediction was significantly different from the experimental result; the deviation was about 20%. For these reasons, the first model is rejected.

The second model is displayed in Figure 27B. Instead of specifying the boundary conditions at the propelled and outlet streams, the jet ejector is located in a big space. The pressure in the space is maintained constant at 101.3 kPa. The motive-stream velocity is defined at the nozzle exit. Because it consumes a lot of computational time and memory space due to the big space, and the additional parameter for adjusting the pinch valve still remains, this model was impractical and inconvenient to implement.

The final model is displayed in Figure 27C. The big space is placed at the jet ejector outlet only instead of the entire domain. The computational time was reduced by 60% from the second model. Additionally, no pinch valve was required in the model, thus eliminating the need for an adjustable parameter that simulates the valve. The motive-stream velocity is specified at the nozzle exit. For the propelled-stream boundary condition, both the mass flow rate and total pressure boundary condition are examined, the result is presented in the next section. The pressure in the big space is maintained constant at 101.3 kPa. The total pressure boundary condition is specified for the wall boundary condition. This model consumes the least computational time plus it did not require a pinch valve; therefore, this model was selected for the research.

CFD Modeling Reliability

Model Accuracy

The model accuracy is verified by comparing the simulation and experimental results with various motive velocities. The jet ejector geometry in the model is exactly the same as in the experiment. The experimental results were obtained from Manohar Vishwanathappa, a graduate chemical engineering student at Texas A&M University. Figure 28 demonstrates how accurately the CFD model predicted the static pressure difference obtained from experiments with various motive velocities. The simulation results are obtained directly from first principles; no adjustable parameters were used.

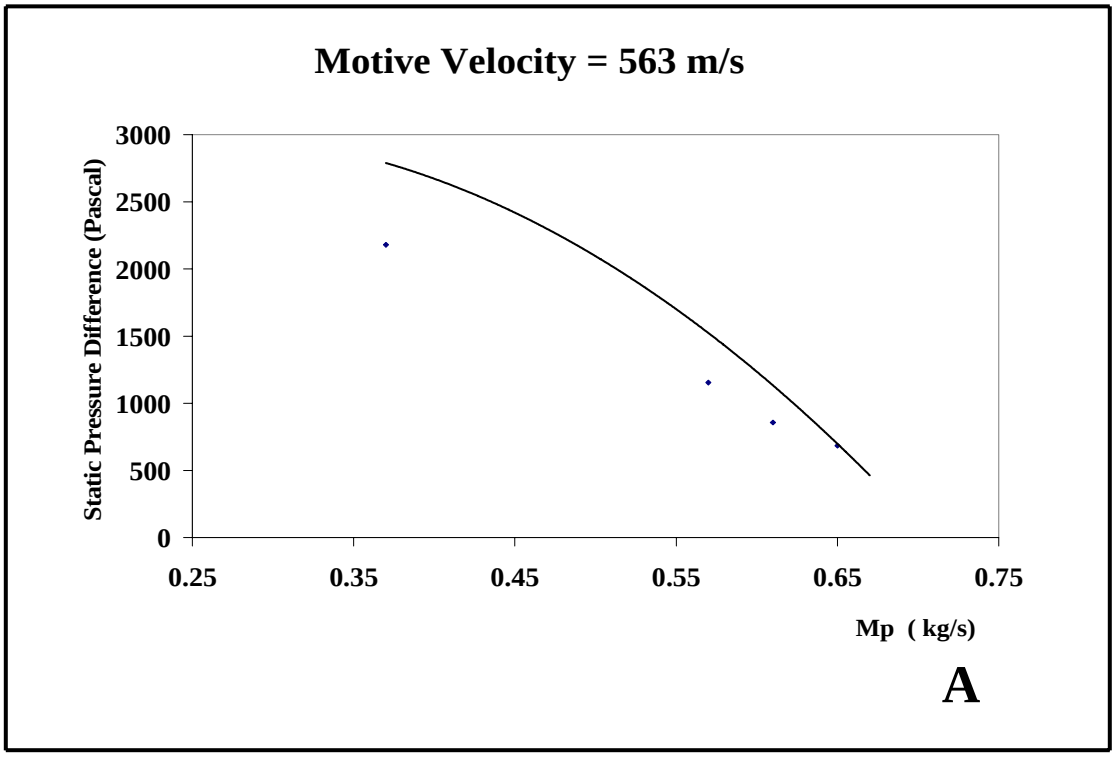

Figure 28. Simulation result comparing the experiment result with various motive velocities.

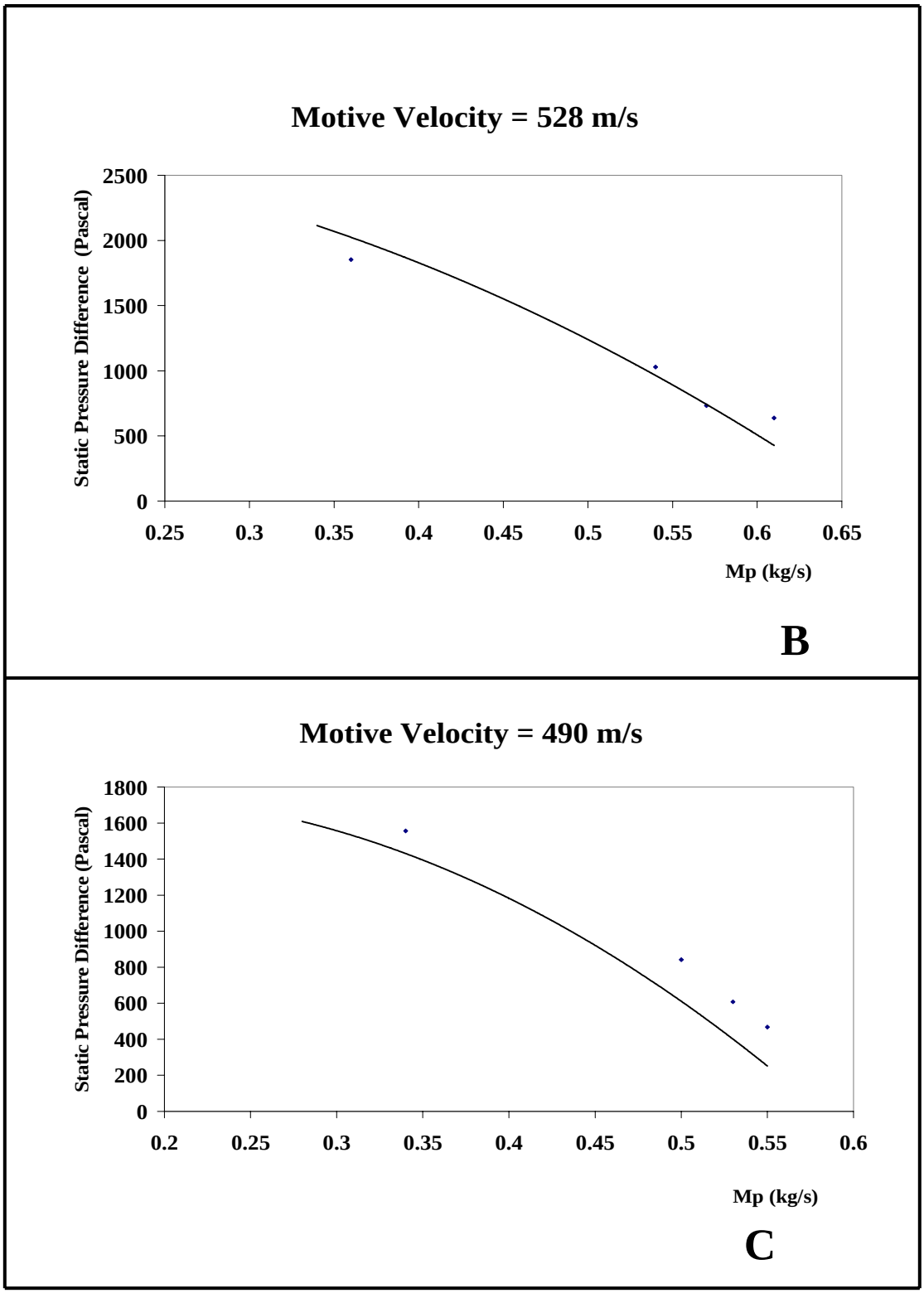

Figure 28. (Continued).

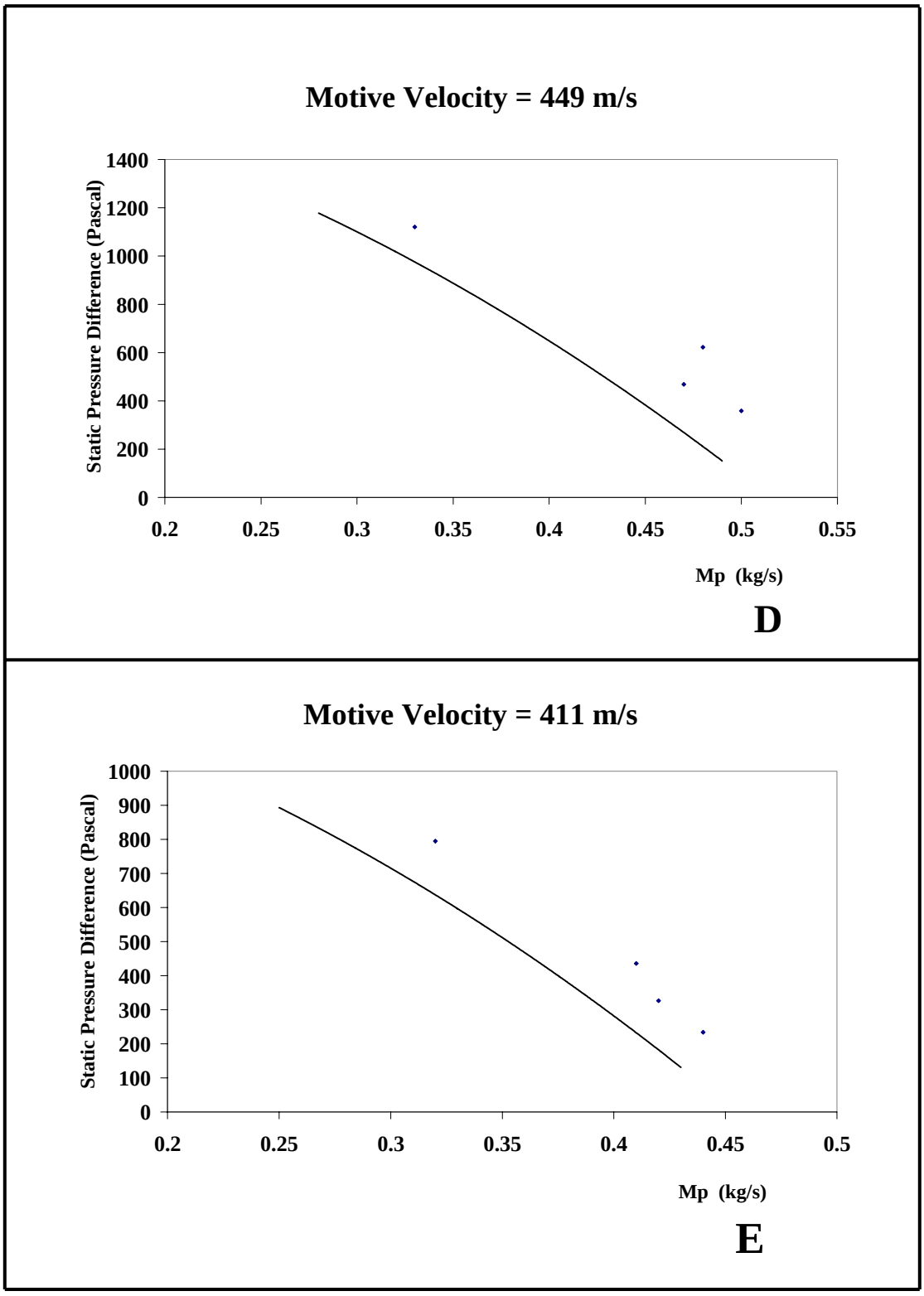

Figure 28. (Continued).

The simulation results lie approximately on the experiment results in every case. The average overall deviation between the simulations and experiments is 8.19%, thus confirming the model accuracy in simulating fluid flow.

Discretation

The grid size and number of iterations are examined in this experiment. The smaller the grid size; the more accuracy is obtained. However, the very fine grid-size model consumes excessive computational resources as a consequence. Also, more iterations provide more accuracy, but require greater computational time and memory. Because efficiency is used to determine the optimum condition, it is used to determine the proper grid size and number of iteration. The results with a variety number of iterations of coarser and finer grid-size models are demonstrated in Tables 15 and 16, respectively.

Table 15. Simulation result of the coarser grid-size model.

Number of iterations	Pressure (Pa)			Efficiency	Computational Time consumed (h)
	Motive	Propelled	Outlet		
2,500	97,842.3	98,124.1	101,325.5	0.9769	2
4,500	97,784.8	98,031.5	101,324.9	0.9783	3
6,000	97,784.7	98,031.5	101,325	0.9783	4

Table 16. Simulation result of the finer grid-size model.

Number of iterations	Pressure (Pa)			Efficiency	Computational Time consumed (h)
	Motive	Propelled	Outlet		
2,500	97,792.5	98,061.1	101,325.3	0.9782	5
4,500	97,764.3	98,008.0	101,327.1	0.9786	7
6,000	97,762.1	98003.4	101,327.2	0.9786	10

Regardless of computational time consumed, the efficiency of every case is almost the same at 97%. The pressure difference among the cases is less than 130 Pa, which is very small compared to the outlet pressure of 101,325 Pa. The computational time presented in the last column deviates so much among the cases due to the effect of grid size and number of iterations. The coarser grid-size at 2,500 iterations consumes five times less computational resource than the finer grid-size at 6,000 iterations, whereas the deviation in efficiency is only 0.0017. So, the coarser grid-size at 2,500 iterations is applied in the optimization study.

Model Boundary Condition

The propelled-stream boundary condition is examined in this experiment. There are two available boundary conditions (mass flow rate and total pressure). The largest nozzle diameter ratio and motive-stream velocity at Mach 0.79 model is applied in the experiment. The results of the experiment are displayed in Figure 29.

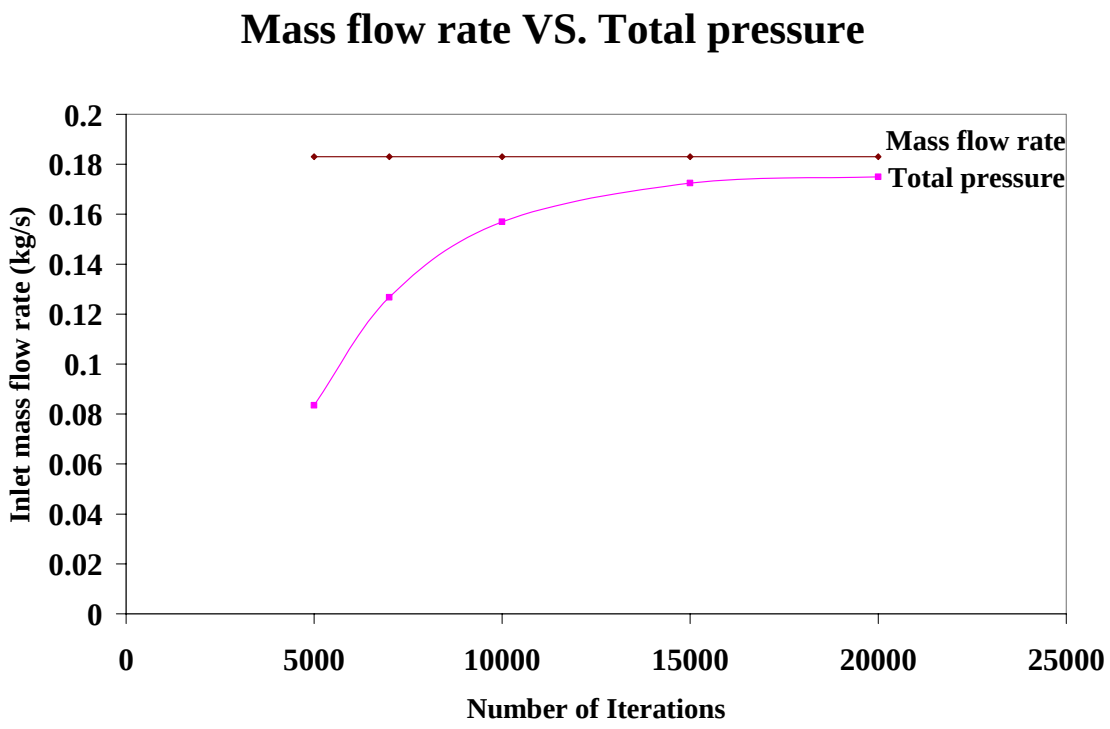

Figure 29. Simulation results of both kinds of boundary condition.

From Figure 29, both boundary conditions provide the same results, but require different numbers of iterations. The total pressure boundary condition requires more than 20,000 iterations to provide a converged solution. To provide a good result, the mass flow rate boundary condition requires only 2,500 iterations, as shown in the previous experiment. Consequently, the computational resources used with the mass flow rate boundary condition are much less than the total pressure boundary condition. Thus, the mass flow rate boundary condition is applied in the research.

Dimensionless Group Analysis

By working closely with Ganesh Mohan, a graduate mechanical engineering student at Texas A&M University, the effect of fluid, geometric scale, and operating pressure on the jet ejector performance was investigated. Steam, air, hydrogen, carbon dioxide, and nitrogen were employed in the dimensionless analysis.

In the first-stage investigation, operating pressure was varied from 0.1 to 10.0 atm. Two different geometric scales (4×, and 8×) were compared in the analysis.

In this stage, the effect of the motive stream velocity was investigated by using two different approaches, which are

3. Maintain the Mach number of the motive stream and C_p value
4. Maintain the velocity magnitude of the motive stream and C_p value

The result of these methods is presented in Tables 17 and 18, respectively. Reynolds number is applied primarily because the Reynolds number is considered as the standard dimensionless group of fluid flow in pipe. C_p value is maintained constant at 31.99 in both cases.

Table 17. Result of maintaining constant Mach number of motive stream (1.184) and C_p (31.99).

Operating Pressure (atm)	Efficiency				C_{pm}				Reynolds Ratio			
	Steam		Air		Steam		Air		Steam		Air	
	4×	8×	4×	8×	4×	8×	4×	8×	4×	8×	4×	8×
0.1	0.902	0.902	0.929	0.929	2.13	2.13	2.13	2.13	3.00	2.98	3.04	3.01
0.2	0.903	0.903	0.932	0.932	2.16	2.16	2.16	2.16	2.98	2.95	3.01	2.99
0.3	0.904	0.904	0.933	0.933	2.17	2.17	2.17	2.17	2.96	2.94	3.00	2.98
0.5	0.905	0.905	0.934	0.934	2.19	2.19	2.19	2.19	2.95	2.93	2.98	2.97
0.6	0.905	0.905	0.935	0.935	2.19	2.19	2.19	2.19	2.94	2.93	2.98	2.96
1.0	0.907	0.907	0.936	0.936	2.21	2.21	2.21	2.21	2.93	2.92	2.96	2.95
3.0	0.907	0.907	0.938	0.938	2.21	2.22	2.22	2.22	2.91	2.91	2.94	2.93
6.0	0.907	0.907	0.938	0.938	2.22	2.22	2.22	2.22	2.91	2.91	2.93	2.94
8.0	0.908	0.907	0.939	0.938	2.22	2.22	2.22	2.22	2.91	2.91	2.93	2.94
10.0	0.908	0.907	0.938	0.938	2.22	2.22	2.22	2.22	2.90	2.90	2.92	2.93

To visualize the result, the jet ejector efficiency, C_{pm}, and Reynolds ratio are plotted as a function operating pressure as shown in Figures 30A-C, respectively.

A. Jet ejector efficiency and operating pressure

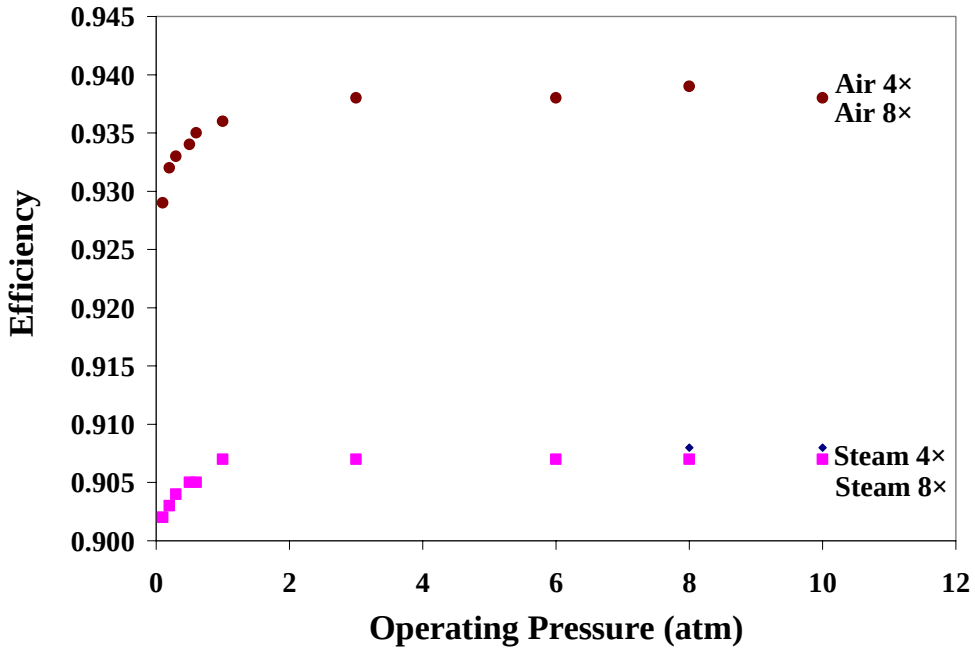

B. C_{pm} and operating pressure

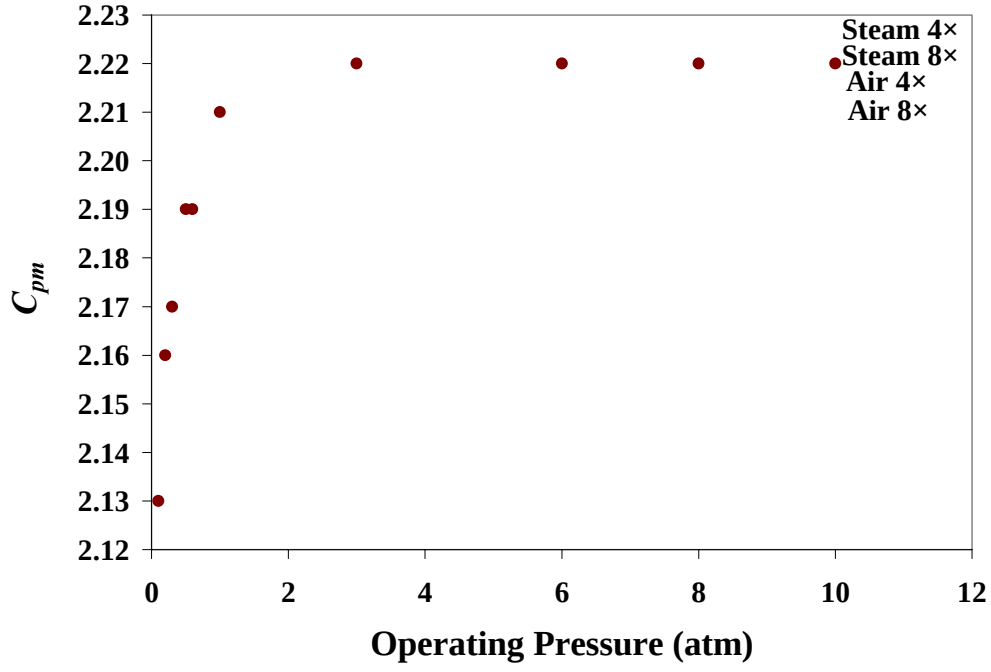

Figure 30. Value of jet ejector efficiency, C_{pm}, and Reynolds ratio of maintaining constant Mach number of the motive stream (1.184) and C_p (31.99).

C. Reynolds ratio and operating pressure

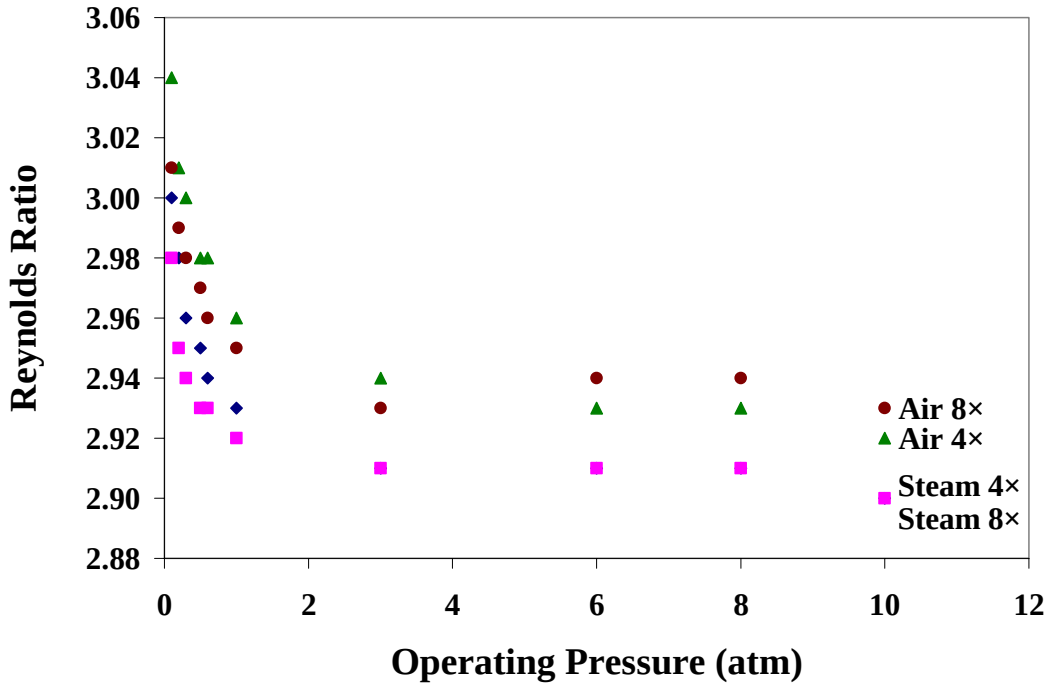

Figure 30. (Continued).

In the first approach (maintaining constant C_p and Mach number of the motive streams), the jet ejector efficiency is significantly different between fluid types (steam and air). Further, the efficiency of each fluid type decreases when operating pressure decreases. However, efficiency is not affected by geometric scale. C_{pm} decreases at low operating pressures, but it is independent of fluid type and geometric scale. Reynolds ratio increases at low operating pressures. The Reynolds ratio difference between steam and air is only 0.03 due to numerical error from simulation. The Reynolds ratio does not depend much on geometric scale.

Table 18. Result of maintaining constant motive-stream velocity (407 m/s) and C_p (31.99).

Operating Pressure (atm)	Efficiency				C_{pm}				Reynolds Ratio			
	Steam		Air		Steam		Air		Steam		Air	
	4×	8×	4×	8×	4×	8×	4×	8×	4×	8×	4×	8×
0.1	0.944	0.945	0.929	0.929	42.4	42.8	2.13	2.13	2.63	2.62	3.04	3.01
0.2	0.945	0.947	0.932	0.932	42.8	43.0	2.16	2.16	2.62	2.59	3.01	2.99
0.3	0.945	0.947	0.933	0.933	42.9	43.1	2.17	2.17	2.60	2.59	3.00	2.98
0.6	0.946	0.948	0.935	0.935	43.0	43.2	2.19	2.19	2.59	2.57	2.98	2.96
1.0	0.947	0.948	0.936	0.936	43.2	43.3	2.21	2.21	2.58	2.56	2.96	2.95
3.0	0.949	0.949	0.938	0.938	43.4	43.4	2.22	2.22	2.55	2.56	2.94	2.93
6.0	0.949	0.949	0.938	0.938	43.5	43.4	2.22	2.22	2.54	2.55	2.93	2.94
10.0	0.949	0.949	0.938	0.938	43.6	43.6	2.22	2.22	2.54	2.55	2.91	2.93

At constant motive-stream velocity, the value of jet ejector efficiency, C_{pm}, and Reynolds ratio are shown as a function of operating pressure in Figures 31A-C.

A. Jet ejector efficiency and operating pressure

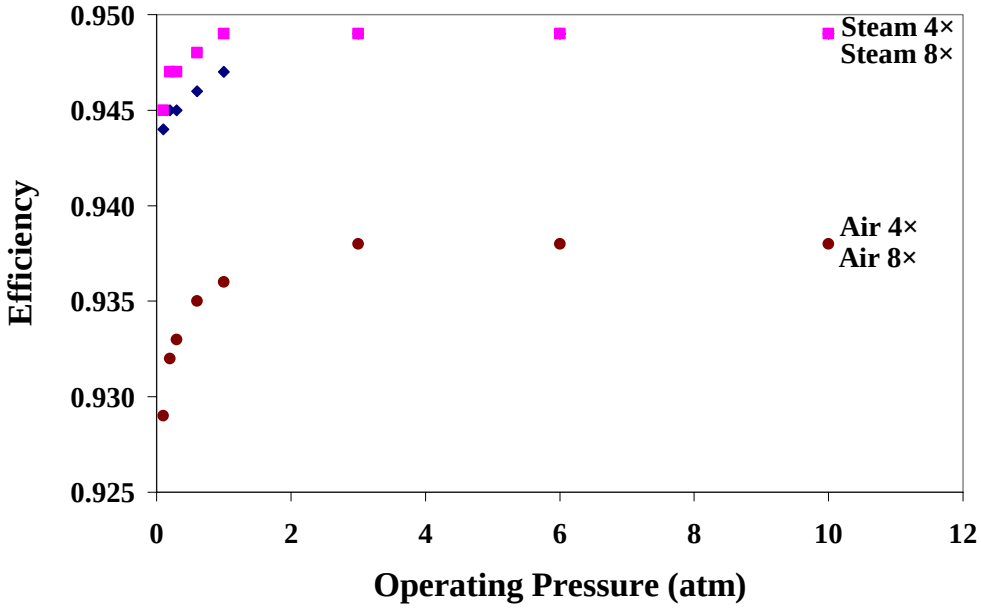

B. C_{pm} and operating pressure

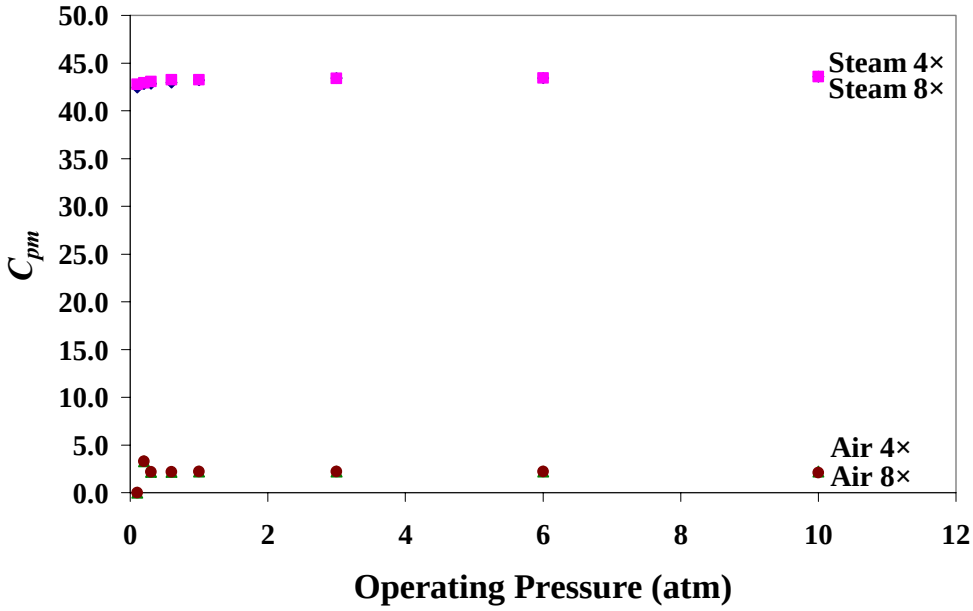

Figure 31. Value of jet ejector efficiency, C_{pm}, and Reynolds ratio of maintaining constant motive-stream velocity (407 m/s) and C_p (31.99).

C. Reynolds ratio and operating pressure

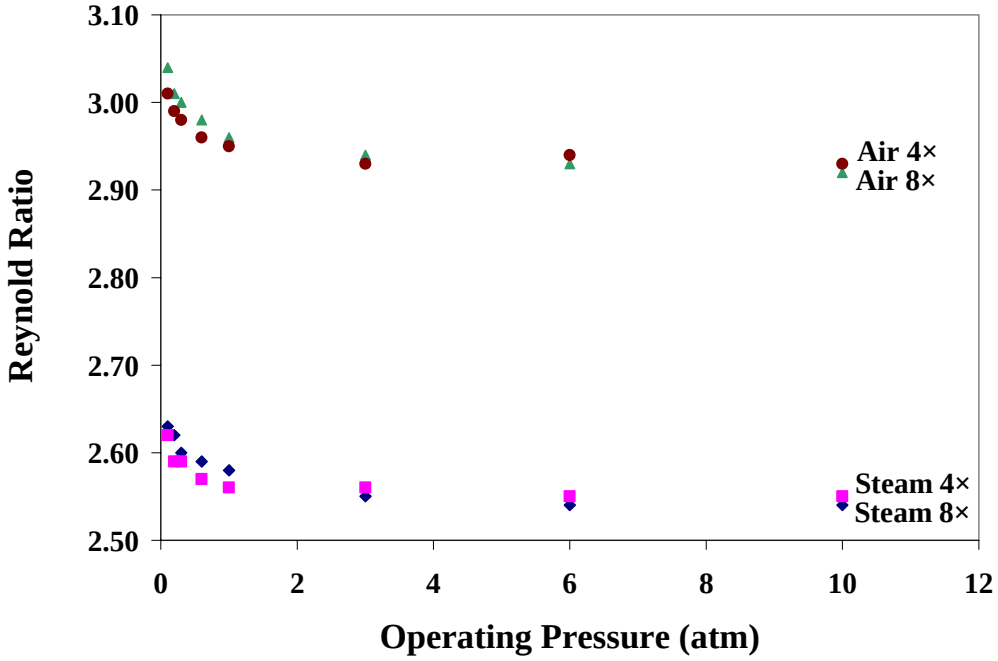

Figure 31. (Continued).

In the case of maintaining constant motive-stream velocity, the jet ejector efficiency between stream and air is not the same, but the differences are less than the constant Mach number condition. For a constant motive-stream velocity, the C_{pm} and Reynolds ratio between steam and air are significantly different. Comparing the two approaches, the motive-stream Mach number should be selected as the proper dimensionless condition, rather than the velocity magnitude. When the motive-stream Mach number and Reynolds ratio are constant, C_p and C_{pm} can be predicted regardless as fluid type, geometric scale, and operating pressure (almost). The jet ejector efficiency is calculated from the newly defined efficiency equation (see Appendix A).

Next, the dimensionless group analysis is further investigated on fluid type and geometric scale. Hydrogen, nitrogen, and carbon dioxide are employed as additional fluid types, and 2× scale is employed as an additional geometric scale. The motive-stream Mach number (1.184) and C_p (31.99) are the same as the earlier experiment. The results are summarized in Table 19.

Table 19. Result of further investigation (motive-stream Mach number = 1.184, C_p = 31.99).

Independent Parameters			Dependent Parameters		
Operating Pressure (atm)	Geometric Scale	Fluid Type	Efficiency	C_{pm}	Reynolds Ratio
1.0	2×	steam	0.904	2.21	2.95
		air	0.933	2.21	2.98
		hydrogen	0.847	2.22	2.96
	4×	nitrogen	0.931	2.22	2.97
		carbon dioxide	0.985	2.22	2.98

The result shows that C_{pm} and Reynolds ratio are almost similar in this investigation.

By maintaining constant motive-stream Mach number and Reynolds ratio, this confirms that C_p and C_{pm} from the research results are applicable to any kind of fluid, geometric scale, and operating pressure (almost). From Table 19, it is clear that the jet ejector efficiency increases when molecular weight increases.

From the result of the first stage analysis, C_{pm} and Reynolds ratio are not constant along a wide range of the operating pressure. C_{pm} decreases when operating pressure decreases, whereas Reynolds ratio increases when operating pressure decreases. Therefore, an investigation of the effect of operating pressure on C_{pm} and Reynolds ratio is necessary. In this investigation, the velocity of the motive stream varies from Mach 0.75 to 1.98 and C_p varies from 4.30 to 101.12, which covers the domain of the optimization results. The results of this investigation including the deviation of C_{pm} and Reynolds ratio are present in Table 20. The C_{pm} and Reynolds ratio deviations are calculated by the following equations:

$$\left(C_{pm}\right)_{deviate} = \frac{\left(C_{pm}\right)_{opt} - \left(C_{pm}\right)_{ref}}{\left(C_{pm}\right)_{ref}} \tag{1}$$

$$\left(\mathrm{Re}\right)_{deviate} = \frac{\left(\mathrm{Re}\right)_{opt} - \left(\mathrm{Re}\right)_{ref}}{\left(\mathrm{Re}\right)_{ref}} \tag{2}$$

where

$\left(C_{pm}\right)_{deviate}$ = the deviation of C_{pm}

$\left(C_{pm}\right)_{opt}$ = C_{pm} value of each particular operating pressure

$\left(C_{pm}\right)_{ref}$ = C_{pm} value of the operating pressure at 1 atm

$\left(\mathrm{Re}\right)_{deviate}$ = the deviation of Reynolds ratio

$\left(\mathrm{Re}\right)_{opt}$ = Reynolds ratio of each particular operating pressure

$\left(\mathrm{Re}\right)_{ref}$ = Reynolds ratio of the operating pressure at 1 atm

Table 20. C_{pm} and Reynolds ratio of the operating pressure investigation. A) C_p = 4.30 and Mach 0.747, B) C_p = 31.99 and Mach 1.184, C) C_p = 51.38 and Mach 1.431, D) C_p = 72.13 and Mach 1.168, E) C_p = 101.12 and Mach 1.981.

A) C_p = 4.30 and Mach 0.747

Operating Pressure (atm)	C_{pm}	Reynolds ratio	Deviation	
			C_{pm}	Reynolds ratio
0.01	28.79	2.07	-0.14	0.44
0.03	30.28	1.72	-0.09	0.19
0.06	31.07	1.65	-0.07	0.15
0.10	31.80	1.62	-0.05	0.13
0.30	32.64	1.57	-0.02	0.09
0.60	33.13	1.56	-0.01	0.08
1.00	33.33	1.44	0.00	0.00
3.00	33.43	1.45	0.00	0.00
6.00	33.50	1.45	0.00	0.01
10.00	33.73	1.44	0.01	0.00

Table 20. (Continued).

B) C_p = 31.99 and Mach 1.184

Operating Pressure (atm)	C_{pm}	Reynolds ratio	Deviation	
			C_{pm}	Reynolds ratio
0.01	1.79	3.28	-0.19	0.12
0.03	2.04	3.07	-0.08	0.05
0.06	2.08	3.03	-0.06	0.03
0.10	2.13	3.00	-0.04	0.02
0.20	2.16	2.98	-0.02	0.02
0.30	2.17	2.96	-0.02	0.01
0.50	2.19	2.95	-0.01	0.01
0.60	2.19	2.94	-0.01	0.00
1.00	2.21	2.93	0.00	0.00
3.00	2.21	2.91	0.00	-0.01
6.00	2.22	2.91	0.01	-0.01
8.00	2.22	2.91	0.01	-0.01
10.00	2.22	2.90	0.01	-0.01

Table 20. (Continued).

C) C_p = 51.28 and Mach 1.431

Operating Pressure (atm)	C_{pm}	Reynolds ratio	Deviation	
			C_{pm}	Reynolds ratio
0.01	0.62	4.33	-0.26	0.08
0.03	0.75	4.15	-0.09	0.03
0.06	0.77	4.09	-0.08	0.02
0.10	0.78	4.07	-0.06	0.01
0.30	0.81	4.04	-0.03	0.01
0.60	0.82	4.01	-0.01	0.00
1.0	0.83	4.01	0.00	0.00
3.0	0.86	4.02	0.03	0.00
6.0	0.86	4.02	0.04	0.00
8.0	0.86	4.02	0.03	0.00
10.0	0.86	4.02	0.04	0.00

Table 20. (Continued).

D) C_p = 72.13 and Mach 1.168

Operating Pressure (atm)	C_{pm}	Reynolds ratio	Deviation	
			C_{pm}	Reynolds ratio
0.01	0.34	5.69	-0.21	0.07
0.03	0.41	5.50	-0.10	0.03
0.06	0.40	5.44	-0.11	0.02
0.10	0.41	5.42	-0.09	0.02
0.30	0.43	5.39	-0.05	0.01
0.60	0.44	5.37	-0.02	0.01
1.00	0.45	5.33	0.00	0.00
3.00	0.46	5.32	0.02	0.00
6.00	0.46	5.31	0.01	0.00
10.00	0.46	5.30	0.01	-0.01

Table 20. (Continued).

E) C_p = 101.12 and Mach 1.981

Operating Pressure (atm)	C_{pm}	Reynolds ratio	Deviation	
			C_{pm}	Reynolds ratio
0.01	0.32	8.02	-0.16	0.04
0.03	0.35	7.83	-0.08	0.02
0.06	0.36	7.78	-0.06	0.01
0.10	0.36	7.76	-0.05	0.01
0.30	0.37	7.74	-0.03	0.00
0.60	0.38	7.70	-0.01	0.00
1.00	0.38	7.70	0.00	0.00
3.00	0.39	7.71	0.02	0.00
6.00	0.39	7.71	0.02	0.00
10.00	0.39	7.71	0.02	0.00

From the above study, the reference Reynolds ratio varies from 1.44 to 7.70. The deviation of C_{pm} and Reynolds ratio are plotted in 3-D curve surface diagram by TableCurve 3-D software as a function of operating pressure and reference Reynolds ratio. These graphs are applied corporately with the results of the optimization study when the operating pressure is outside 1atm. The deviation C_{pm} and Reynolds ratio are presented in Figures 32 and 33, respectively.

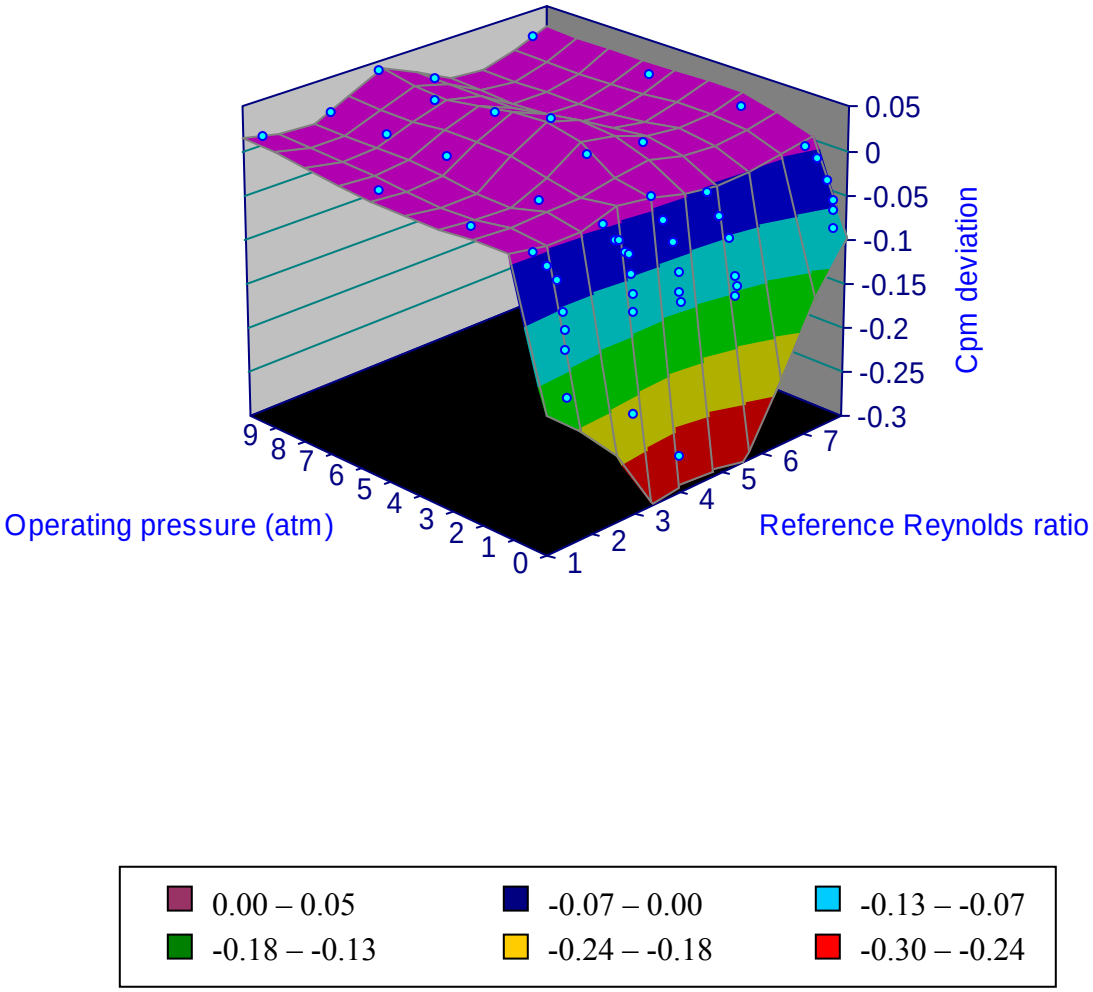

Figure 32. 3-D compilation of C_{pm} deviation.

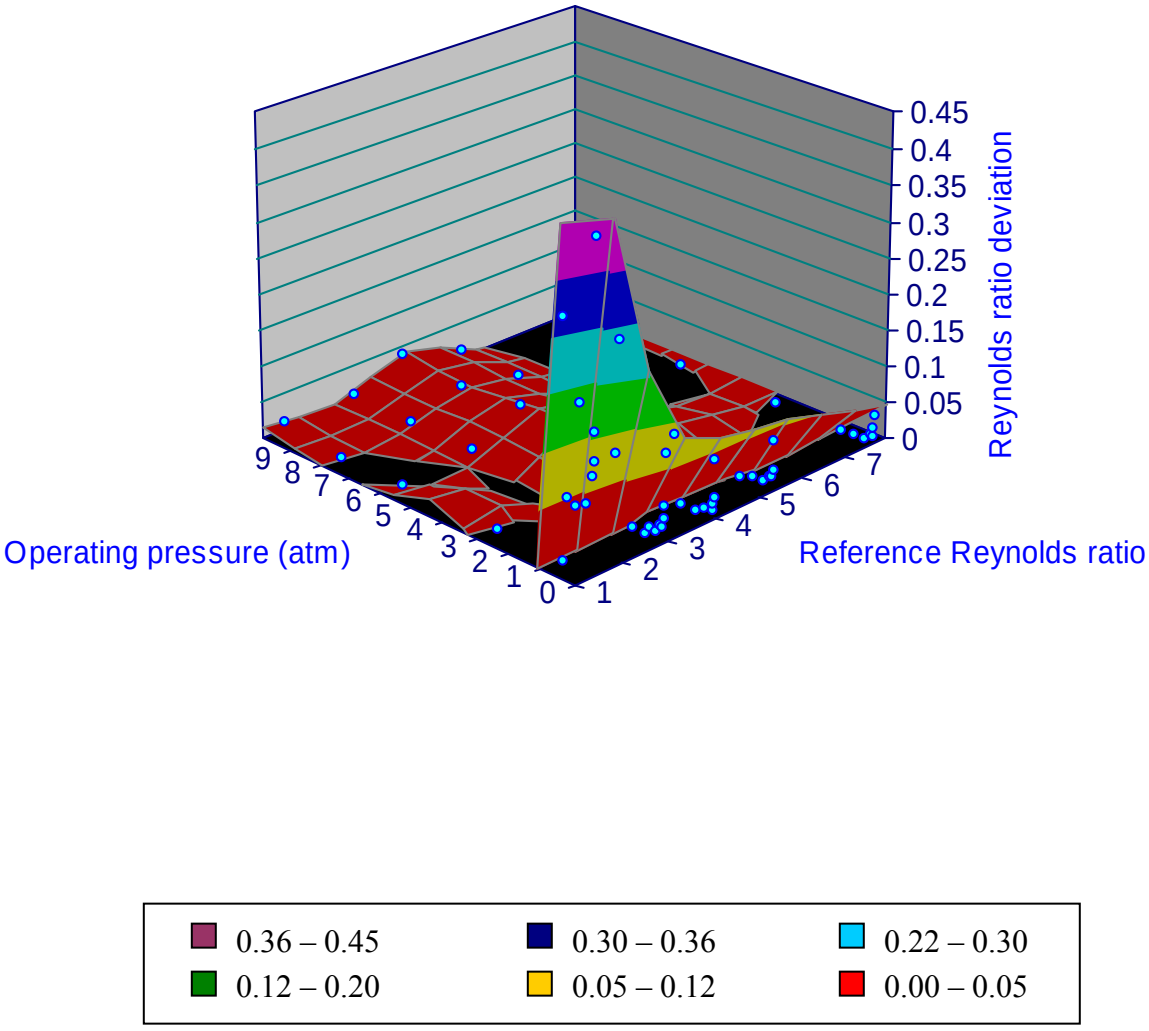

Figure 33. 3-D compilation of Reynolds ratio deviation.

Jet-Ejector Optimization

In the optimization study, the optimum propelled mass, length, and diameter of the throat section, nozzle position, and radius of inlet curvature are investigated over a wide range of motive velocity and nozzle diameters. For this dimensionless group analysis, all dimensions are expressed relative to the inlet diameter and the motive velocity is expressed relative to the speed of sound. The research results are summarized in Table 21, and results are categorized into four different groups, which are

1. The independent parameter group
2. The geometric parameter group
3. The flow parameter group
4. The design parameter group

The independent parameter group consists of the nozzle diameter and motive-stream Mach number. For design purposes, these parameters must be decided initially and are completely independent.

The geometric parameter group consists of the optimum length and diameter of the throat section, the optimum nozzle position, and the optimum radius of inlet curvature. The values in this column were obtained from the optimization study by adjusting the jet ejector geometry until the optimum condition was found. To achieve maximum performance, the jet ejector geometry must follow the information in this group. Therefore, the length and diameter of the throat section, and the nozzle position are located. From the optimization study, the radius of inlet curvature does not affect the jet ejector performance very much. To simplify the problem, the optimum radius of inlet curvature may be ignored.

The design parameter group consists of the optimum mass flow rate ratio based on atmospheric pressure and Reynolds ratio. To achieve maximum efficiency, the mass flow rate and Reynolds ratio of the motive and propelled stream must agree with the information in this group. If a jet ejector is operated with a different fluid type, geometric scale, and operating pressure, C_p and C_{pm} still hold, which was proven in the dimensionless analysis section. For fluids other than steam, the jet ejector efficiency is calculated from the newly defined efficiency equation (Appendix A) when the density, mass flow rate, pressure, velocity, and temperature of the propelled, motive, and outlet streams are known.

.

Table 21. Optimization result (steam, P_o = 1.0 atm).

Independent Parameter		Geometric Parameter				Design Parameter		Flow Parameter		
Nozzle diameter ratio	Mach number	$\frac{L}{D_p}$	$\frac{D_t}{D_p}$	$\frac{x}{D_p}$	$\frac{r}{D_p}$	$\frac{M_m}{M_p}$	Reynolds Ratio	C_p	C_{pm}	$\eta*$
0.03	0.39	1.80	0.38	0.05	0.12	0.0415	5.62	12.84	-25.11	0.997
	0.79	2.40	0.42	0.00	0.10	0.0399	5.69	10.98	-62.85	0.989
	1.18	2.40	0.44	-0.05	0.08	0.0412	6.61	10.30	-21.42	0.975
	1.58	2.60	0.44	0.00	0.08	0.0449	8.50	9.90	-10.69	0.953
	1.97	2.00	0.44	-0.05	0.06	0.0378	0.92	0.81	-6.06	0.930
0.06	0.39	2.40	0.44	0.00	0.10	0.0867	2.93	12.46	19.71	0.995
	0.79	2.60	0.42	0.00	0.08	0.0871	3.00	10.11	30.78	0.980
	1.18	2.60	0.44	0.00	0.10	0.0685	3.44	6.44	-3.78	0.963
	1.58	2.80	0.44	0.00	0.10	0.0959	4.55	8.18	-2.75	0.916
	1.97	2.80	0.46	0.05	0.14	0.1129	7.07	7.73	-3.09	0.859
0.11	0.39	2.60	0.38	0.05	0.14	0.2169	1.82	10.74	61.14	0.991
	0.79	2.80	0.42	0.05	0.00	0.2129	1.90	12.84	41.50	0.965
	1.18	2.80	0.44	0.20	0.12	0.2874	2.89	30.17	2.15	0.905
	1.58	2.60	0.44	0.55	0.08	0.4598	5.21	60.15	0.96	0.785
	1.97	1.20	0.44	0.10	0.00	0.7665	11.32	85.66	0.10	0.586
0.23	0.39	2.40	0.36	0.00	0.06	1.1494	2.32	83.00	236.10	0.987
	0.58	2.40	0.38	0.20	0.10	1.0452	2.27	74.80	205.18	0.969
	0.79	2.40	0.40	0.20	0.02	1.0448	2.34	90.94	180.82	0.956

$*$ steam only

The flow parameters consist of the dimensionless pressures of the propelled and motive streams plus the jet ejector efficiency. Once the jet ejector geometry and the independent parameters are defined, and the jet ejector is operated following the design parameter, the static pressure of the propelled and motive stream is calculated from C_p and C_{pm}. Also the jet ejector efficiency for steam is indicated.

The fluid velocity at the inlet to the convergent section is checked to verify that it is less than Mach 1.0. A convergent nozzle can produce an exit velocity less than, or equal to, Mach 1.0. The fluid velocity depends on the inlet velocity of propelled stream and distance between the nozzle and throat diameter. In the optimization study, the maximum velocity at the inlet to the convergent section is Mach 0.6. Thus, the CFD modeling is valid.

Following the above procedure when designing the jet ejector, all variables will be resolved, and the highest performance is expectable

Fluent also provides flow field visualization in the jet ejector. The flow velocity, pressure, temperature, turbulence energy, and turbulence dissipation ratio are presented in Figures 34 to 38, respectively. These pictures compare between the original (Appendix F) and optimized model.

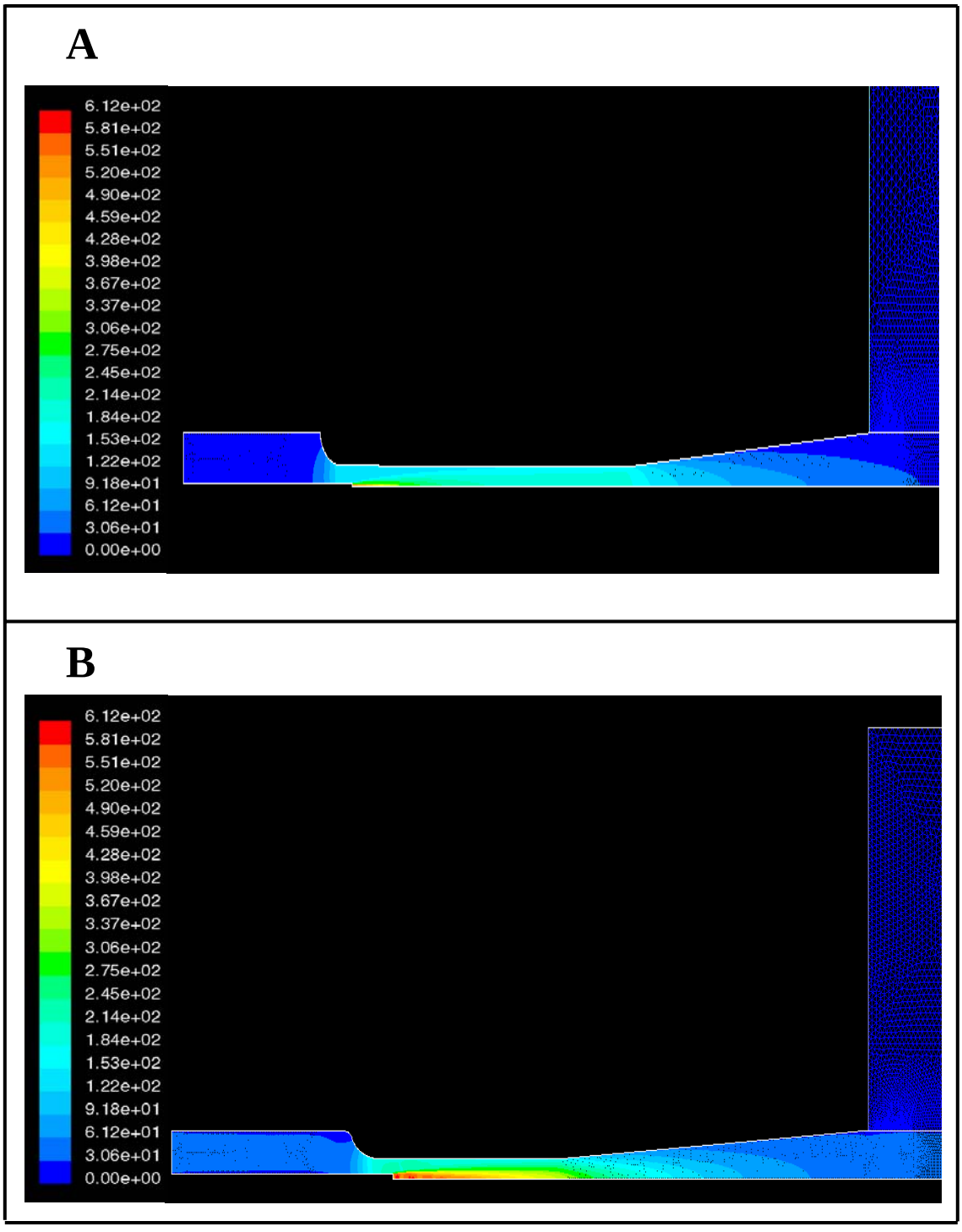

Figure 34. Velocity field inside the jet ejector A) original model, B) optimized model (unit: m/s).

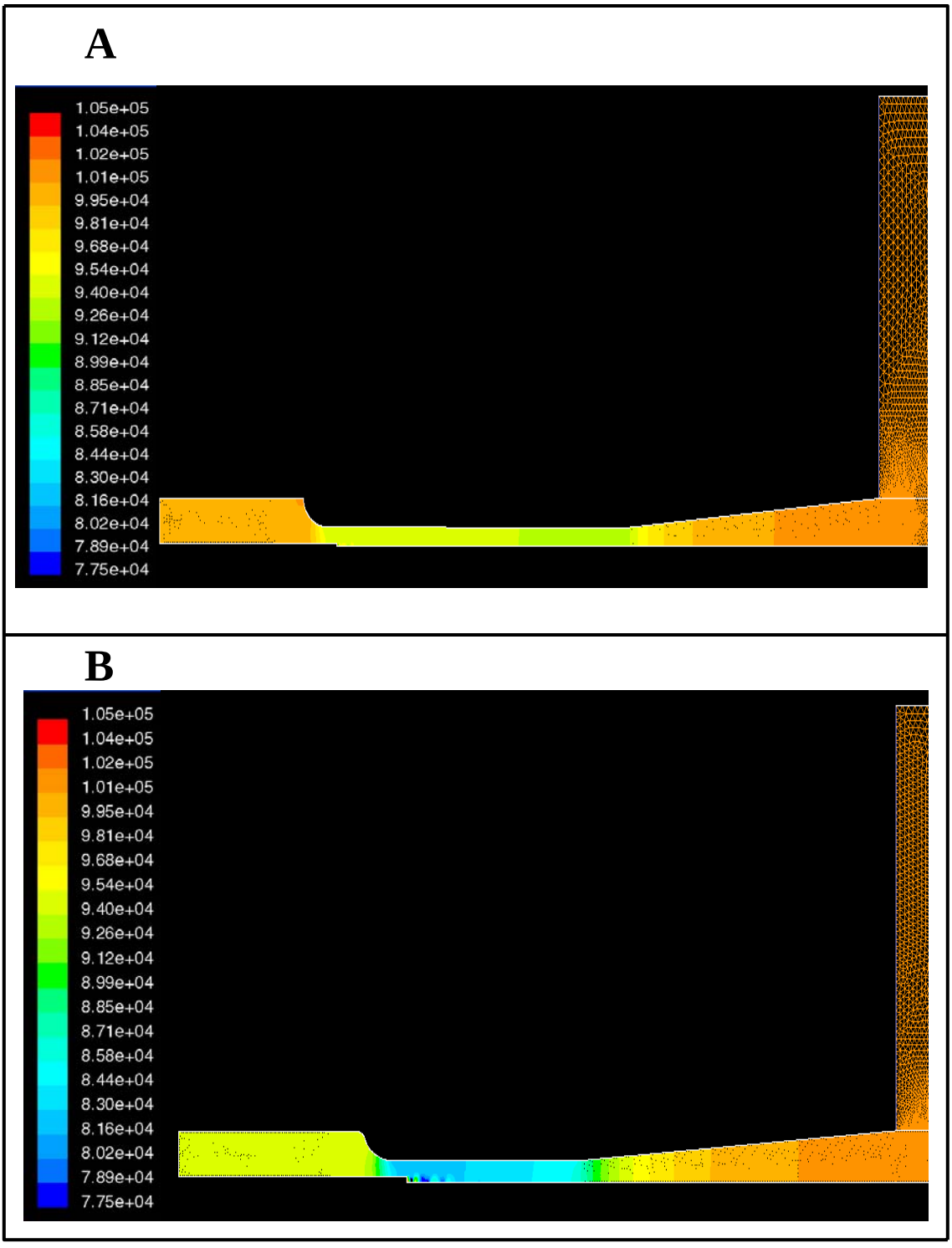

Figure 35. Pressure field inside the jet ejector A) original model, B) optimized model (unit: Pascal).

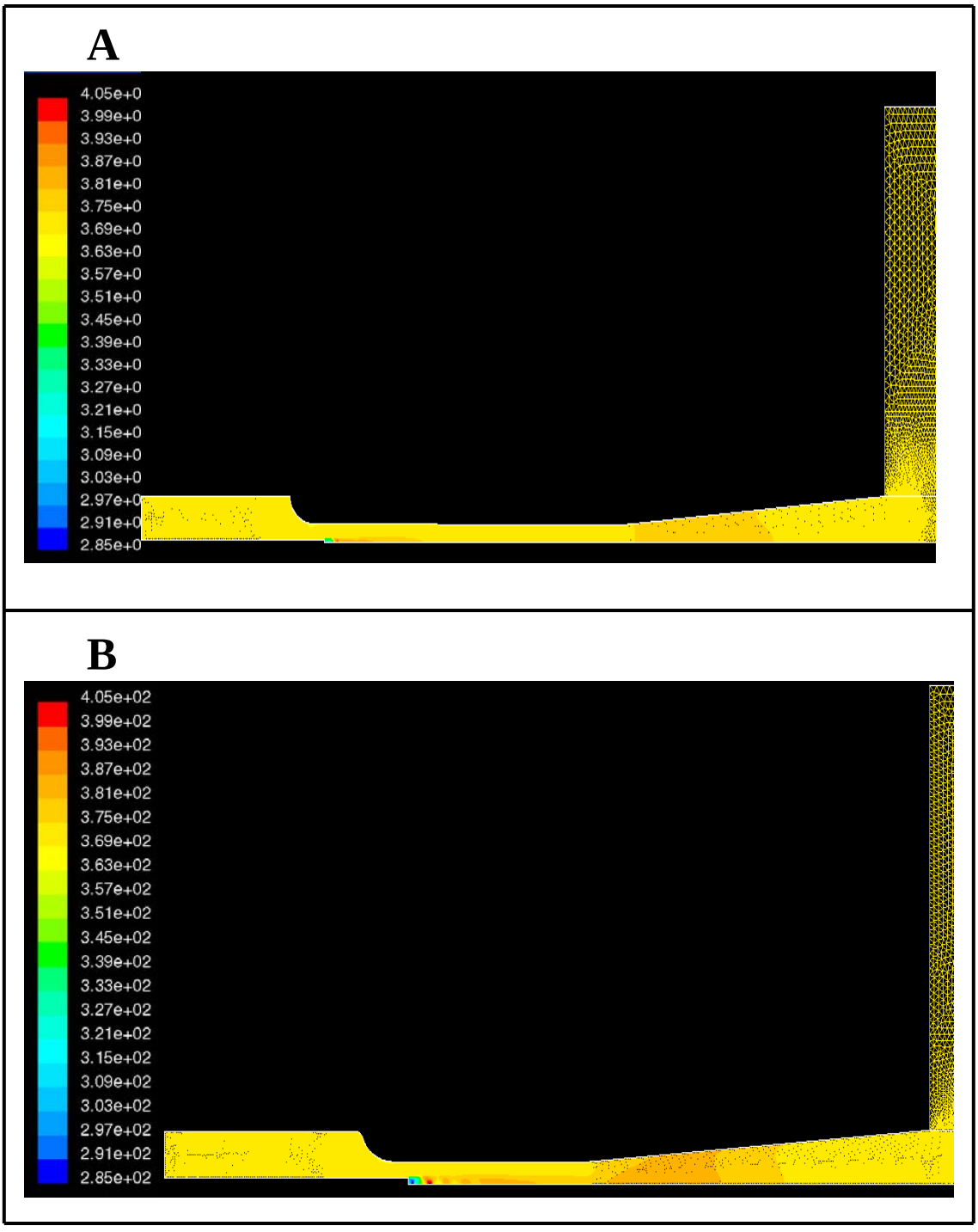

Figure 36. Temperature field inside the jet ejector A) original model, B) optimized model (unit: Kelvin).

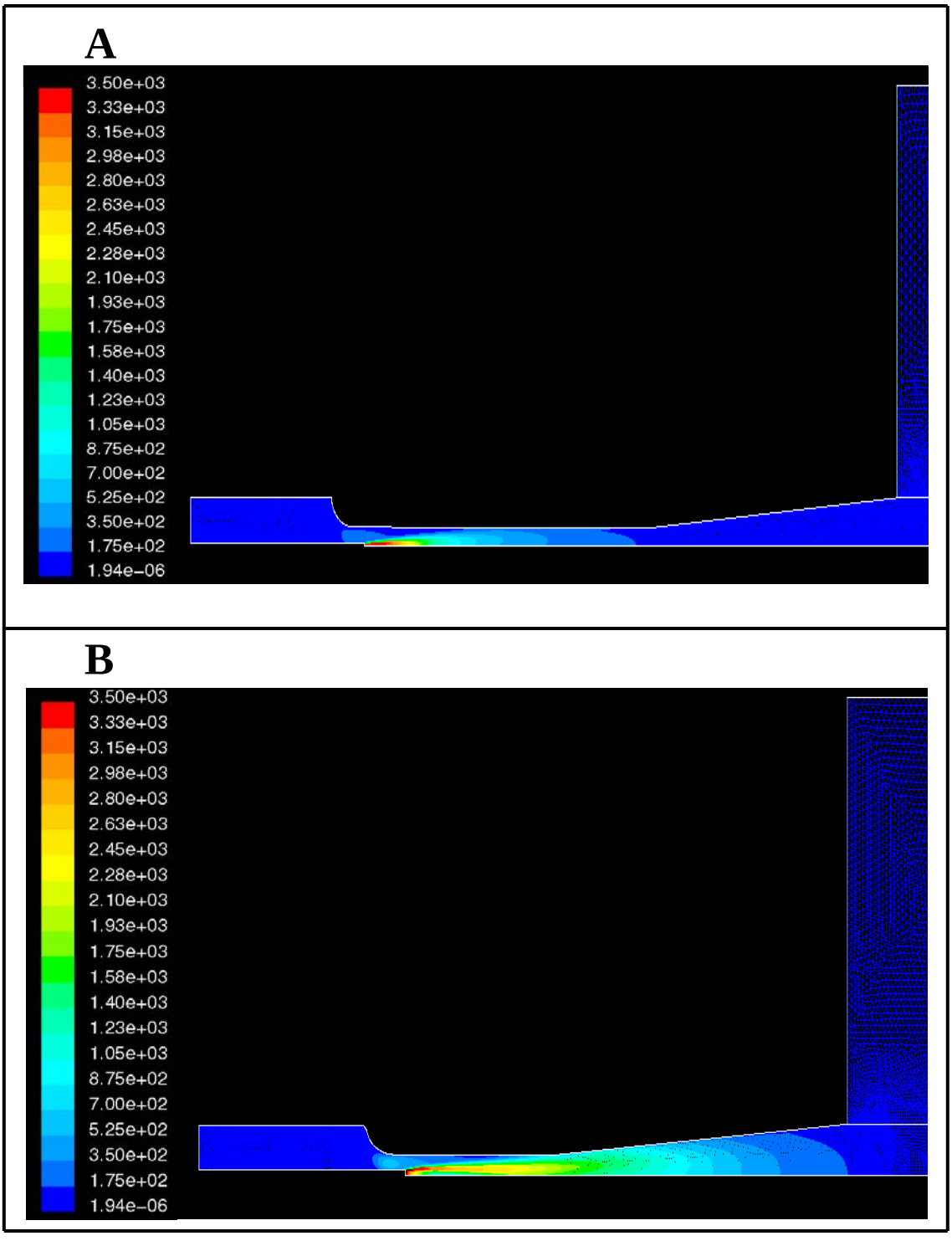

Figure 37. Turbulence energy field inside the jet ejector A) original model, B) optimized model (unit: m^2/s^2).

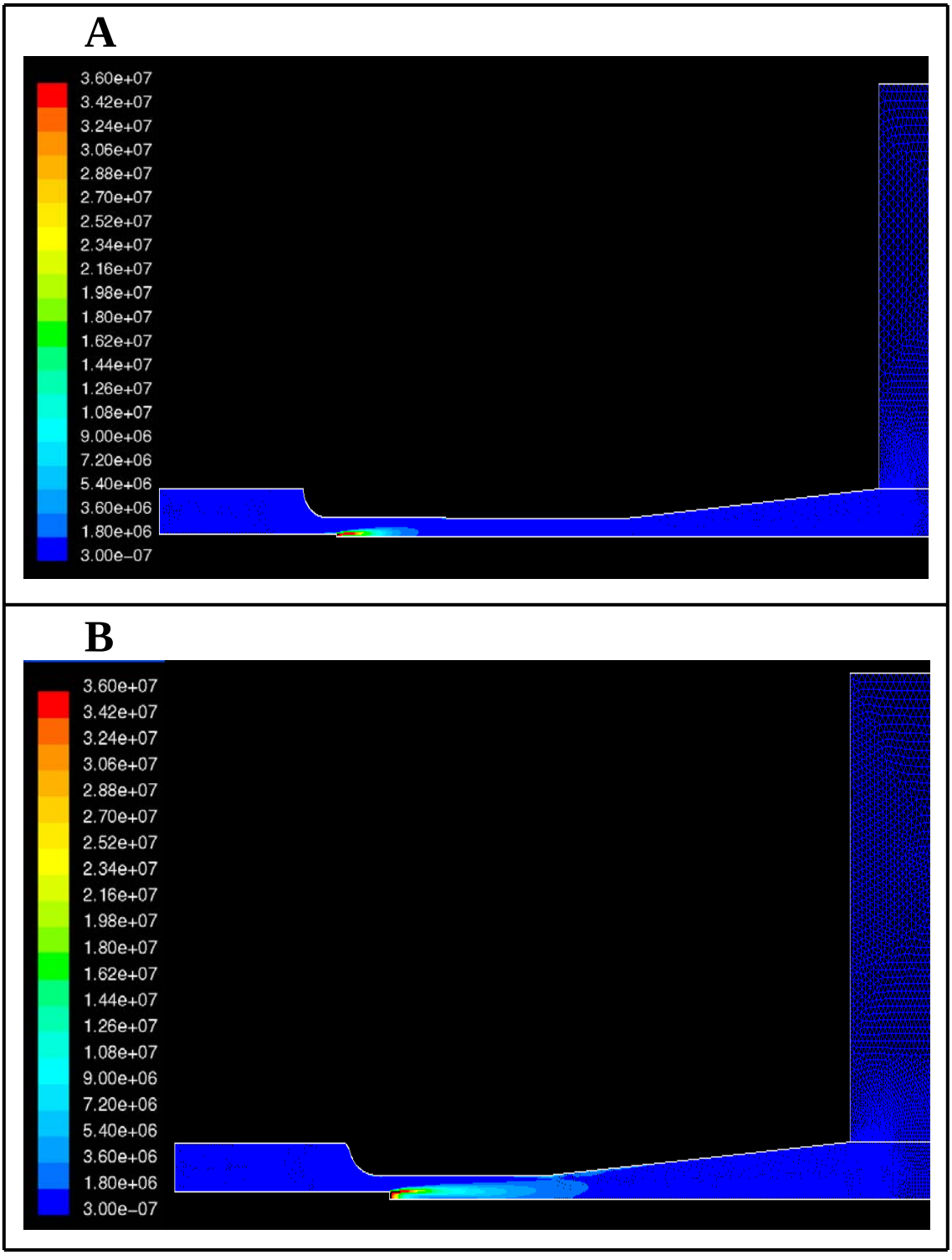

Figure 38. Turbulence dissipation rate field in the jet ejector A) original model, B) optimized model (unit: m^2/s^3).

In the diffuser section, kinetic energy is converted to pressure energy, and thus the fluid velocity decreases in this section, as shown in Figure 34. Pressure and temperature increase in the diffuser section as a consequence; the temperature increase is due to inherent energy losses from the mechanism. From the velocity diagram (Figure 34), after the mixing point, the flow velocity of the original model drops much faster than the optimized model. The motive-stream kinetic energy suddenly drops, and thus there are a lot of energy losses in the original model. This loss mechanism is also shown in the turbulence energy field and turbulence dissipation rate diagram (Figures 37 and 38, respectively). The turbulence energy and turbulence dissipation rate are greater in the original model than the optimized model at the mixing point because the kinetic energy suddenly drops in the original model. The above reasons explain the improvements in the optimized model. Also, the length of the throat section is considerably shorter in the optimized than the original model; therefore, friction loss is reduced, and thus the jet ejector efficiency increases.

Next, for more convenience in applications, the optimization information presented in Table 24 is converted to a 3-D curve-surface diagram. Curve fitting software (TableCurve 3D) is used to transform the data. In Figures 39 to Figure 47, the optimum length and diameter ratio of the throat section, the nozzle position, the dimensionless pressure term of propelled and motive stream, the efficiency, and an optimum mass flow rate ratio are plotted in the 3-D curve surfaces as a function of nozzle diameter ratio and motive velocity. Equations corresponding to the surfaces are also presented as a function of motive-stream Mach number and nozzle diameter ratio.

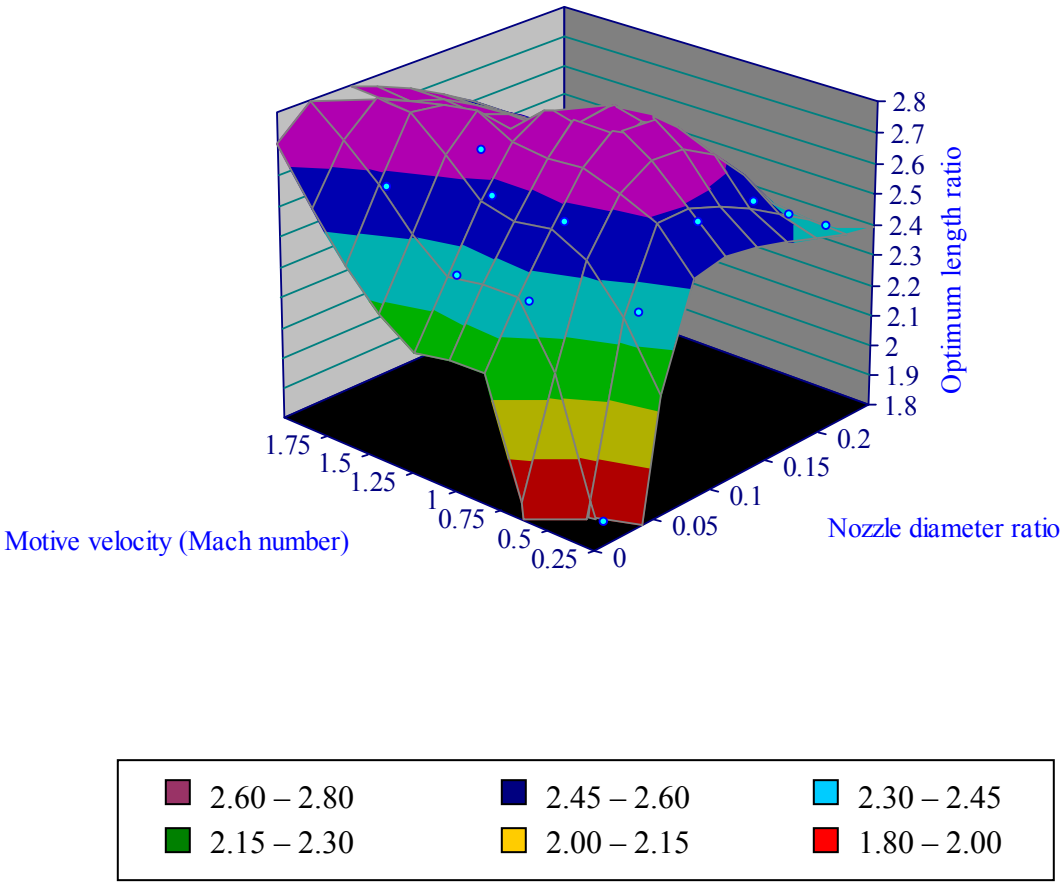

Figure 39. 3-D compilation of optimum length ratio.

A mathematical equation to calculate optimum length ratio

$$z = a + bx + cy + dx^2 + ey^2 + fxy + gx^3 + hy^3 + ixy^2 + jx^2y \qquad (3)$$

z = optimum length ratio

x = nozzle diameter ratio, y = motive-stream Mach number $a = 0.4993$

$b = 32.4252$ $c = 2.2223$ $d = 182.3512$

$e = -1.0643$ $f = -10.5451$ $g = 318.4801$

$h = 0.2103$ $i = 0.4739$ $j = 20.4609$

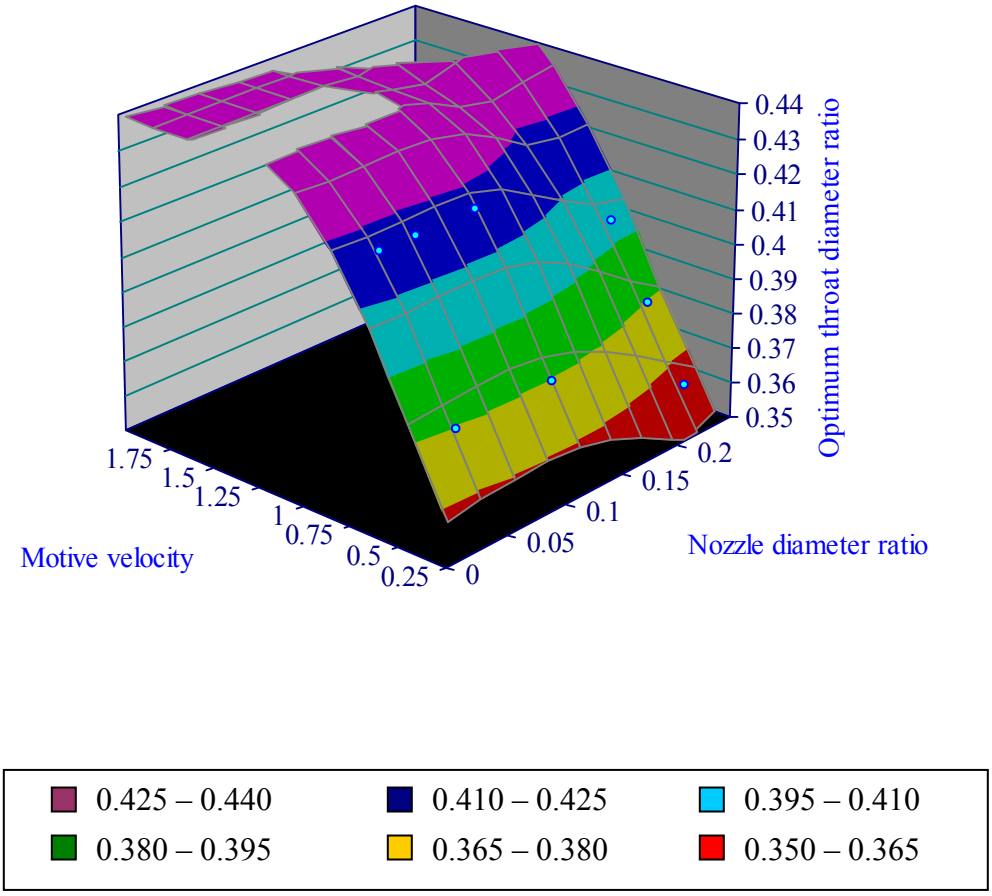

Figure 40. 3-D compilation of optimum throat diameter ratio.

A mathematical equation to calculate optimum throat diameter ratio

$$z = a + bx^{1.5} + cx^{2} + dx^{2.5} + e\frac{\ln y}{y} + \frac{f}{y} + \frac{g}{y^{1.5}} + h\frac{\ln y}{y^{2}} + \frac{i}{y^{2}} \qquad (4)$$

z = optimum throat diameter ratio

x = nozzle diameter ratio, y = motive-stream Mach number

a = 1.3520	b = -1.5131	c = -2.1463
d = -0.8353	e = -10.9840	f = 32.1638
g = -55.3664	h = 4.7102	i = 22.2874

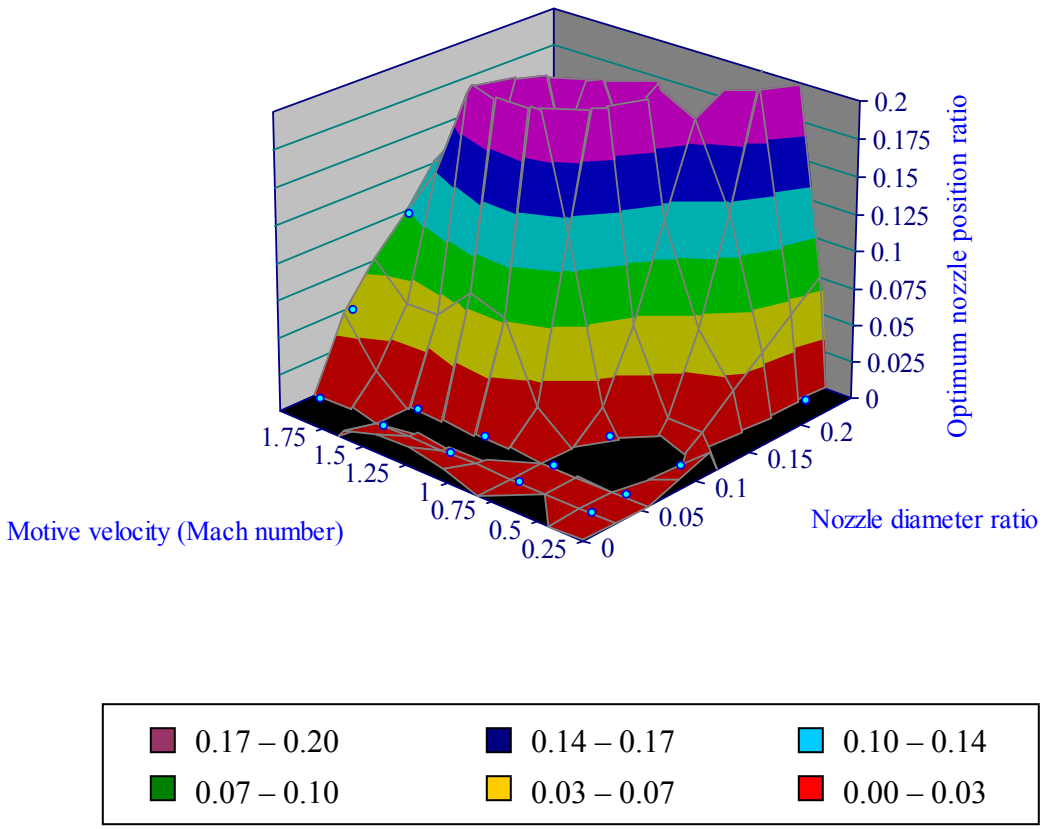

Figure 41. 3-D compilation of optimum nozzle position ratio.

A mathematical equation to calculate optimum nozzle position ratio

$$z = a + bx + cy + dx^2 + ey^2 + fxy + gx^3 + hy^3 + ixy^2 + jx^2y \qquad (5)$$

z = optimum nozzle position ratio

x = nozzle diameter ratio, y = motive-stream Mach number a = 0.2287

b = -6.8517 c = -0.3172 d = 45.3028

e = 0.1198 f = 6.2800 g = -105.4628

h = -0.0097 i = -1.6657 j = -5.7138

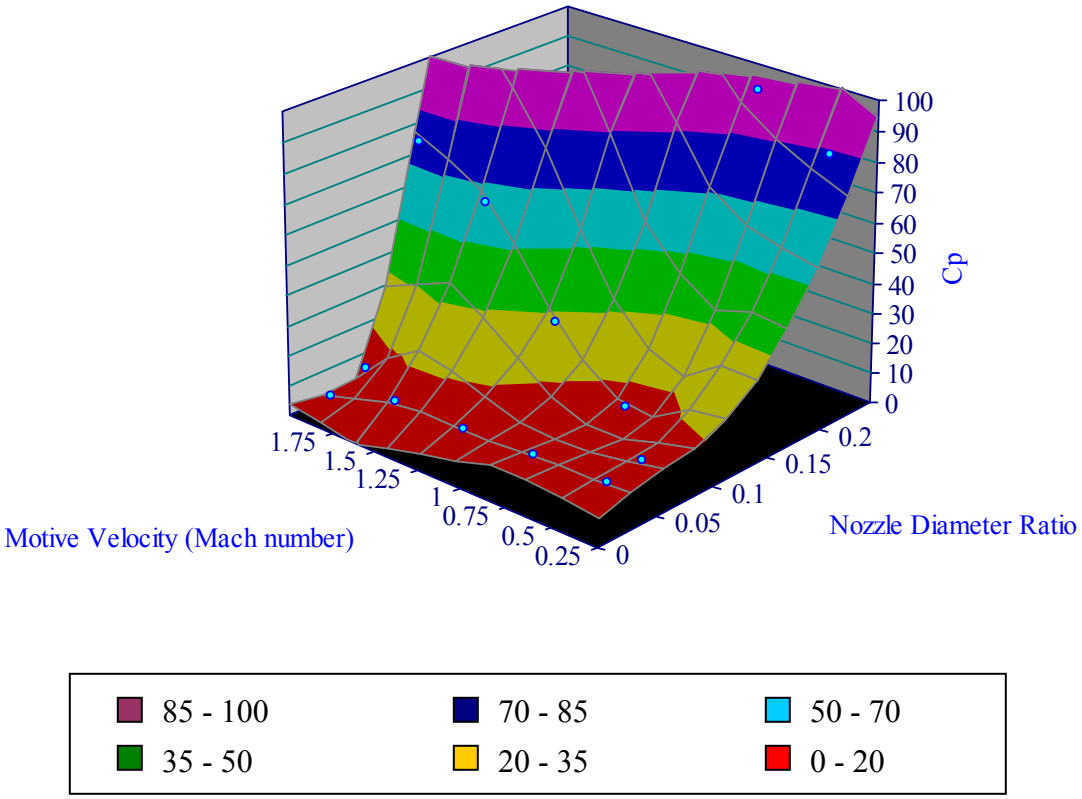

Figure 42. 3-D compilation of C_p.

A mathematical equation to calculate C_p

$$z = a + bx + cy + dx^2 + ey^2 + fxy \tag{6}$$

$z = C_p$

x = nozzle diameter ratio, y = motive-stream Mach number

$a = 41.0708$ $b = -678.7825$ $c = -35.2336$

$d = 2956.6883$ $e = 4.0871$ $f = 505.1732$

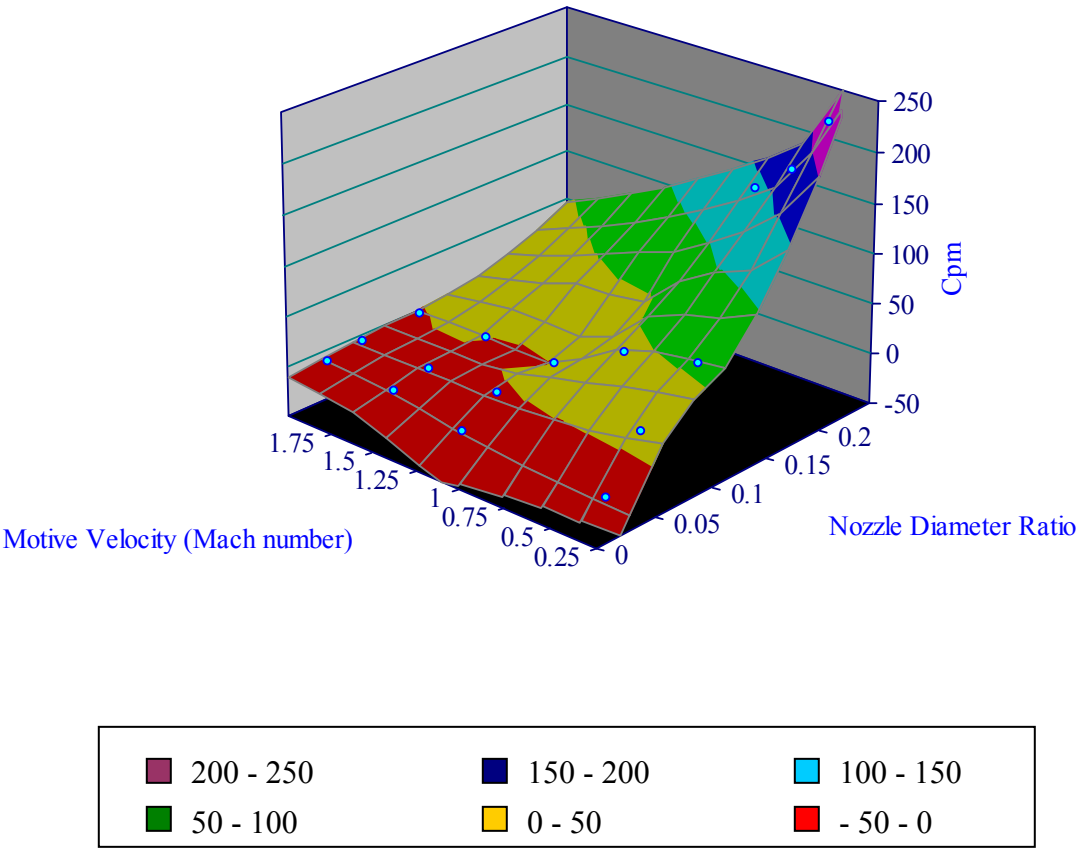

Figure 43. 3-D compilation of C_{pm}.

A mathematical equation to calculate C_{pm}

$$z = a + bx + cy + dx^2 + ey^2 + fxy \tag{7}$$

$z = C_{pm}$

x = nozzle diameter ratio, y = motive-stream Mach number

a = -54.2998	b = 123.1851	c = -7.4812
d = 1066.0700	e = 14.0903	f = -621.3600

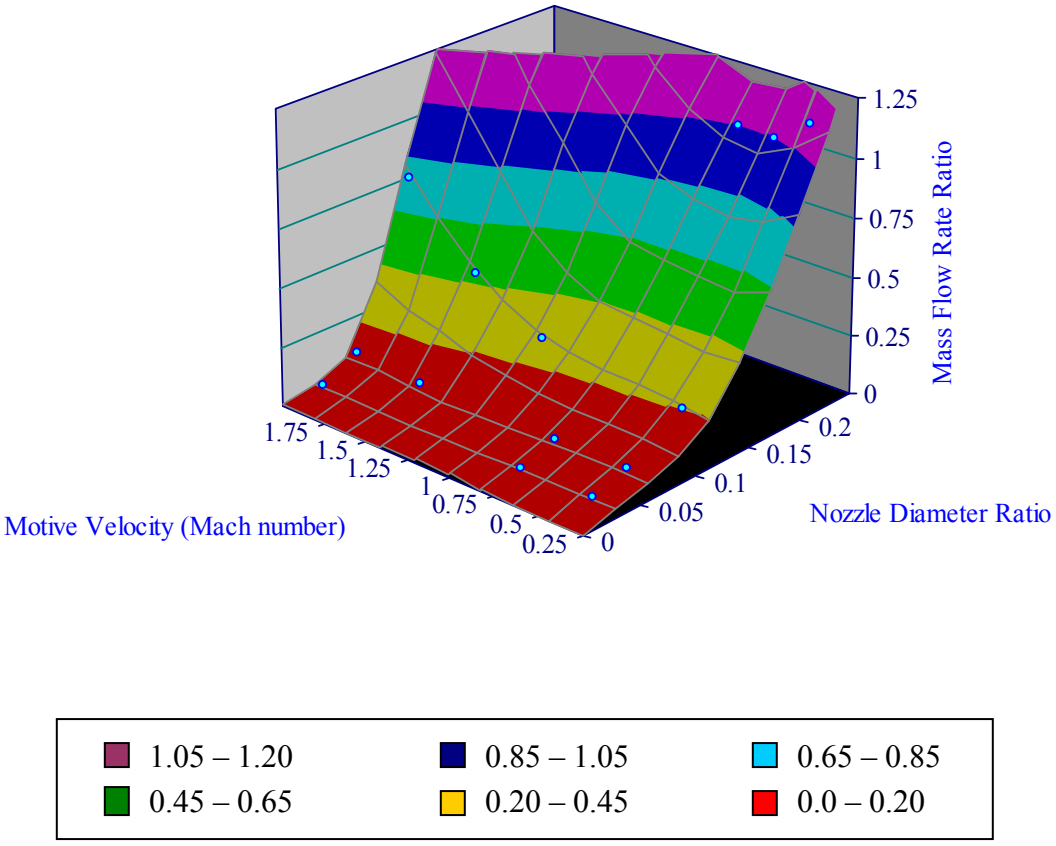

Figure 44. 3-D compilation of optimum mass flow rate ratio.

A mathematical equation to calculate optimum mass flow rate ratio

$$z = a + b\ln x + \frac{c}{x^{0.5}} + dy^{1.5} + ey^2 \ln y + fy^{2.5} \tag{8}$$

z = optimum mass flow rate ratio

x = nozzle diameter ratio, y = motive-stream Mach number

a = -9.3082	b = 15.5430	c = 15.8514
d = -26.8980	e = -27.9546	f = 26.6767

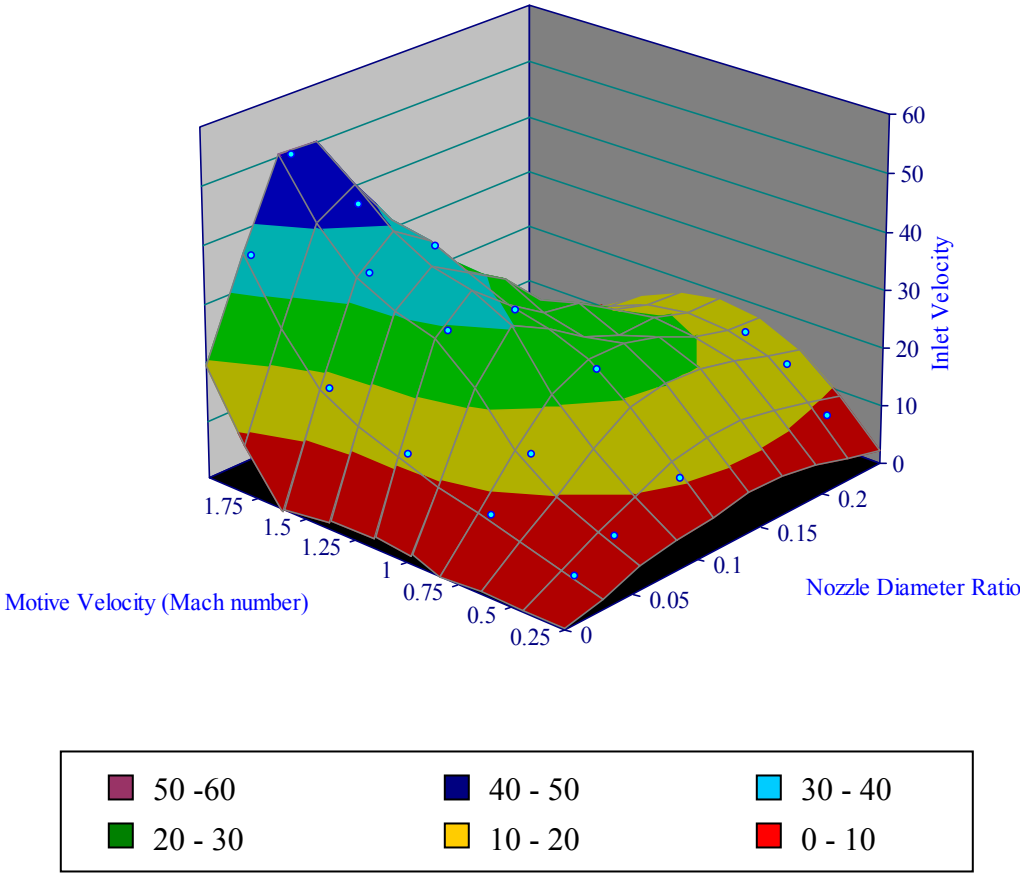

Figure 45. 3-D compilation of optimum inlet velocity.

A mathematical equation to calculate optimum inlet velocity

$$z = a + bx + cy + dx^2 + ey^2 + fxy + gx^3 + hy^3 + ixy^2 + jx^2y \qquad (9)$$

z = optimum inlet velocity

x = nozzle diameter ratio, y = motive-stream Mach number a = -14.1552

b = 437.9519 c = 4.3672 d = -5400.8602

e = -8.3698 f = 751.1445 g = 15614.4770

h = 4.3605 i = -179.6070 j = -2034.0570

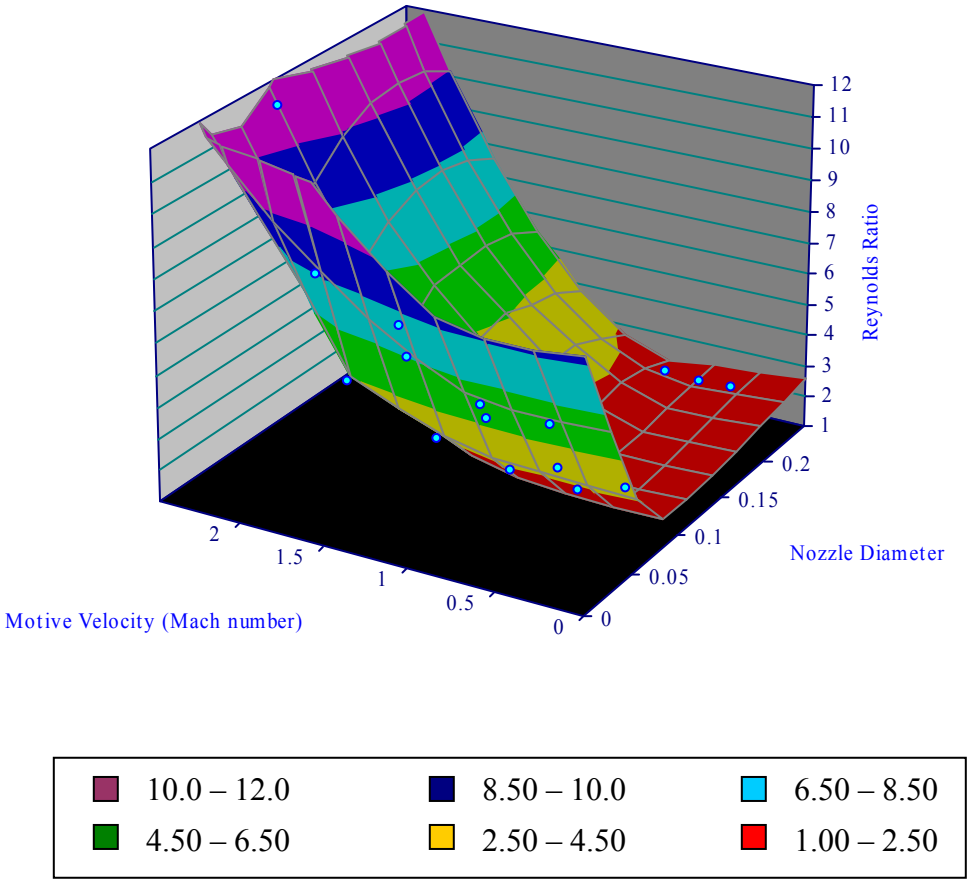

Figure 46. 3-D compilation of optimum Reynolds ratio.

A mathematical equation to calculate optimum inlet velocity

$$z = a + b\ln x + cy + d(\ln x)^2 + ey^2 + fy(\ln x) + g(\ln x)^3 + hy^3 + iy^2 \ln x + jy(\ln x)2 \quad (10)$$

z = optimum inlet velocity

x = nozzle diameter ratio, y = motive-stream Mach number a = 0.3347

b = -3.4896 c = 3.7693 d = -1.8229

e = 5.3977 f = 6.8428 g = -0.3528

h = 0.0929 i = 1.3085 j = 1.6498

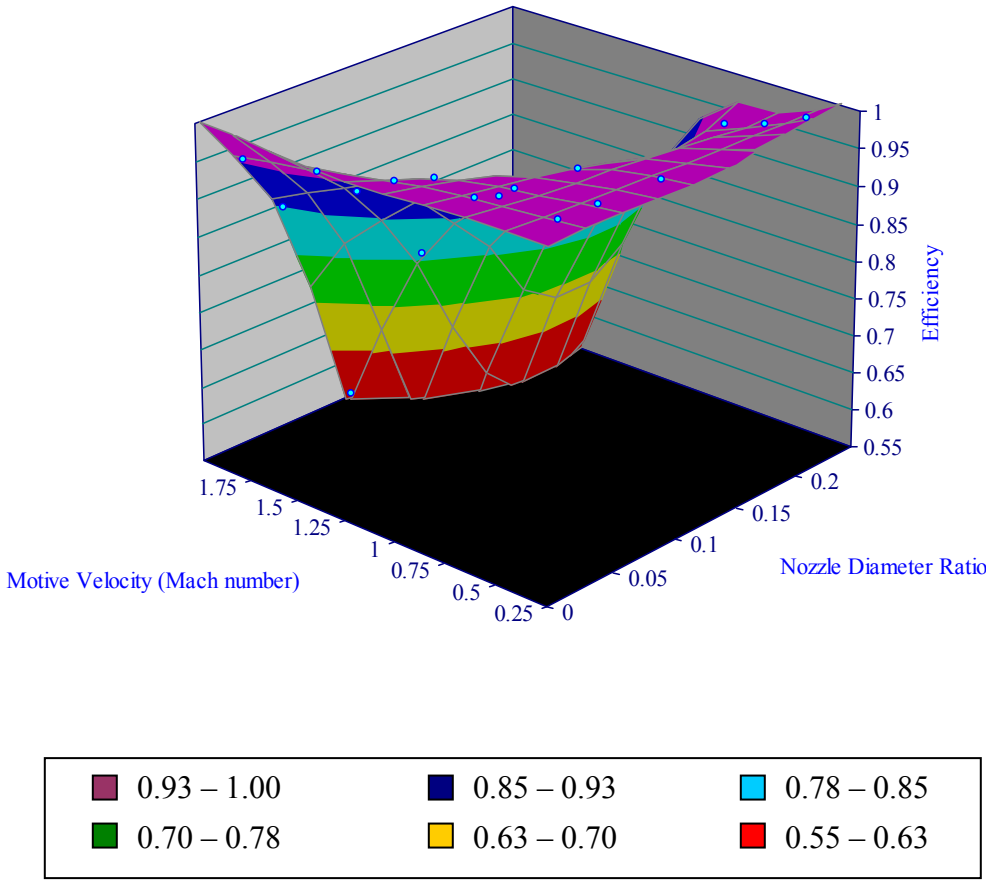

Figure 47. 3-D compilation of the jet ejector efficiency.

A mathematical equation to calculate jet ejector efficiency

$$z = \frac{a + bx + cx^2 + dx^3 + ey + fy^2}{1 + gx + hx^2 + iy} \tag{11}$$

z = jet ejector efficiency

x = nozzle diameter ratio, y = motive-stream Mach number

a = 1.0098	b = -10.2811	c = 34.2369
d = -9.7852	e = -0.0946	f = -0.0093
g = -9.9334	h = 30.7074	i = -0.0907

Multi-Stage Jet Ejector System

The objective of this section is to demonstrate how to implement the optimization results to design a multi-stage jet ejector cascade system. The system with an overall 1.2 compression ratio is analyzed as an example. As the motive stream, superheated steam at 18 atm and 719 K is fed at the top stage of the system. To minimize superheated steam consumption, the high-pressure outlet stream of the upper stage is fed as the motive stream of the lower stage. At the first stage, the large nozzle diameter ratio model is selected to achieve a high compression ratio per stage and minimize the number of jet ejectors. The motive-stream velocity is limited below sonic velocity to avoid shock waves. The motive velocity at Mach 0.99 is applied in the first two stages, and Mach 0.95 is applied for the rest of the system. To maximize system efficiency, jet ejectors with smaller nozzle diameters are used after the second stage. The calculation of fluid property is presented in the methodology section. To achieve the 1.2 compression ratio, 85 jet ejectors and 244 streams are required. The system flow diagram is shown in Figure 48. The SH-S symbol in the diagram represents the external superheated steam. The pressure and mass flow rate of the stream in each stage are summarized in Table 22. The jet ejector specification for each stage is summarized in Table 23.

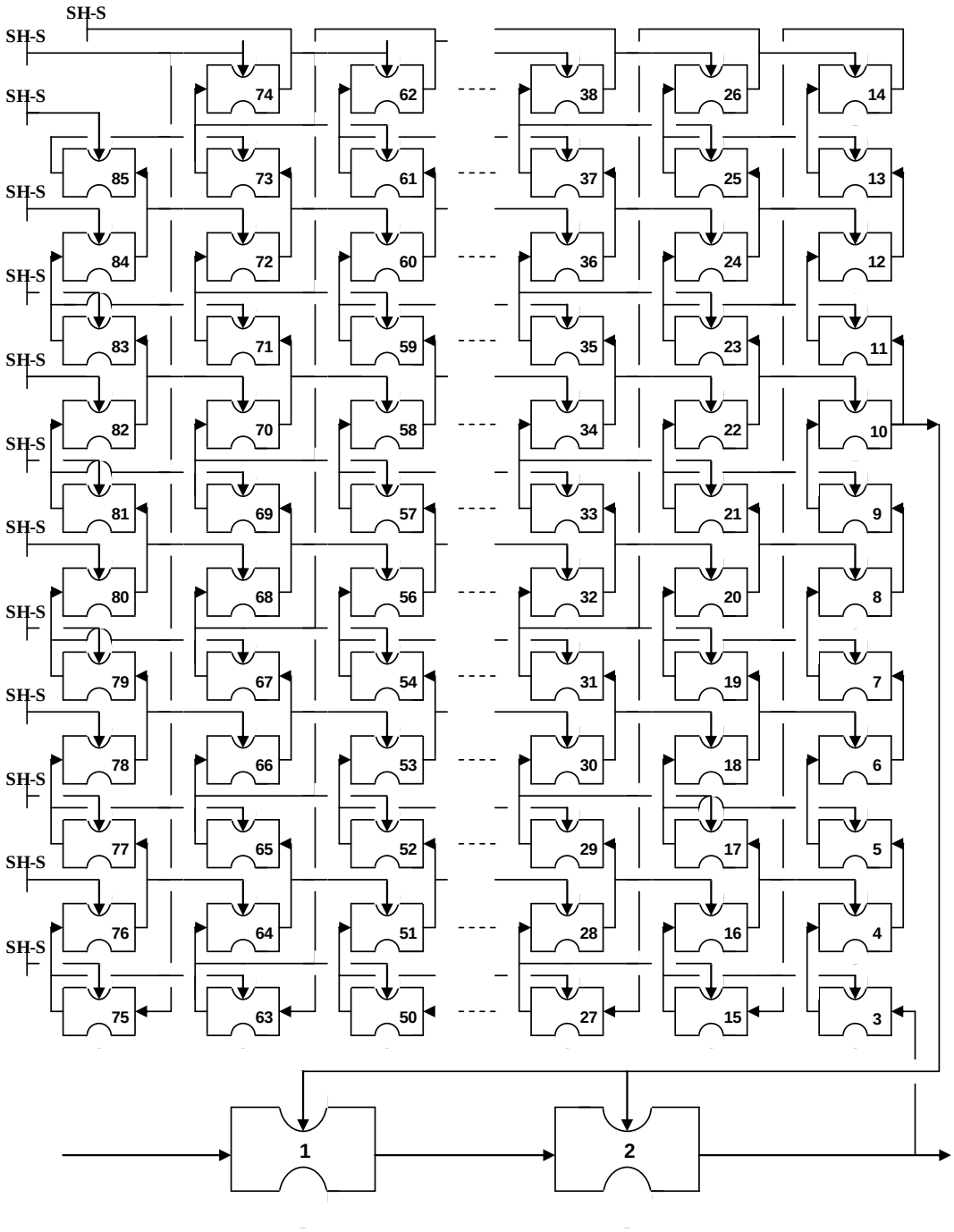

Figure 48. Cascade diagram.

Table 22. Pressure and mass flow rate of jet ejector in the cascade.

Stage number	Pressure (Pa)				Mass flow rate (kg/s)		
	Propelled Stream	Outlet Stream	Motive Stream		Stream		
			Inlet	Outlet	Propelled	Outlet	Motive
1	101,325	111,909	144,820	94,586	17.0	45.0	28.0
2	111,909	120,927	144,270	107,179	45.0	90.2	45.2
3	120,927	125,719	190,600	121,325	28.5	35.1	6.6
4	125,719	130,656	197,400	126,129	35.1	43.2	8.1
5	130,656	135,741	204,400	131,078	43.2	53.2	10.0
6	135,741	140,979	211,500	136,178	53.2	65.5	12.3
7	140,979	146,369	218,900	141,426	65.5	80.8	15.2
8	146,369	151,918	226,450	146,830	7.6	9.3	1.8
9	151,918	157,628	234,200	152,393	9.3	11.5	2.2
10	157,628	163,502	242,150	158,116	11.5	14.2	2.7
11	163,502	169,544	250,350	164,005	14.2	17.5	3.3
12	169,544	175,761	258,700	170,061	17.5	21.5	4.0
13	175,761	182,148	267,300	176,292	21.5	26.5	5.0
14	182,148	188,714	276,100	182,694	26.5	32.6	6.1
15	188,714	195,461	285,100	189,275	32.6	40.2	7.6
16	195,461	202,392	294,300	195,973	33.6	41.4	7.8
17	202,392	209,513	303,900	202,985	33.3	41.0	7.7
18	209,513	216,824	313,650	210,121	31.0	38.2	7.2
19	216,824	224,332	323,600	217,449	25.8	31.8	6.0
20	224,332	232,039	333,800	224,973	16.6	20.4	3.8

Table 22. (Continued).

Stage number	Pressure (Pa)				Mass flow rate (kg/s)		
	Propelled Stream	Outlet Stream	Motive Stream		Stream		
			Inlet	Outlet	Propelled	Outlet	Motive
21	232,039	239,949	344,300	232,697	18.7	23.0	4.3
22	239,949	248,065	355,000	240,624	20.9	25.7	4.8
23	248,065	256,392	366,000	248,758	23.0	28.4	5.3
24	256,392	264,934	377,200	257,107	25.1	30.9	5.8
25	264,934	273,693	388,660	265,662	26.8	33.1	6.2
26	273,693	282,675	400,450	274,440	28.1	34.6	6.5
27	282,675	291,884	412,500	283,441	28.5	35.1	6.6
28	291,884	301,321	424,800	292,668	27.5	33.9	6.4
29	301,321	310,993	437,400	302,125	26.1	32.1	6.1
30	310,993	320,612	450,300	311,793	24.4	30.1	5.7
31	320,612	330,758	463,100	321,456	22.9	28.2	5.3
32	330,758	341,150	476,500	331,622	22.2	27.4	5.2
33	341,150	351,793	490,300	342,035	23.5	29.0	5.5
34	351,793	362,690	504,400	352,699	24.6	30.3	5.7
35	362,690	373,847	518,750	363,618	25.5	31.4	5.9
36	373,847	385,268	533,500	374,794	26.1	32.1	6.1
37	385,268	396,956	548,500	386,240	26.3	32.4	6.1
38	396,956	408,916	563,800	397,950	26.2	32.3	6.1
39	408,916	421,153	579,400	409,934	25.8	31.7	6.0
40	421,153	433,672	595,500	422,194	25.1	31.0	5.8

Table 22. (Continued).

Stage number	Pressure (Pa)				Mass flow rate (kg/s)		
	Propelled Stream	Outlet Stream	Motive Stream		Stream		
			Inlet	Outlet	Propelled	Outlet	Motive
41	433,672	466,476	640,000	435,736	24.6	30.3	5.7
42	466,476	480,166	656,800	467,614	24.2	29.8	5.6
43	480,166	494,166	674,600	481,330	24.2	29.8	5.6
44	494,166	508,478	692,800	495,356	24.5	30.2	5.7
45	508,478	523,110	711,400	509,695	25.0	30.8	5.8
46	523,110	538,064	730,300	524,353	25.4	31.2	5.9
47	538,064	553,348	749,700	539,335	25.5	31.5	5.9
48	553,348	568,964	769,500	554,646	25.5	31.5	5.9
49	568,964	584,920	789,600	570,291	25.4	31.3	5.9
50	584,920	601,219	810,000	586,275	25.2	31.0	5.8
51	601,219	617,868	831,000	602,604	25.0	30.8	5.8
52	617,868	634,871	852,400	619,282	24.8	30.5	5.7
53	634,871	652,233	874,100	636,314	24.7	30.4	5.7
54	652,233	669,961	896,300	653,707	24.7	30.5	5.7
55	669,961	688,059	919,000	671,466	24.8	30.6	5.8
56	688,059	706,533	942,100	689,595	25.0	30.8	5.8
57	706,533	725,388	965,600	708,101	25.1	30.9	5.8
58	725,388	744,630	989,600	726,988	25.1	31.0	5.8
59	744,630	764,265	1,014,000	746,263	25.1	30.9	5.8
60	764,265	784,297	1,039,000	765,931	25.0	30.8	5.8

Table 22. (Continued).

Stage number	Pressure (Pa)				Mass flow rate (kg/s)		
	Propelled Stream	Outlet Stream	Motive Stream		Stream		
			Inlet	Outlet	Propelled	Outlet	Motive
61	784,297	804,733	1,064,300	785,997	24.9	30.6	5.8
62	804,733	825,578	1,090,200	806,467	24.7	30.5	5.7
63	825,578	846,838	1,116,600	827,346	24.6	30.4	5.7
64	846,838	868,519	1,143,500	848,641	24.6	30.3	5.7
65	868,519	890,627	1,170,800	870,358	24.5	30.2	5.7
66	890,627	913,167	1,198,500	892,501	24.5	30.1	5.7
67	913,167	936,146	1,226,800	915,078	24.4	30.1	5.7
68	936,146	959,570	1,255,700	938,094	24.3	29.9	5.6
69	959,570	983,444	1,285,000	961,554	24.1	29.7	5.6
70	983,444	1,007,774	1,315,000	985,466	23.9	29.5	5.5
71	1,007,774	1,032,568	1,345,500	1,009,836	23.6	29.1	5.5
72	1,032,568	1,057,831	1,376,400	1,034,669	23.3	28.7	5.4
73	1,057,831	1,083,569	1,407,850	1,059,972	22.9	28.2	5.3
74	1,083,569	1,109,789	1,440,000	1,085,750	22.4	27.6	5.2
75	1,109,789	1,136,497	1,472,700	1,112,010	21.9	27.0	5.1
76	1,136,497	1,163,699	1,506,000	1,138,759	21.3	26.2	4.9
77	1,163,699	1,191,403	1,539,600	1,166,003	20.5	25.2	4.8
78	1,191,403	1,219,613	1,573,500	1,193,277	19.6	24.1	4.5
79	1,219,613	1,248,337	1,609,000	1,222,002	18.4	22.7	4.3
80	1,248,337	1,277,582	1,644,500	1,250,825	17.0	21.0	4.0

Table 22. (Continued).

Stage number	Pressure (Pa)				Mass flow rate (kg/s)		
	Propelled Stream	Outlet Stream	Motive Stream		Stream		
			Inlet	Outlet	Propelled	Outlet	Motive
81	1,277,582	1,307,354	1,680,700	1,280,058	15.3	18.9	3.6
82	1,307,354	1,337,639	1,717,400	1,309,854	13.3	16.4	3.1
83	1,337,639	1,368,483	1,754,850	1,340,202	10.8	13.4	2.5
84	1,368,483	1,399,877	1,793,000	1,371,094	7.9	9.7	1.8
85	1,399,877	1,431,824	1,831,500	1,402,534	4.3	5.3	1.0

Table 23. Jet ejector model specification of each stage.

Number of Stage	Parameters					
	(D_n/D_p)	v_m (Mach number)	C_p	C_{pm}	Reynolds Ratio	η
1	0.25	0.99	104.02	170.22	3.690	0.9264
2	0.23	0.99	96.59	147.26	3.444	0.9551
3-85	0.11	0.95	21.86	20.04	2.162	0.9472

The overall mass flow rate ratio of the cascade is 1.381, which means 1 kg of superheated steam (18 atm, 719 K) compresses 1.381 kg of steam from 1.0 to 1.2 atmospheres.

CONCLUSIONS

Jet ejectors are widely used in the chemical industrial process because they are highly reliable with low capital and maintenance costs. However, jet ejectors have a low efficiency compared with mechanical compressors. A high-efficiency jet ejector, which was designed and presented in the High Efficiency Jet Ejector invention disclosure of Holtzapple (2001) is an engaging solution to resolve the low efficiency problem. This research was conducted to investigate the optimal geometry and operating conditions for a high-efficiency jet ejector.

CFD software was applied in this research. Many experiments were done to verify the reliability of CFD modeling. The results confirm that CFD modeling can provide high-quality solutions that agree well with experiment data. Therefore, the research results from CFD modeling have high accuracy and reliability.

The dimensionless group analysis indicated that the dimensionless principle could apply together with the research result to make the result valid for any fluid, geometric scale, and operating pressure. For a given Reynolds ratio and the motive-stream Mach number, the static pressure of the propelled and motive streams is calculated from C_p and C_{pm} in the research results, respectively. The inlet and outlet static pressures calculated from C_p allow the jet ejector efficiency to be calculated, regardless of the fluid type, using newly defined efficiency equation when the density, mass flow rate, pressure, velocity, and temperature of the propelled, motive, and outlet streams are known.

The optimal geometry of a high-efficiency jet ejector was discovered. The research results indicated that optimum length of the throat is 2 to 3 times the inlet diameter. This is approximately 5 to 7 times the throat diameter, which is consistent with the literature. The optimum throat diameter is about 0.44 times the inlet diameter, which allows for complete mixing of the propelled and motive streams before flowing to the divergence section. The flow visualized diagram of the optimized model confirms the complete mixing of both streams. The optimum nozzle position is – 0.05 to 0.05 times the inlet diameter in most cases, which is compatible with the ESDU (1986) recommendation. The optimum radius inlet curvature fluctuated because this parameter provided so little improvement on jet ejector performance. As a consequence, the result was easily obscured with numerical error from CFD modeling. The jet-ejector efficiency after the optimization study is above 90% provided the motive velocity is below Mach 1.2 with all nozzle diameters. This is remarkable improvement from a conventional jet ejector design.

Finally, a multi-stage jet ejector cascade system was analyzed using the optimized results. Unfortunately, the ratio of propelled mass to motive mass is small. Perhaps the performance will improve using mixing vanes inside the throat section. The mixing vanes help mix both streams giving higher compression ratios as a consequence. Optimizing mixing-vane jet ejector design is recommended for future research.

FUTURE RESEARCH

Because the cascade of jet ejectors requires a lot of superheated steam and has too many jet-ejector stages, this system is impractical to operate. Some experimental results of a jet ejector with mixing vanes indicates that the compression ratio improves with only a slight decrease of efficiency, by a few percentage points. Therefore, a jet ejector with mixing vanes may decrease the amount of superheated steam consumed, and decrease the number of stages in the system. The optimization of the jet ejector with mixing vanes should be further researched to obtain the maximum efficiency.

LITERATURE CITED

Bailey, A., and S. A. Wood, "An Investigation of the Principles of the Air Ejector," Technical Report of the Aeronautical Research Committee R and M, United Kingdom (1945).

Birgenheier, D B., T. Butzbach., D. E. Bolt., R. Bhatnagar., and R. E. Ojala, "Designing Steam-Jet Vacuum Systems," *Chem. Eng. J*., **100**, 7(1993).

Berkeley, F. D., "Ejectors Give Any Suction Pressure," *Chem Eng. J.*, **64**, 4(1957).

Chandrasekhara, M. S., A. Krothapalli, and D. Baganoff, "Performance Characteristics of an Underexpanded Multiple Jet Ejector," *J. Propul. Power*, **7**, 3(1991).

Croft, D. R., and D. G. Lilley, "Jet Pump Design and Performance Analysis," AIAA 14th Aerospace Science Meeting, AIAA Paper 76183, New York (1976).

Croll, W. S., "Keeping Steam Ejectors," *Chem. Eng. J*., **105**, 4(1998).

Da-Wen, S., and I. W. Eames, "Recent Developments in the Design Theories and Applications of Ejectors," *J.Inst. Energy*, **68** (1995).

Deen, W. M., *Analysis of Transport Phenomena*, Oxford University Press, New York (1998).

DeFrate, L. A., and A. E. Hoerl, "Optimum Design of Ejectors Using Digital Computers," *Chem. Eng. Prog. Symp. Series*, **21** (1959).

Djebedjian, B., S. Abdalla, and M. A. Rayan, "Parametric Investigation of Boost Jet Pump Performance," *Proceedings of FEDSM, ASME Fluids Engineering Summer Conference*, Boston (2000).

Ducharme, R., P. Kapadia, J. Dowden, M. Thornton, I. Richardson, "A Mathematical Model of the Arc in Electric Arc Welding including Shielding Gas Flow and Cathode Spot Location," *J. Phys. : Appl. Phys*., **28,** 9 (1995).

Dutton, J. C., and B. F. Carroll, "Optimal Supersonic Ejector Designs," *ASME J.Fluids Eng*., **108** (1986).

El-Dessouky, H., H. Ettouney, I. Alatiqi, and G. Al-Nuwaibit, "Evaluation of Steam Jet Ejectors," *Chem. Eng. Process.*, **41**, 6 (2002).

Engineering Sciences Data Unit (ESDU), *Ejector and Jet Pump; Design for Steam Driven Flow,* Item number 86030, ESDU International Ltd., London (1986).

Fletcher, C. A. J., *Computational Techniques for Fluid Dynamics*, Volumes I & II, 2nd ed., Springer-Verlag, Orlando, FL (1991).

Fluent User Guides, Fluent Inc., www.fluent.com, (2001).

Habashi, W. G., *Solution Techniques for Large-Scale CFD Problems*, John Wiley & Sons, New York (1995).

Happle J., and H. Brenner, *Low Reynolds Number Hydrodynamics(Mechanics of Fluids and Transport Processes),* McGraw Hill, New York (1965).

Hedges, K. R., and P. G. Hill, "Compressible Flow Ejectors; Flow Field Measurements and Analysis," *ASME Trans. Fluid Eng.,* **96**, 3 (1974).

Hoggarth, M. L., "The Design and Performance of High-Pressure Injectors as Gas Jet Boosters," *Process Inst. Mech. Eng*., **185** (1970).

Holton, W. C., "Effect of Molecular Weight and Entrained Fluid on the Performance of Steam-Jet Ejectors," *Trans. Am. Soc. Mech. Eng.*, **73** (1951).

Holton, W. C., and E. J. Schulz, "Effect of Temperature of Entrained Fluid on the Performance of Steam-Jet Ejectors," *Trans. Am. Soc. Mec. Eng.*, **73** (1951).

Holtzapple, M. T., "High-Efficiency Jet Ejector," (Invention Disclosure) Department of Chemical Engineering, Texas A&M University, College Station, Texas (2001).

Keenan, J. H., and J. Kaye, *Gas Tables*, John Wiley & Sons, New York (1948).

Keenan, J. H., and E. P. Neumann, "A Simple Air Ejector," *ASME J. Appl. Mech*., **9** (1942).

Keenan, J. H., E. P. Neumann, and F. Lustwerk, " An Investigation of Ejector Design by Analysis and Experiment," *J. Appl. Mech*., **17**, 3 (1950).

Kim, H. D., T. Setoguchi, S. Yu, and S. Raghunathan, "Navier-Stokes Computations of the Supersonic Ejector-Diffuser System with a Second Throat," *J. Therm. Sci*., **8**, 2 (1999).

Knight, G. B., "Five Ways to Automatically Control Pressure for Ejector Vacuum Systems," *Chem. Eng. J*., **66**, 6 (1959).

Kroll, A. E., "The Design of Jet Pumps," *Chem. Eng. Prog*., **1**, 2 (1947).

Mains, W. D., and R. E. Richenberg, "Steam Jet Ejectors in Pilot and Production Plants," *Chem. Eng. Process.,* **63**, 3 (1967).

Manohar, D.V., "High-Efficiency Jet Ejector," (Research Progress Report) Department of Chemical Engineering, Texas A&M University, College Station, Texas (2001).

Mark, M. and Foster, A. R., *Thermodynamics Principles and Applications*, Allyn and Bacon, Inc., Boston, MA (1979).

Matsuo, K, and H. D. Kim, "Shock Train and Pseudo-Shock Phenomena in Internal Gas Flows," *Prog. Aero. Sci*., **35**, 1 (1999).

Neve, R. S., "Computational Fluid Dynamics Analysis of Diffuser Performance in Gas-Powered Jet Pumps," *Int. J. Heat Fluid Fow.,* **14**, 4 (1993).

Reinke, B., M. Neal, and S. K. Gupta, "Flow Inside A Jet-Ejector Pump for Vacuum Applications," *J. Ind. Inst. Chem. Engrs*., **44**, 3 (2002).

Riffat, S. B., and P. Everitt, "Experimental and CFD Modeling of an Ejector System for Vehicle Air Conditioning*," J. Inst. Ener*gy, **72** (1999).

Riffat, S. B., G. Gam, and S. Smith, "Computational Fluid Dynamics Applied to Ejector Pumps," *Appl. Therm. Eng. J*., **16**, 4 (1996).

Riffat, S. B., and S. A. Omer, "CFD Modelling and Experimental Investigation of an Ejector Refrigeration System Using Methanol as the Working Fluid," *Int. J. Energy Res.*, **25**, 2 (2001).

Schmitt, H., *Diversity of Jet Pump and Ejector Techniques*, The Second Symposium on Jet Pumps & Ejectors and Gas Lift Techniques*,* BHRA Fluid Engineering, Bedford, UK (1975).

Sissom, L. E., and D. R. Pitts, *Elements of Transport Phenomena*, Mc-Graw Hill, New York (1972).

Smith, J. M., and H. C. Van Ness, *Introduction to Chemical Engineering Thermodynamics*, 3rd ed., McGraw-Hill, New York (1975).

Steam Jet Syphons; Design, Construction, and Operation, AMETEK Inc., Cornwells Heights, PA (1979).

Talpallikar, M. V., C. E. Smith, M. C. Lai, and J. D. Holdeman, " CFD Analysis of Jet Mixing in Low NOx Flametube Combustors," *ASME J. Eng. Gas Turbines Power*, **114** (1998).

APPENDIX A

MATHEMATICAL DERIVATION OF AN EFFICIENCY EQUATION

An efficiency equation is needed to determine the performance of the jet ejector, and to determine the optimal geometry. Unfortunately, the conventional efficiency equation cannot be applied directly in our research for two reasons, which are explained below; therefore, a new efficiency equation is derived. Before applying this new equation in the optimization study, the accuracy of the equation must be verified first.

The traditional efficiency equation is presented in Equation A1.

$$\eta = \frac{M_p\left(H_o - H_p\right)}{M_m\left(H_m - H_o\right)} \tag{A1}$$

where,

M_p = mass flow rate of the propelled stream $\left(\text{kg/s}\right)$

M_m = mass flow rate of the motive stream $\left(\text{kg/s}\right)$

H_m = specific enthalpy of the motive stream $\left(\text{J/kg}\right)$

H_o = specific enthalpy of the outlet stream $\left(\text{J/kg}\right)$

H_p = specific enthalpy of the propelled stream $\left(\text{J/kg}\right)$

The traditional efficiency equation cannot be applied for the following reasons:

1. The traditional efficiency equation accounts for only the effect of stream enthalpy. The effect of kinetic energy is not included in the equation, which is incorrect.
2. The traditional efficiency equation is inconvenient to interface with CFD, because CFD does not allow us to specify fluid enthalpy directly.

The derivation and verification of the newly defined efficiency equation are presented in the following section.

In the jet ejector, there are three major energy components concerned.

1. Kinetic energy
2. Pressure energy
3. Flow work

Kinetic Energy

Kinetic energy was introduced by Lord Kelvin in 1856. The importance of this quantity was earlier recognized by Thomas Young, an English physicist, who in 1807 called it simply energy, the first recorded instance of the use of this word (Smith et al., 1975). Kinetic energy has the following general formation:

$$E_k = \frac{1}{2} m\left(u_2^2 - u_1^2\right) = \Delta \frac{mu^2}{2} \tag{A2}$$

where,

E_k = kinetic energy (J)

m = mass of the object (kg)

u_2 = final velocity (m/s)

u_1 = initial velocity (m/s)

From Equation A2, the energy need to accelerate an object from initial velocity u_1 to final velocity u_2 is the kinetic energy.

Pressure Energy

The pressure energy is used to compress the fluid from initial pressure P_1 to final pressure P_2. For compressible fluids, the pressure energy equals to

$$E_P = \dot{m}\left(P\hat{V}\right)\frac{\gamma}{\gamma-1}\left(\left(\frac{P_2}{P_1}\right)^{\frac{\gamma-1}{\gamma}}-1\right) \tag{A3}$$

where,

E_P = pressure energy (J)

$\dot{m}$ = fluid mass flow rate (kg/s)

P = pressure (Pa)

$\hat{V}$ = specific volume (m^3/kg)

γ = ratio of heat capacities = C_P / C_V

P_1 = initial pressure (Pa)

P_2 = final pressure (Pa)

Assume the ideal gas law;

$$PV = nRT = \frac{m}{MW}RT \tag{A4}$$

where,

V = volume $\left(\mathrm{m}^3\right)$

n = number of moles

R = universal gas constant = 8.314 $\frac{\mathrm{J}}{\mathrm{gmol}\cdot\mathrm{K}}$

T = temperature $\left(\mathrm{K}\right)$

MW = molecular weight (g/gmol)

Rearrange Equation A3;

$$\frac{PV}{m} = P\hat{V} = \frac{RT}{MW} \tag{A5}$$

Substituting Equation A5 into Equation A3 gives rise to Equation A6.

$$E_P = \dot{m}\left(\frac{RT}{MW}\right)\frac{\gamma}{\gamma-1}\left(\left(\frac{P_2}{P_1}\right)^{\frac{\gamma-1}{\gamma}} - 1\right) \tag{A6}$$

Flow Work

Flow energy relates to the mass flowing into or out of the system (Mark et al., 1979). If the mass is flowing into the system, the surroundings provide the energy to the mass; conversely, the system must do work on the surroundings if the mass is flowing out of the system. Figure A1 displays the mechanism of flow work.

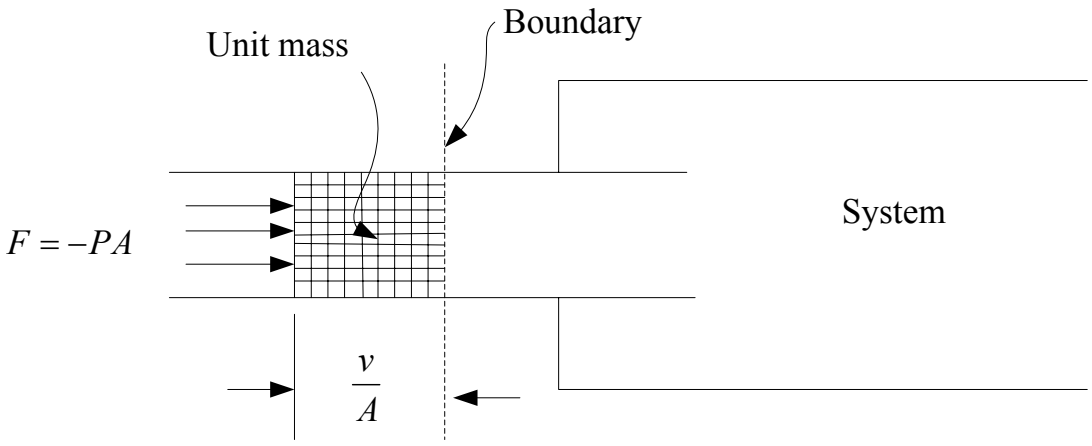

Figure A1. As a unit mass crosses the boundary upon entering the system, the surroundings do an amount of work $-PV$ on the system. This energy necessary to cross the boundary is known as flow energy or flow work (Mark and Foster, 1979).

As shown in Figure A1, if the unit mass is to enter the system, a force is necessary to overcome the pressure at the entry position (Mark et al., 1979). The amount of force to push the unit mass to enter the system equals a factor between pressure and the cross-sectional area which the unit mass moves through. If we multiply the cross-sectional area with the distance which the unit mass has gone through, it will equal the volume of the unit mass; which is called the specific volume of the substance.

$$\hat{V} = A \times \text{Distance} \tag{A7}$$

Consequently,

$$\text{Distance} = \frac{\hat{V}}{A} \tag{A8}$$

To derive the flow work, the work definition is applied first.

$$\text{Flow work} = \text{Force} \times \text{Distance} \tag{A9}$$

which is;

$$\text{Flow work} = PA \times \frac{\hat{V}}{A} = P\hat{V} \tag{A10}$$

Note that P and $\hat{V}$ are both properties that relate to the fluid entering or leaving the system. As such, the flow work will be associated with the mass entering or leaving the system (Mark et al., 1979).

The Efficiency Equation Derivation

As stated above, there are three major energy components associated in the system: kinetic energy, pressure energy, and flow work. Figure A2 displays the relationship of the energy in the system.

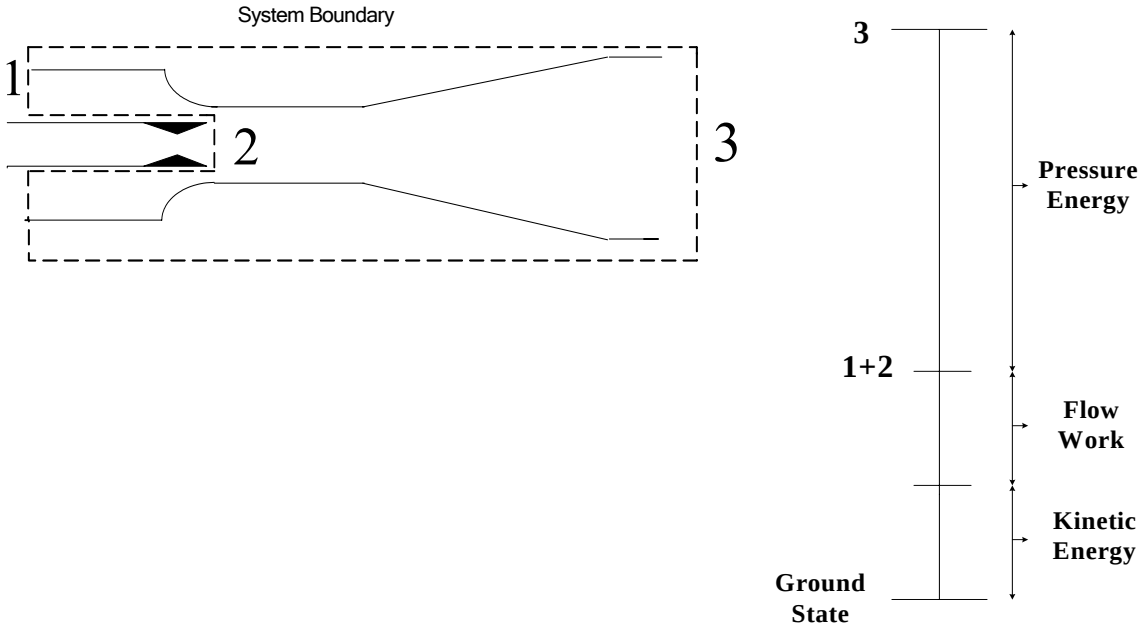

Figure A2. Energy diagram in jet ejector.

The efficiency equation is formulated as follows:

$$\eta = \frac{\text{Total Energy Output}}{\text{Total Energy Input}} \tag{A11}$$

From Figure A2,

$$\text{Total Energy Output} = [\text{Kinetic Energy} + \text{Flow Work} + \text{Pressure Work}]_{\text{output}} \tag{A12}$$

$$\text{Total Energy Input} = [\text{Kinetic Energy} + \text{Flow Work}]_{\text{propelled}} + [\text{Kinetic Energy} + \text{Flow Work}]_{\text{motive}} \tag{A13}$$

which is,

$$\text{Total Energy Output} = \frac{1}{2}\dot{m}_1 v_1^2 + \frac{1}{2}\dot{m}_m v_m^2 + \dot{m}_1 \frac{RT_1}{MW} + \dot{m}_m \frac{RT_m}{MW} + \dot{m}_1 \left(\frac{RT_1}{MW}\right)\frac{\gamma}{\gamma-1}\left[\left(\frac{P_2}{P_1}\right)^{\frac{\gamma-1}{\gamma}} - 1\right] + \dot{m}_m \left(\frac{RT_m}{MW}\right)\frac{\gamma}{\gamma-1}\left[\left(\frac{P_2}{P_m}\right)^{\frac{\gamma-1}{\gamma}} - 1\right] \tag{A14}$$

$$\text{Total Energy Input} = \frac{1}{2}\dot{m}_1 v_1^2 + \frac{1}{2}\dot{m}_m v_m^2 + \dot{m}_1 \frac{RT_1}{MW} + \dot{m}_m \frac{RT_m}{MW} \tag{A15}$$

where,

P_2 = outlet pressure (Pa)

P_1 = inlet pressure of propelled stream (Pa)

P_m = inlet pressure of motive stream (Pa)

v_2 = outlet velocity (m/s)

v_1 = inlet velocity of propelled stream (m/s)

v_m = inlet velocity of motive stream (m/s)

m_1 = inlet mass flow rate of propelled stream $(\mathrm{kg/s})$

m_m = inlet mass flow rate of motive stream $(\mathrm{kg/s})$

T_1 = temperature of propelled stream (K)

T_m = temperature of motive stream (K)

Combining Equations A14 and A15, the newly defined efficiency equation is:

$$\eta = \frac{\frac{1}{2}\left(\dot{m}_m+\dot{m}_1\right)v_2^2+\dot{m}_1\frac{RT_1}{MW}+\dot{m}_m\frac{RT_m}{MW}+\dot{m}_1\left(\frac{\gamma}{\gamma-1}\right)\frac{RT_1}{MW}\left[\left(\frac{P_2}{P_1}\right)^{\frac{\gamma-1}{\gamma}}-1\right]+\dot{m}_m\left(\frac{\gamma}{\gamma-1}\right)\frac{RT_m}{MW}\left[\left(\frac{P_2}{P_m}\right)^{\frac{\gamma-1}{\gamma}}-1\right]}{\frac{1}{2}\dot{m}_1 v_1^2+\frac{1}{2}\dot{m}_m v_m^2+\dot{m}_1\frac{RT_1}{MW}+\dot{m}_m\frac{RT_m}{MW}} \qquad \text{(A16)}$$

Next, the validation of the efficiency equation is described. The model to verify the equation is presented in Figure A3. It is assumed that every device operates at 100% efficiency. Given this assumption, if the efficiency equation is defined properly, the outlet conditions should equal the inlet conditions.

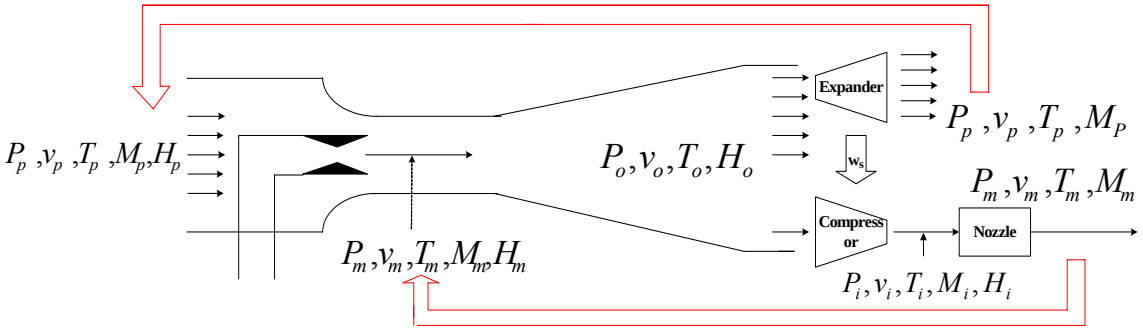

Figure A3. Ejector including the turbine-compressor cycle.

Restated, by going through reversible processes (jet ejector, expander, compressor and nozzle) the outlet conditions will be identical to the initial conditions, provided the newly defined efficiency equation is correct. The verification procedure is presented as follows:

1. The propelled and motive stream conditions (e.g., mass flow rate, static pressure, density, velocity, temperature) are defined at the inlet.
2. The static pressure of outlet stream is calculated from the newly defined efficiency equation by assuming that jet ejector operates at 100% efficiency (i.e., the efficiency term on the left hand side of Equation A17 equals 1.0).
3. The outlet stream is separated to two parts. The mass of the first part equals the propelled stream, whereas the second part equals the motive stream.
4. The first part is injected to an isentropic expander. To get back to the initial specified propelled stream, shaft energy is extracted from the outlet stream by the expander.
5. The second part is injected to an isentropic compressor. Energy from the isentropic expander is injected into the isentropic compressor to compress the stream to an intermediate stage before feeding through the isentropic nozzle. The intermediate condition is obtained from this step.
6. The intermediate stream goes through the isentropic nozzle. The stream exiting the nozzle must equal the initial specified motive-stream velocity.

Next, the calculation procedure is explained with a step-by-step instruction.

Step 1: An arbitrary jet ejector is chosen for an analysis. The fluid properties of the propelled and motive streams are specified and displayed in Table A1. Each equipment performs isentropically (frictionless, adiabatic, and 100% efficiency). The static pressure of the outlet stream is calculated from the newly defined efficiency equation.

Table A1. The specified valued of fluid properties.

	Fluid Properties		
	Propelled	Motive	Outlet
Static Pressure (Pa)	101,325	101,325	**Be evaluated**
Temperature (K)	373	373	373
Mass Flow Rate (kg/s)	0.67	0.5	1.17
Velocity (m/s)	10	300	10

Step 2: Assuming that the jet ejector operates at 100% efficiency, the value of the efficiency term of the left-hand side equals 1.0. The denominator of Equation A16 moves to the left hand side (Equation A17).

$$\begin{aligned}&\frac{1}{2}\dot{m}_1 v_1^2+\frac{1}{2}\dot{m}v_m^2+\dot{m}_1\frac{RT_1}{MW}+\dot{m}_m\frac{RT_m}{MW}\\&=\frac{1}{2}\left(\dot{m}_1+\dot{m}_m\right)v_2^2+\dot{m}_1\frac{RT_1}{MW}+\dot{m}_m\frac{RT_m}{MW}+\dot{m}_1\left(\frac{\gamma}{\gamma-1}\right)\frac{RT_1}{MW}\left[\left(\frac{P_2}{P_1}\right)^{\frac{\gamma-1}{\gamma}}-1\right]\\&+\dot{m}_n\left(\frac{\gamma}{\gamma-1}\right)\frac{RT_m}{MW}\left[\left(\frac{P_2}{P_m}\right)^{\frac{\gamma-1}{\gamma}}-1\right]\end{aligned} \tag{A17}$$

To extract the outlet-stream pressure, Equation A17 gives Equation A18.

$$P_2=\left\{\left[\frac{1}{2}\dot{m}_m\left(v_m^2-v_2^2\right)\left(\frac{\gamma-1}{\gamma}\right)\frac{MW}{R}+T_m\dot{m}_m+T_1\dot{m}_1\right]\times\left[\frac{\left(P_1+P_m\right)^{\frac{\gamma-1}{\gamma}}}{\left(T_m\dot{m}_m P_1^{\frac{\gamma-1}{\gamma}}+T_1\dot{m}_1 P_m^{\frac{\gamma-1}{\gamma}}\right)}\right]\right\}^{\frac{\gamma}{\gamma-1}} \tag{A18}$$

All parameters in Equation A18 are substituted by the values providing in Table A1. The static pressure of the outlet stream is

$$P_2=113{,}117.20 \quad \text{Pa}$$

The answer can be checked by back substituting P_2 in Equation A16. If the answer is correct, the value of the efficiency term will equal to unity.

Step 3: A following energy balance equation is applied to calculate the temperature of the outlet stream.

$$\Delta E_K+\Delta E_P+\Delta\left(H+PV\right)=W+Q \tag{A19}$$

where,

ΔE_K = kinetic energy change (J)

ΔE_P = potential energy change (J)

H = enthalpy (J)

PV = flow work (J)

W = shaft work (J)

Q = heat exchanging between the system and surrounding (J)

The flow work and potential energy difference are zero, so only the shaft work and enthalpy term appear in the system. Equation 19 is reduced to Equation A20.

$$\Delta KE = -\Delta H \tag{A20}$$

which is:

$$\Delta KE = \frac{1}{2}\dot{m}_m\left(v_2^2 - v_m^2\right) + \frac{1}{2}\dot{m}_1\left(v_2^2 - v_1^2\right) \tag{A21}$$

$$\Delta H = \dot{m}_1 C_P\left(T_2 - T_1\right) + \dot{m}_m C_P\left(T_2 - T_m\right) \tag{A22}$$

where,

C_P = heat capacity at constant pressure $(\mathrm{J/(mol \cdot K)})$

An ideal gas law is applied to evaluate C_P

$$C_P = \frac{\gamma}{\gamma - 1}R = \frac{1.3}{0.3}R = 4.333R \tag{A23}$$

Equations (A20), (A21), (A22) are substituted into Equation A19. Equation A19 is rearranged to compute the temperature of the outlet stream, which is

$$T_2 = \frac{1}{2}\left(\frac{MW}{C_P}\right)\frac{\dot{m}_m}{\left(\dot{m}_m + \dot{m}_1\right)}\left(v_m^2 - v_2^2\right) + \frac{\left(\dot{m}_1 T_1 + \dot{m}_m T_m\right)}{\left(\dot{m}_1 + \dot{m}_m\right)} \tag{A24}$$

$$T_2 = 382.60 \text{ K}$$

Step 4: The shaft work from the turbine is evaluated by

$$W_S = \dot{m}_1\left(\frac{\gamma}{\gamma - 1}\right)\left(\frac{RT_2}{MW}\right)\left[1 - \left(\frac{P_1}{P_2}\right)^{\frac{\gamma-1}{\gamma}}\right] \tag{A25}$$

where,

$W_S =$ shaft work (J)

$$W_S = 12{,}870.70 \text{ J}$$

Step 5: The shaft work powers the compressor, which compresses the second part of the outlet stream. An intermediate condition before going though the nozzle is expected after this stage. The pressure can be computed by the following Equation A26.

$$W_S = \dot{m}_m\left(\frac{\gamma}{\gamma - 1}\right)\left(\frac{RT_2}{MW}\right)\left[\left(\frac{P_3}{P_2}\right)^{\frac{\gamma-1}{\gamma}} - 1\right] \tag{A26}$$

To extract P_3, Equation A26 is rearranged and gives rise to Equation A27.

$$P_3 = P_2 \times \left[\left(\frac{\gamma - 1}{\gamma}\right)\frac{MW \cdot W_S}{RT_2 \cdot \dot{m}_m} + 1\right]^{\frac{\gamma}{\gamma-1}} \tag{A27}$$

$$P_3 = 130{,}541.89 \text{ Pa}$$

Step 6: The temperature of the intermediate stream is calculated by the ideal gas law for a compressible gas, which is

$$\frac{T_3}{T_2} = \left(\frac{P_3}{P_2}\right)^{\frac{\gamma-1}{\gamma}} \tag{A28}$$

where,

P_3 = static pressure at the intermediate stage (Pa)

T_3 = temperature at the intermediate stage (K)

$$T_3 = T_2 \times \left(\frac{P_3}{P_2}\right)^{\frac{\gamma-1}{\gamma}} = 395.46 \text{ K} \tag{A29}$$

Step 7: The intermediate stream is fed through the nozzle. The velocity at the nozzle exit is calculated by Equation A30.

$$\frac{1}{2}\left(v_m^2 - v_3^2\right) = \left(\frac{\gamma}{\gamma-1}\right)\left(\frac{RT_3}{MW}\right)\left[1 - \left(\frac{P_m}{P_3}\right)^{\frac{\gamma-1}{\gamma}}\right] \tag{A30}$$

where,

v_3 = fluid velocity at the intermediate stage (m/s)

$$v_m = \sqrt{v_3^2 + \frac{2 \cdot RT_3}{MW}\left(\frac{\gamma}{\gamma-1}\right)\left[1 - \left(\frac{P_m}{P_3}\right)^{\frac{\gamma-1}{\gamma}}\right]} \tag{A31}$$

$$v_m = 300.005 \text{ m/s}$$

Step 8: Finally, the analysis is extended by adjusting propelled and motive stream mass flow rate with a wide range from 0.1 to 1.0 kg/s. The calculation result of both cases is displayed in Table A2 and A3 respectively.

Table A2. Calculation result from adjusting propelled-stream mass flow rate.

Stream Properties of Each Stage	M_p (kg/s)					
	0.1	0.3	0.5	0.7	0.9	1.0
P_2 (Pa)	125,270.6	118,914.6	115,222.0	112,809.7	111,110.6	110,436.5
T_2 (K)	391.7	387.0	384.2	382.4	381.0	380.5
W_s (J/s)	3781.8	8612.0	11566.6	13560.4	14996.5	15573.8
P_3 (Pa)	130,540.8	130,540.8	130,540.8	130,540.8	130,540.8	130,540.8
T_3 (K)	395.5	395.5	395.5	395.5	395.5	395.5
V_m (m/s)	**300.00**	**300.00**	**300.00**	**300.00**	**300.00**	**300.00**

Table A3. Calculation result from adjusting motive-stream mass flow rate.

Stream Properties of Each Stage	M_m (kg/s)					
	0.1	0.3	0.5	0.7	0.9	1.0
P_2 (Pa)	104,803.30	109,758.61	113,116.81	115,541.89	117,374.97	118,133.30
T_2 (K)	375.92	379.95	382.60	384.48	385.87	386.45
W_s (J/s)	4,114.78	9,695.20	13,303.66	15,828.46	17,694.01	18,455.32
P_3 (Pa)	130,540.82	130,540.82	130,540.82	130,540.82	130,540.82	130,540.82
T_3 (K)	395.46	395.46	395.46	395.46	395.46	395.46
V_m (m/s)	**300.00**	**300.00**	**300.00**	**300.00**	**300.00**	**300.00**

Conclusion, the condition of the outlet stream is identical to the initial specified condition over a wide range of propelled and motive stream mass flow rates. This validates the newly defined efficiency equation.

APPENDIX B

RESULTS OF MODEL ACCURACY EXPERIMENT

In the model accuracy experiment, the simulation results are compared to experimental results obtained from Manohar Vishwanathappa, a graduate chemical engineering student at Texas A&M University. Both of the simulation and experimental results are summarized in this section. The experimental results are shown in Table B1, whereas the simulation results are shown in Table B2.

Table B1. Experimental data.

v_m (m/s)	Pinch 0		Pinch 1		Pinch 2		Pinch 3	
	M_p (kg/s)	ΔP (Pa)	M_p (kg/s)	ΔP (Pa)	M_p (kg/s)	ΔP (Pa)	M_p (kg/s)	ΔP (Pa)
562.86	0.65	684.96	0.61	856.82	0.57	1,153.22	0.37	2,179.41
527.86	0.61	637.63	0.57	732.28	0.54	1,028.68	0.36	1,853.12
490.03	0.55	468.26	0.53	607.75	0.5	841.87	0.34	1,556.72
448.95	0.5	358.67	0.47	468.26	0.48	622.69	0.33	1,120.84
411.19	0.44	234.13	0.42	326.28	0.41	435.88	0.32	794.55

The pinch valve is located at the downstream of jet ejector to produce back pressure. The number behind the pinch indicates the diameter of the pinch valve. Pinch 0 (see Figure B1-A) indicates that the diameter is largest (perfectly open). Pinch 3 (see Figure B1-D) indicates that the diameter is smallest. The geometry of the jet ejector is detailed in Appendix F.

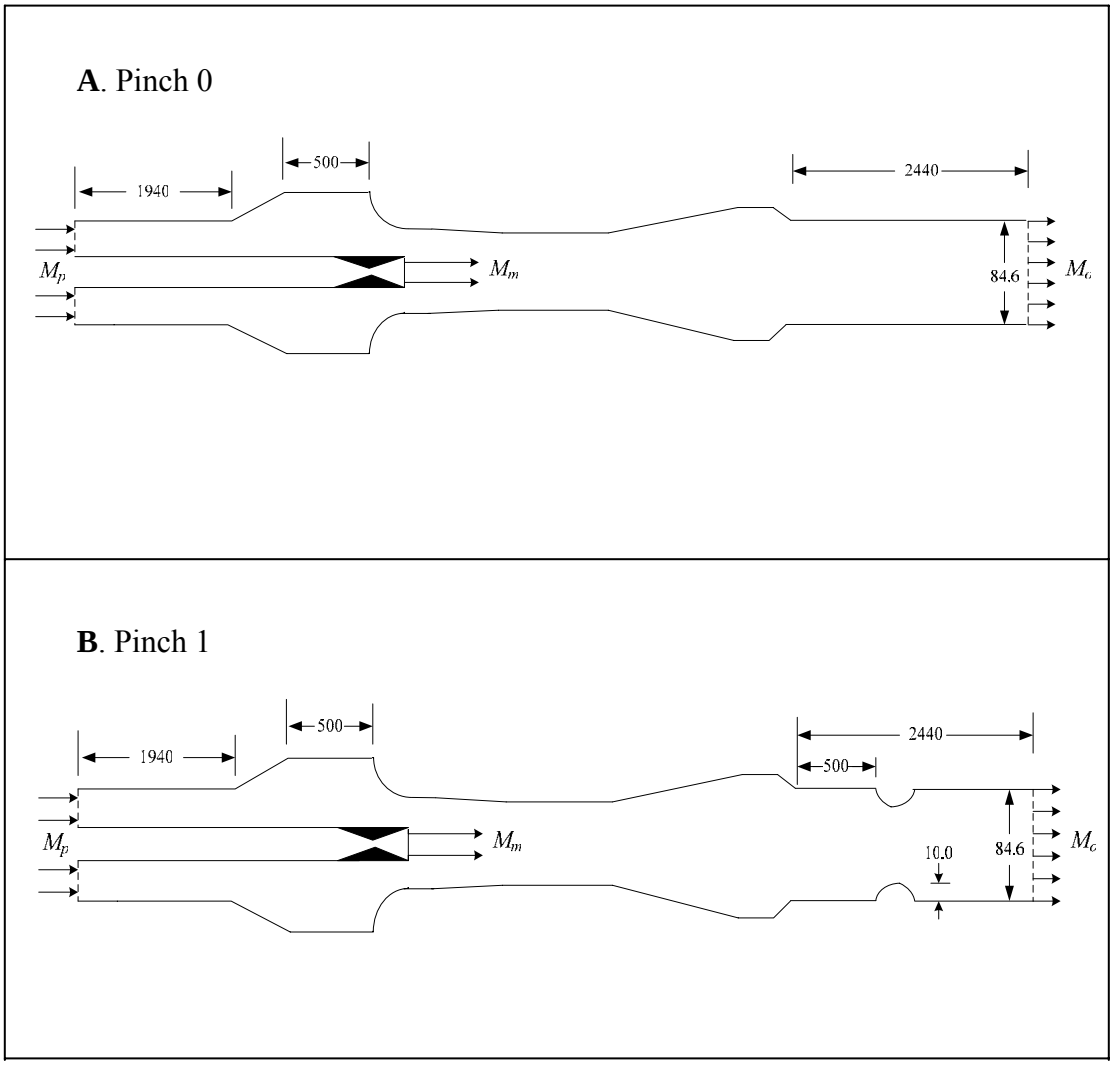

Figure B1. Location and dimension of pinch valve in an experimental set A) pinch 0, B) pinch 1, C) pinch 2, D) pinch 3 (unit: millimeter).

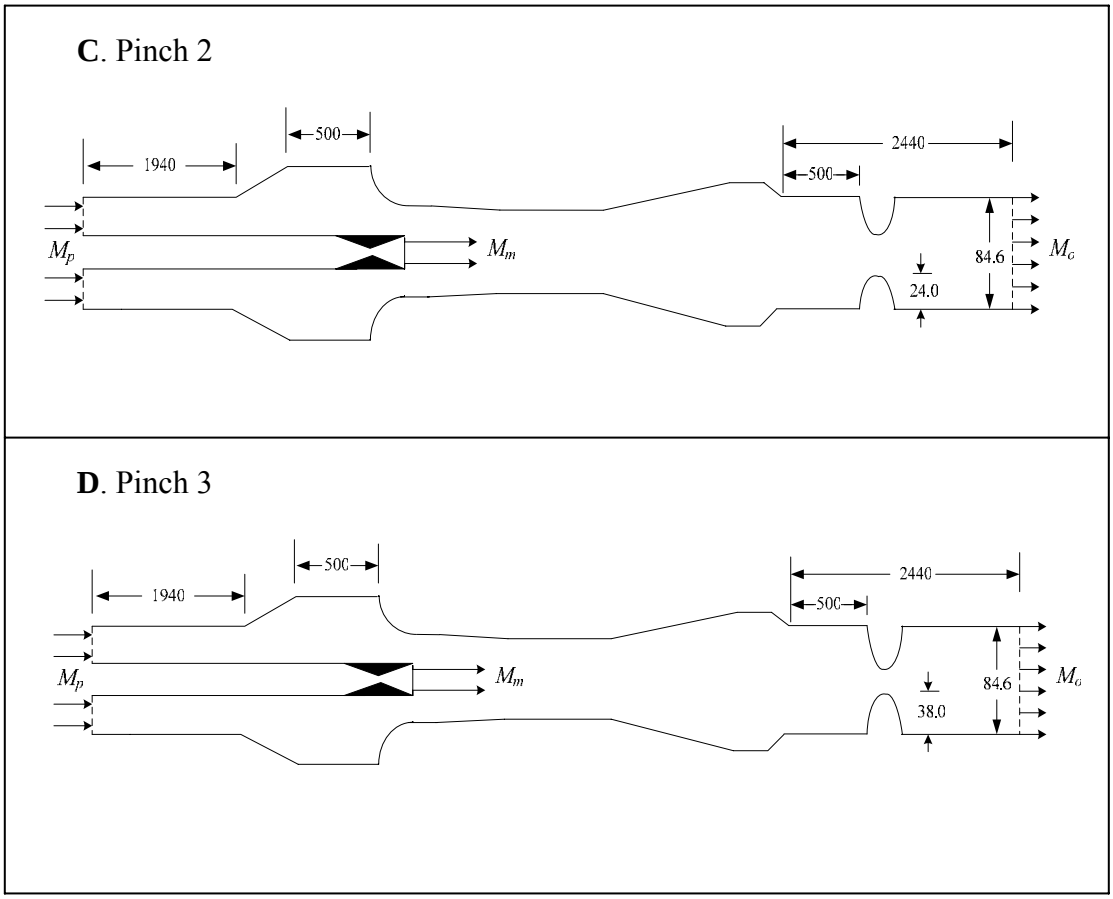

Figure B1. (Continued)

Because the pinch valve itself is not included in the simulation model, the propelled-stream mass flow rate is adjusted to match the back pressure produced by the pinch valve. This removes the complexity of trying to simulate the flow through the pinch valve. In the simulation experiment, the propelled mass flow rate is adjusted over a wide range to cover the experimental region. All the simulation results according to the motive stream velocity are summarized as follows:

Table B2. Simulation data A) motive stream velocity at 563 m/s, B) at 528 kg/s, C) at 490 m/s, D) at 449 m/s, E) at 411 m/s.

A. Motive stream velocity = 563 m/s

v_m (m/s)	M_p (kg/s)	Pressure (Pa)		
		Inlet	Outlet	Difference
563	0.67	100,990	101,320	330
	0.65	100,535	101,321	786
	0.61	100,106	101,321	1,215
	0.58	99,851	101,322	1,471
	0.55	99,617	101,322	1,705
	0.52	99,400	101,322	1,922
	0.49	99,195	101,322	2,127
	0.46	99,002	101,322	2,320
	0.43	98,822	101,322	2,500
	0.4	98,649	101,322	2,673
	0.37	98,484	101,322	2,838

Table B2. (Continued).

B. Motive stream velocity = 528 m/s

v_m (m/s)	M_p (kg/s)	Pressure (Pa)		
		Inlet	Outlet	Difference
528	0.61	100,906	101,321.3	415.3
	0.58	100,654.5	101,321.5	667
	0.55	100,423.4	101,321.6	898.2
	0.52	100,209.3	101,321.8	1,112.5
	0.49	100,009.8	101,322	1,312.2
	0.46	99,821.4	101,322.1	1,500.7
	0.43	99,649	101,322.3	1,673.3
	0.40	99,484.7	101,322.4	1,837.7
	0.37	99,446	101,322.5	1,876.5
	0.34	99,144	101,322.8	2,178.8

C. Motive stream velocity = 490 m/s

v_m (m/s)	M_p (kg/s)	Pressure (Pa)		
		Inlet	Outlet	Difference
490	0.55	101,062	101,321.7	259.7
	0.52	100,649.4	101,321.9	472.5
	0.49	100,651.5	101,322	670.5
	0.46	100,467	101,322.2	855.2
	0.43	100,300	101,322.4	1,022.4
	0.40	100,139	101,322	1,183
	0.37	99,969.5	101,322.6	1,333.1
	0.28	99,705	101,323	1,618

Table B2. (Continued).

D. Motive stream velocity = 449 m/s

v_m (m/s)	M_p (kg/s)	Pressure (Pa)		
		Inlet	Outlet	Difference
449	0.49	101,176	101,322	146
	0.46	100,993	101,322	329
	0.43	100,823	101,322	499
	0.40	100,670	101,323	653
	0.37	100,531	101,323	792
	0.34	100,399	101,323	924
	0.31	100,266	101,323	1,057
	0.28	100,139	101,323	1,184

E. Motive stream velocity = 411 m/s

v_m (m/s)	M_p (kg/s)	Pressure (Pa)		
		Inlet	Outlet	Difference
411	0.43	101,194	101,322	128
	0.40	101,038	101,323	285
	0.37	100,896	101,323	427
	0.31	100,651	101,323	672
	0.28	100,535	101,323	788
	0.25	100,427	101,323	896

APPENDIX C

FLUID PROPERTIES OF DIMENSIONLESS ANALYSIS

There are two stages involved in the dimensionless analysis. The first stage is to investigate the proper dimensionless group. And the second stage is further investigation on different fluid type and geometric scale. There are two approaches applied in the first stage, which are

1. Maintain the motive-stream Mach number and C_p value
2. Maintain the motive-stream velocity and C_p value

In the second stage, additional fluid types (hydrogen, nitrogen, and carbon dioxide) and geometric scale (2×) are included. The detail of fluid properties (e.g., pressure, mass flow rate, velocity, density, speed of sound, and viscosity) are included in this section. The fluid properties of the first approach (maintaining the Mach number and C_p) are summarized in Table C1, and the second approach (maintaining the velocity and *Cp*) are summarized in Table C2. The fluid properties of the second stage are summarized in Table C3.

Because the results of the first stage experiment show that C_{pm} and Reynolds ratio deviate significantly on operating pressure, the influence of the operating pressure is studied explicitly. Steam and 4× scale geometry are applied in this experiment. The fluid properties are summarized in Table C4.

Table C1. Fluid properties of maintaining the Mach number and *Cp*. A) static pressure, B) mass flow rate, C) velocity, D) density, and E) speed of sound and viscosity.

A Static pressure.

Fluid Type	Geometric Scale	Operating Pressure (atm)	Static Pressure (Pa)		
			Motive Stream	Propelled Stream	Outlet Stream
Steam	4×	0.1	10,087.3	9,414.0	10,135.2
		0.2	20,171.1	18,804.5	20,270.2
		0.3	30,254.0	28,179.5	30,405.1
		0.5	50,418.4	46,928.1	50,674.9
		0.6	60,500.9	56,300.5	60,809.6
		1.0	100,825.1	93,768.0	101,349.1
		3.0	302,444.4	280,930.6	304,044.1
		6.0	604,844.9	561,745.9	608,063.5
		8.0	806,057.8	751,575.7	810,129.4
		10.0	1,007,319.2	940,908.4	1,012,277.2
	8×	0.1	10,086.2	9,400.7	10,135.1
		0.2	20,169.5	18,778.5	20,270.0
		0.3	30,251.9	28,150.2	30,404.8
		0.5	50,415.6	46,884.5	50,674.5
		0.6	60,497.4	56,257.5	60,809.2
		1.0	100,820.4	93,688.4	101,348.6

Table C1. (Continued).

A Static pressure (Continued).

Fluid Type	Geometric Scale	Operating Pressure (atm)	Static Pressure (Pa)		
			Motive Stream	Propelled Stream	Outlet Stream
Steam	8×	3.0	302,428.8	280,895.8	304,031.8
		6.0	604,888.3	561,880.5	608,088.3
		8.0	806,486.5	749,014.3	810,763.7
		10.0	1,008,087.5	935,951.1	1,013,472.9
Air	4×	0.1	10,084.8	9,376.4	10,135.4
		0.2	20,166.4	18,724.7	20,270.6
		0.3	30,247.1	28,065.8	30,405.6
		0.5	50,406.0	46,733.9	50,675.8
		0.6	60,485.5	56,056.8	60,810.7
		1.0	100,798.6	93,359.9	101,350.8
		3.0	302,356.4	279,659.6	304,048.9
		6.0	604,680.8	559,087.2	608,080.6
		8.0	806,149.2	746,456.5	810,589.7
		10.0	1,007,537.8	933,484.6	1,013,058.2
	8×	0.1	10,083.8	9,362.3	10,135.3
		0.2	20,164.2	18,699.5	20,270.3
		0.3	30,244.2	28,030.2	30,405.3
		0.5	50,402.5	46,682.7	50,675.4

Table C1. (Continued).

A Static pressure (Continued).

Fluid Type	Geometric Scale	Operating Pressure (atm)	Static Pressure (Pa)		
			Motive Stream	Propelled Stream	Outlet Stream
Air	8×	0.6	60,480.9	55,997.4	60,810.2
		1.0	100,793.6	93,277.5	101,350.2
		3.0	302,342.4	279,544.4	304,040.2
		6.0	604,721.6	559,421.8	608,097.6
		8.0	806,278.1	745,542.6	810,797.14
		10.0	1,007,827.6	931,861.7	1,013,491.5

B Mass flow rate.

Fluid Type	Geometric Scale	Operating Pressure (atm)	Mass Flow Rate (kg/s)		
			Motive Stream	Propelled Stream	Outlet Stream
Steam	4×	0.1	0.270	0.911	1.178
		0.2	0.541	1.833	2.369
		0.3	0.811	2.778	3.589
		0.5	1.352	4.627	5.939
		0.6	1.622	5.558	7.170
		1.0	2.704	9.314	11.988
		3.0	8.112	28.049	36.161
		6.0	16.224	56.165	72.389

Table C1. (Continued).

B Mass flow rate (Continued).

Fluid Type	Geometric Scale	Operating Pressure (atm)	Mass Flow Rate (kg/s)		
			Motive Stream	Propelled Stream	Outlet Stream
Steam	4×	8.0	21.632	73.865	94.697
		10.0	27.040	91.733	117.273
	8×	0.1	1.082	3.660	4.741
		0.2	2.163	7.371	9.534
		0.3	3.245	11.095	14.340
		0.5	5.408	18.566	23.973
		0.6	6.490	22.284	28.774
		1.0	10.816	37.312	48.128
		3.0	32.448	112.270	144.718
		6.0	64.896	224.422	289.318
Air	4×	8.0	86.528	299.786	386.314
		10.0	108.160	374.720	482.880
		0.1	0.367	1.183	1.545
		0.2	0.734	2.426	3.160
		0.3	1.102	3.592	4.680
		0.5	1.836	6.052	7.888
		0.6	2.203	7.288	9.491
		1.0	3.672	12.162	15.833

Table C1. (Continued).

B Mass flow rate (Continued).

Fluid Type	Geometric Scale	Operating Pressure (atm)	Mass Flow Rate (kg/s)		
			Motive Stream	Propelled Stream	Outlet Stream
Air	4×	3.0	11.015	36.599	47.614
		6.0	22.031	73.080	95.111
		8.0	29.375	97.157	125.932
		10.0	36.718	124.272	160.990
	8×	0.1	1.469	4.751	6.219
		0.2	2.937	9.572	12.510
		0.3	4.406	14.411	18.817
		0.5	7.344	24.115	31.458
		0.6	8.812	28.997	37.809
		1.0	14.687	48.464	63.152
		3.0	44.062	146.165	190.226
		6.0	88.123	292.101	380.224
		8.0	117.498	389.633	507.130
		10.0	146.872	487.143	634.015

Table C1. (Continued).

C Velocity magnitude.

Fluid Type	Geometric Scale	Operating Pressure (atm)	Velocity Magnitude (m/s)		
			Motive Stream	Propelled Stream	Outlet Stream
Steam	4×	0.1	510.760	28.71	33.07
		0.2	510.760	28.96	33.27
		0.3	510.760	29.15	33.41
		0.5	510.760	29.30	33.53
		0.6	510.760	29.35	33.57
		1.0	510.760	29.49	33.67
		3.0	510.760	29.75	33.85
		6.0	510.760	29.78	33.89
		8.0	510.760	28.94	33.32
		10.0	510.760	28.56	33.04
	8×	0.1	510.760	28.99	33.29
		0.2	510.760	29.23	33.47
		0.3	510.760	29.35	33.56
		0.5	510.760	29.49	33.67
		0.6	510.760	29.50	33.67
		1.0	510.760	29.66	33.79
		3.0	510.760	29.76	33.87
		6.0	510.760	29.74	33.86

Table C1. (Continued).

C Velocity magnitude (Continued).

Fluid Type	Geometric Scale	Operating Pressure (atm)	Velocity Magnitude (m/s)		
			Motive Stream	Propelled Stream	Outlet Stream
Steam	8×	8.0	510.760	29.75	34.10
		10.0	510.760	29.82	33.94
Air	4×	0.1	406.890	23.27	27.00
		0.2	406.890	23.50	27.17
		0.3	406.890	23.62	27.26
		0.5	406.890	23.75	27.36
		0.6	406.890	23.81	27.41
		1.0	406.890	23.93	27.49
		3.0	406.890	24.15	27.65
		6.0	406.890	24.21	27.70
		8.0	406.890	23.97	27.53
		10.0	406.890	23.88	27.42
	8×	0.1	406.890	23.50	27.17
		0.2	406.890	23.70	27.33
		0.3	406.890	23.81	27.40
		0.5	406.890	23.92	27.48
		0.6	406.890	23.97	27.53
		1.0	406.890	24.06	27.59

Table C1. (Continued).

C Velocity magnitude (Continued).

Fluid Type	Geometric Scale	Operating Pressure (atm)	Velocity (m/s)		
			Motive Stream	Propelled Stream	Outlet Stream
Air	8×	3.0	406.890	24.21	27.70
		6.0	406.890	24.13	27.64
		8.0	406.890	24.19	27.69
		10.0	406.890	24.21	27.70

D Density.

Fluid Type	Geometric Scale	Operating Pressure (atm)	Density (kg/m^3)		
			Motive Stream	Propelled Stream	Outlet Stream
Steam	4×	0.1	0.070	0.055	0.059
		0.2	0.139	0.109	0.118
		0.3	0.209	0.164	0.177
		0.5	0.348	0.273	0.294
		0.6	0.417	0.327	0.353
		1.0	0.695	0.545	0.588
		3.0	2.084	1.633	1.765
		6.0	4.170	3.270	3.529
		8.0	5.434	4.371	4.699
		10.0	6.688	5.470	5.870

Table C1. (Continued).

D Density (Continued).

Fluid Type	Geometric Scale	Operating Pressure (atm)	Density (kg/m^3)		
			Motive Stream	Propelled Stream	Outlet Stream
Steam	8×	0.1	0.070	0.055	0.059
		0.2	0.139	0.109	0.118
		0.3	0.210	0.164	0.177
		0.5	0.347	0.273	0.294
		0.6	0.417	0.327	0.353
		1.0	0.695	0.545	0.588
		3.0	2.084	1.633	1.765
		6.0	4.168	3.266	3.529
		8.0	5.560	4.360	4.679
		10.0	6.946	5.441	5.882
Air	4×	0.1	0.118	0.088	0.095
		0.2	0.236	0.175	0.189
		0.3	0.355	0.262	0.284
		0.5	0.591	0.437	0.473
		0.6	0.709	0.524	0.567
		1.0	1.182	0.873	0.946
		3.0	3.544	2.614	2.837
		6.0	7.087	5.226	5.673

Table C1. (Continued).

D Density (Continued).

Fluid Type	Geometric Scale	Operating Pressure (atm)	Density (kg/m^3)		
			Motive Stream	Propelled Stream	Outlet Stream
Air	4×	8.0	9.353	6.978	7.560
		10.0	11.630	8.725	9.439
	8×	0.1	0.118	0.088	0.095
		0.2	0.236	0.175	0.189
		0.3	0.354	0.262	0.284
		0.5	0.591	0.434	0.473
		0.6	0.709	0.524	0.574
		1.0	1.181	0.872	0.946
		3.0	3.543	2.613	2.837
		6.0	7.087	5.229	5.673
		8.0	9.449	6.970	7.564
		10.0	11.811	8.710	9.455

Table C1. (Continued).

E Speed of sound and viscosity.

Fluid Type	Geometric Scale	Operating Pressure (atm)	Speed of Sound (m/s)		Viscosity ($\times 10^{-5}$; kg/(m·s))	
			Motive Stream	Propelled Stream	Motive Stream	Propelled Stream
Steam	4×	0.1	431.52	472.44	1.257	1.517
		0.2	431.52	472.43	1.257	1.517
		0.3	431.52	472.43	1.257	1.517
		0.5	431.51	472.43	1.257	1.517
		0.6	431.51	472.43	1.257	1.517
		1.0	431.51	472.43	1.257	1.517
		3.0	431.51	472.43	1.257	1.517
		6.0	431.50	472.43	1.257	1.517
		8.0	431.53	472.43	1.257	1.517
		10.0	431.57	472.44	1.257	1.517
	8×	0.1	431.52	472.43	1.257	1.517
		0.2	431.52	472.43	1.257	1.517
		0.3	431.51	472.43	1.257	1.517
		0.5	431.51	472.43	1.257	1.517
		0.6	431.51	472.43	1.257	1.517

Table C1. (Continued).

E Speed of sound and viscosity (continued).

Fluid Type	Geometric Scale	Operating Pressure (atm)	Speed of Sound (m/s)		Viscosity ($\times 10^{-5}$; kg/(m·s))	
			Motive Stream	Propelled Stream	Motive Stream	Propelled Stream
Steam	8×	1.0	431.51	472.43	1.257	1.517
		3.0	431.50	472.43	1.257	1.517
		6.0	431.50	472.43	1.257	1.517
		8.0	431.46	472.43	1.257	1.517
		10.0	431.50	472.43	1.257	1.517
Air	4×	0.1	343.73	386.88	1.804	2.111
		0.2	343.73	386.88	1.804	2.111
		0.3	343.73	386.87	1.804	2.111
		0.5	343.72	386.87	1.803	2.111
		0.6	343.72	386.87	1.803	2.111
		1.0	343.72	386.87	1.803	2.111
		3.0	343.72	386.87	1.803	2.111
		6.0	343.71	386.87	1.803	2.111
		8.0	343.71	386.87	1.803	2.111
		10.0	343.78	386.89	1.803	2.111

Table C1. (Continued).

E Speed of sound and viscosity (Continued).

Fluid Type	Geometric Scale	Operating Pressure (atm)	Speed of Sound (m/s)		Viscosity ($\times 10^{-5}$; kg/(m·s))	
			Motive Stream	Propelled Stream	Motive Stream	Propelled Stream
Air	8×	0.1	343.73	386.87	1.804	2.111
		0.2	343.73	386.87	1.804	2.111
		0.3	343.72	386.87	1.803	2.111
		0.5	343.72	386.87	1.803	2.111
		0.6	343.72	386.87	1.803	2.111
		1.0	343.72	386.87	1.803	2.111
		3.0	343.71	386.87	1.803	2.111
		6.0	343.72	386.87	1.803	2.111
		8.0	343.71	386.87	1.803	2.111
		10.0	343.71	386.87	1.803	2.111

Table C2. Fluid properties of maintaining velocity and *Cp*. A) static pressure, B) mass flow rate, C) velocity, D) density, and E) speed of sound and viscosity.

A Static pressure.

Fluid Type	Geometric Scale	Operating Pressure (atm)	Static Pressure (Pa)		
			Motive Stream	Propelled Stream	Outlet Stream
Steam	4×	0.1	9,611.8	9,740.3	10,134.0
		0.2	19,203.4	19,472.5	20,267.8
		0.3	28,779.9	29,190.9	30,401.5
		0.6	57,523.7	58,361.5	60,802.6
		1.0	95,801.7	97,239.5	101,337.7
		3.0	287,070.2	291,532.8	304,011.7
		6.0	573,757.8	582,797.9	608,021.1
		10.0	955,570.8	970,930.2	1,013,273.9
	8×	0.1	9,601.0	9,735.5	10,133.9
		0.2	19,179.5	19,456.6	20,267.6
		0.3	28,757.2	29,180.6	30,401.3
		0.6	57,467.0	58,334.4	60,802.4
		1.0	95,713.5	97,179.2	101,337.4
		3.0	286,937.5	291,418.9	304,010.9
		6.0	574,140.5	583,061.8	608,023.9
		10.0	956,542.8	971,656.1	1,013,367.9

Table C2. (Continued).

A Static pressure (continued).

Fluid Type	Geometric Scale	Operating Pressure (atm)	Static Pressure (Pa)		
			Motive Stream	Propelled Stream	Outlet Stream
Air	4×	0.1	10,084.8	9,376.4	10,135.4
		0.2	20,166.4	18,724.7	20,270.6
		0.3	30,247.1	28,065.8	30,405.6
		0.6	60,485.5	56,056.8	60,810.7
		1.0	100,798.6	93,359.9	101,350.8
		3.0	302,356.4	279,659.6	304,048.9
		6.0	604,680.8	55,9087.2	608,080.6
		10.0	1,007,537.8	933,484.6	1,013,518.2
	8×	0.1	10,083.8	9,362.3	10,135.3
		0.2	20,164.2	18,699.5	20,270.3
		0.3	30,244.2	28,030.2	30,405.3
		0.6	60,480.9	55,997.4	60,810.2
		1.0	100,793.6	93,277.5	101,350.2
		3.0	302,342.4	279,544.4	304,040.2
		6.0	604,721.6	559,421.8	608,097.6
		10.0	1,007,827.6	931,861.7	1,013,491.5

Table C2. (Continued).

B Mass flow rate.

Fluid Type	Geometric Scale	Operating Pressure (atm)	Mass Flow Rate (kg/s)		
			Motive Stream	Propelled Stream	Outlet Stream
Steam	4×	0.1	0.189	0.682	0.871
		0.2	0.377	1.370	1.747
		0.3	0.566	2.050	2.616
		0.6	1.311	4.144	5.275
		1.0	1.884	6.950	8.834
		3.0	5.647	21.000	26.647
		6.0	11.290	41.820	53.110
		10.0	18.867	70.000	88.867
	8×	0.1	0.755	2.743	3.498
		0.2	1.509	5.480	6.959
		0.3	2.262	8.312	10.574
		0.6	4.521	16.710	21.231
		1.0	7.535	28.000	35.535
		3.0	22.615	84.356	106.972
		6.0	45.176	168.000	213.176
		10.0	75.265	280.322	355.587
Air	4×	0.1	0.367	1.183	1.545
		0.2	0.734	2.426	3.160

Table C2. (Continued).

B Mass flow rate (Continued).

Fluid Type	Geometric Scale	Operating Pressure (atm)	Mass Flow Rate (kg/s)		
			Motive Stream	Propelled Stream	Outlet Stream
Air	4×	0.3	1.102	3.592	4.680
		0.6	2.203	7.288	9.491
		1.0	3.672	12.162	15.833
		3.0	11.015	36.599	47.614
		6.0	22.031	73.080	95.111
		10.0	36.718	124.272	160.990
	8×	0.1	1.469	4.751	6.219
		0.2	2.937	9.572	12.510
		0.3	4.406	14.411	18.817
		0.6	8.812	28.997	37.809
		1.0	14.687	48.464	63.152
		3.0	44.062	146.165	190.226
		6.0	88.123	292.1008	380.224
		10.0	146.872	487.143	634.015

Table C2. (Continued).

C Velocity magnitude.

Fluid Type	Geometric Scale	Operating Pressure (atm)	Velocity Magnitude (kg/s)		
			Motive Stream	Propelled Stream	Outlet Stream
Steam	4×	0.1	406.89	20.85	24.45
		0.2	406.89	20.96	24.53
		0.3	406.89	21.13	24.49
		0.6	406.89	21.22	24.69
		1.0	406.89	21.29	24.81
		3.0	406.89	21.46	24.94
		6.0	406.89	21.58	24.86
		10.0	406.89	21.64	24.96
	8×	0.1	406.89	20.98	24.56
		0.2	406.89	21.17	24.43
		0.3	406.89	21.22	24.75
		0.6	406.89	21.33	24.84
		1.0	406.89	21.45	24.95
		3.0	406.89	21.56	25.03
		6.0	406.89	21.46	24.94
		10.0	406.89	21.49	24.96
Air	4×	0.1	406.89	23.27	27.00
		0.2	406.89	23.50	27.17

Table C2. (Continued).

C Velocity magnitude (Continued).

Fluid Type	Geometric Scale	Operating Pressure (atm)	Velocity Magnitude (kg/s)		
			Motive Stream	Propelled Stream	Outlet Stream
Air	4×	0.3	406.89	23.62	27.26
		0.6	406.89	23.81	27.41
		1.0	406.89	23.93	27.49
		3.0	406.89	24.15	27.65
		6.0	406.89	24.21	27.70
		10.0	406.89	23.88	27.42
	8×	0.1	406.89	23.50	27.17
		0.2	406.89	23.70	27.33
		0.3	406.89	23.81	27.40
		0.6	406.89	23.97	27.53
		1.0	406.89	24.06	27.59
		3.0	406.89	24.21	27.70
		6.0	406.89	24.13	27.64
		10.0	406.89	24.21	27.70

Table C2. (Continued).

D Density.

Fluid Type	Geometric Scale	Operating Pressure (atm)	Density (kg/m^3)		
			Motive Stream	Propelled Stream	Outlet Stream
Steam	4×	0.1	0.062	0.057	0.059
		0.2	0.120	0.113	0.118
		0.3	0.186	0.170	0.177
		0.6	0.371	0.339	0.353
		1.0	0.618	0.565	0.588
		3.0	1.851	1.694	1.765
		6.0	3.702	3.386	3.530
		10.0	6.180	5.650	5.883
	8×	0.1	0.062	0.057	0.059
		0.2	0.124	0.113	0.118
		0.3	0.190	0.170	0.177
		0.6	0.371	0.339	0.353
		1.0	0.617	0.565	0.588
		3.0	1.866	1.693	1.765
		6.0	3.700	3.390	3.530
		10.0	6.168	5.646	5.883
Air	4×	0.1	0.118	0.088	0.095
		0.2	0.236	0.175	0.189

Table C2. (Continued).

D Density (Continued).

Fluid Type	Geometric Scale	Operating Pressure (atm)	Density (kg/m^3)		
			Motive Stream	Propelled Stream	Outlet Stream
Air	4×	0.3	0.355	0.262	0.284
		0.6	0.709	0.524	0.567
		1.0	1.182	0.873	0.946
		3.0	3.544	2.614	2.837
		6.0	7.087	5.226	5.673
		10.0	11.630	8.725	9.439
	8×	0.1	0.118	0.088	0.095
		0.2	0.236	0.175	0.189
		0.3	0.355	0.262	0.284
		0.6	0.709	0.524	0.474
		1.0	1.181	0.872	0.946
		3.0	3.543	2.613	2.837
		6.0	7.087	5.229	5.673
		10.0	11.811	8.710	9.455

Table C2. (Continued).

E Speed of sound and viscosity.

Fluid Type	Geometric Scale	Operating Pressure (atm)	Speed of Sound (m/s)		Viscosity ($\times 10^{-5}$; kg/(m·s))	
			Motive Stream	Propelled Stream	Motive Stream	Propelled Stream
Steam	4×	0.1	447.23	472.50	1.354	1.517
		0.2	447.26	472.50	1.354	1.517
		0.3	447.27	472.50	1.354	1.517
		0.6	447.24	472.49	1.354	1.517
		1.0	447.24	472.49	1.354	1.517
		3.0	447.22	472.49	1.354	1.517
		6.0	447.23	472.49	1.354	1.517
		10.0	447.18	472.49	1.353	1.517
		0.1	447.24	472.50	1.354	1.517
		0.2	447.27	472.50	1.354	1.517
		0.3	447.23	472.49	1.354	1.517
		0.6	447.23	472.49	1.354	1.517
		1.0	447.20	472.49	1.353	1.517
		3.0	447.14	472.49	1.353	1.517
		6.0	447.22	472.49	1.354	1.517
		10.0	447.22	472.49	1.354	1.517
Air	4×	0.1	343.73	386.88	1.804	2.111

Table C2. (Continued).

E Speed of sound and viscosity (Continued).

Fluid Type	Geometric Scale	Operating Pressure (atm)	Speed of Sound (m/s)		Viscosity ($\times 10^{-5}$; kg/(m·s))	
			Motive Stream	Propelled Stream	Motive Stream	Propelled Stream
Air	4×	0.2	343.73	386.88	1.804	2.111
		0.3	343.73	386.87	1.804	2.111
		0.6	343.72	386.87	1.803	2.111
		1.0	343.72	386.87	1.803	2.111
		3.0	343.71	386.87	1.803	2.111
		6.0	343.71	386.87	1.803	2.111
		10.0	343.78	386.89	1.804	2.111
	8×	0.1	343.73	386.88	1.804	2.111
		0.2	343.72	386.87	1.804	2.111
		0.3	343.72	386.87	1.803	2.111
		0.6	343.72	386.87	1.803	2.111
		1.0	343.72	386.87	1.803	2.111
		3.0	343.71	386.87	1.803	2.111
		6.0	343.71	386.87	1.803	2.111
		10.0	343.71	386.87	1.803	2.111

Table C3. Fluid properties of further investigation. A) static pressure, B) mass flow rate, C) velocity, D) density, and E) speed of sound and viscosity.

A Static pressure.

Fluid Type	Geometric Scale	Operating Pressure (atm)	Static Pressure (Pa)		
			Motive Stream	Propelled Stream	Outlet Stream
Hydrogen	2×	1.0	100817.5	93667.7	101350.4
Steam	2×	1.0	100833.1	93861.5	101349.8
Nitrogen	4×	1.0	100798.0	93387.4	101350.7
Air	2×	1.0	100805.7	93447.4	101351.9
Carbon dioxide	4×	1.0	100821.9	93769.8	101348.7

B Mass flow rate.

Fluid Type	Geometric Scale	Operating Pressure (atm)	Mass Flow Rate (kg/s)		
			Motive Stream	Propelled Stream	Outlet Stream
Hydrogen	2×	1.0	0.242	0.781	1.023
Steam	2×	1.0	0.676	2.308	2.984
Nitrogen	4×	1.0	3.611	11.839	15.450
Air	2×	1.0	0.918	3.000	3.918
Carbon dioxide	4×	1.0	4.207	14.507	18.714

Table C3. (Continued).

C Velocity magnitude.

Fluid Type	Geometric Scale	Operating Pressure (atm)	Velocity Magnitude (m/s)		
			Motive Stream	Propelled Stream	Outlet Stream
Hydrogen	2×	1.0	1537.42	88.80	102.59
Steam	2×	1.0	510.76	29.30	33.52
Nitrogen	4×	1.0	413.76	24.29	27.92
Air	2×	1.0	406.89	23.79	27.38
Carbon dioxide	4×	1.0	326.56	18.87	21.52

D Density.

Fluid Type	Geometric Scale	Operating Pressure (atm)	Density (kg/m^3)		
			Motive Stream	Propelled Stream	Outlet Stream
Hydrogen	2×	1.0	0.082	0.061	0.066
Steam	2×	1.0	0.695	0.546	0.588
Nitrogen	4×	1.0	1.143	0.844	0.914
Air	2×	1.0	1.182	0.873	0.946
Carbon dioxide	4×	1.0	1.691	1.331	1.437

Table C3. (Continued).

E Speed of sound and viscosity.

Fluid Type	Geometric Scale	Operating Pressure (atm)	Speed of Sound (m/s)		Viscosity ($\times 10^{-5}$; kg/(m·s))	
			Motive Stream	Propelled Stream	Motive Stream	Propelled Stream
Hydrogen	2×	1.0	1298.69	1470.65	0.874	1.003
Steam	2×	1.0	431.51	472.43	1.257	1.517
Nitrogen	4×	1.0	349.51	393.39	1.748	2.048
Air	2×	1.0	343.73	386.87	1.804	2.111
Carbon dioxide	4×	1.0	275.85	301.41	1.423	1.752

Table C4. Fluid properties of the operating pressure investigation A) static pressure, B) mass flow rate, C) velocity, D) density, and E) speed of sound and viscosity.

A Static pressure.

.

C_p	Mach number	Operating Pressure (atm)	Static Pressure (Pa)		
			Motive Stream	Propelled Stream	Outlet Stream
4.30	0.7474	0.01	978.7	1,008.3	1,013.5
		0.03	2,886.8	3,018.6	3,040.4
		0.06	6,743.3	6,033.9	6,080.7
		0.1	9,538.3	10,053.7	10,134.3
		0.3	28,459.5	30,146.6	3,040.3
		0.6	56,808.3	60,285.4	60,804.0
		1.0	93,633.5	100,352.1	101,348.5
		3.0	280,987.3	301,049.2	304,006.8
		6.0	561,582.8	602,073.7	608,039.8
		10.0	934,731.4	1,003,1	1,013,108.7
31.99	1.1837	0.01	1,010.2	953.8	1,013.6
		0.03	3,027.5	2,836.2	3,040.6
		0.06	6,053.6	5,655.8	6,081.2
		0.1	10,087.3	9,414.0	10,135.2
		0.2	20,171.1	18,804.5	20,270.2
		0.3	30,254.0	28,179.5	30,405.1
		0.5	50,418.4	46,928.1	50,674.9

Table C4. (Continued).

A Static Pressure (Continued).

C_p	Mach Number	Operating Pressure (atm)	Static Pressure (Pa)		
			Motive Stream	Propelled Stream	Outlet Stream
31.99	1.1837	0.6	60,500.9	56,300.5	60,809.6
		1.0	100,825.1	93,768.0	101,349.1
		3.0	302,444.4	280,930.6	304,044.1
		6.0	604,844.9	561,745.9	608,063.5
		8.0	806,057.8	751,575.7	810,129.4
		10.0	1,007,319.2	940,908.4	1,012,277.2
51.28	1.4313	0.01	1,012.3	907.4	1,013.6
		0.03	3,035.6	2,690.0	3,040.8
		0.06	6,070.5	5,346.8	6,081.4
		0.1	10,117.1	8,914.7	10,135.6
		0.3	30,347.4	26,676.2	30,406.1
		0.6	60,690.4	53,253.2	60,811.7
		1.0	101,146.9	88,661.0	101,352.5
		3.0	303,409.3	265,458.5	304,054.4
		6.0	606,774.9	532,489.6	608,044.2
		8.0	808,503.8	713,987.1	810,112.4
		10.0	1,009,025.8	899,705.3	1,010,897.6

Table C4. (Continued).

A Static Pressure (Continued).

C_p	Mach number	Operating Pressure (atm)	Static Pressure (Pa)		
			Motive Stream	Propelled Stream	Outlet Stream
72.13	1.1677	0.01	1,012.9	851.6	1,013.7
		0.03	3,038.0	2,514.3	3,040.9
		0.06	6,075.7	5,003.6	6,081.7
		0.1	10,125.8	8,322.4	10,136.0
		0.3	30,374.7	24,871.2	30,407.4
		0.6	60,746.7	49,658.9	60,814.1
		1.0	101,239.9	82,464.5	101,356.6
		3.0	303,700.4	246,768.4	304,066.3
		6.0	607,260.8	497,852.1	607,956.4
		10.0	1,007,683.2	851,148.9	1,008,679.8
101.12	1.9811	0.01	1,013.0	769.4	1,013.7
		0.03	3,038.4	2,256.2	3,041.1
		0.06	6,076.4	4,481.6	6,082.1
		0.1	10,127.0	7,451.5	10,136.6
		0.3	30,379.1	22,259.3	30,408.9
		0.6	60,755.9	44,356.3	60,817.2
		1.0	101,257.7	73,870.4	101,361.3
		3.0	303,756.8	222,683.9	304,068.5

Table C4. (Continued).

B Mass flow rate.

C_p	Mach number	Operating Pressure (atm)	Mass Flow Rate (kg/s)		
			Motive Stream	Propelled Stream	Outlet Stream
101.12	1.9811	6.0	607,025.9	438,811.6	607,673.3
		10.0	1,012,537.4	732,504.2	1,013,613
4.30	0.7474	0.01	0.015	0.069	0.084
		0.03	0.0456	0.244	0.289
		0.06	0.090	0.504	0.595
		0.1	0.151	0.855	1.006
		0.3	0.452	2.638	3.090
		0.6	0.900	5.308	6.208
		1.0	1.508	9.503	11.048
		3.0	4.497	28.080	32.877
		6.0	9.000	54.557	63.557
		10.0	15.051	95.100	110.150
31.99	1.1837	0.01	0.027	0.083	0.110
		0.03	0.081	0.266	0.347
		0.06	0.162	0.540	0.702
		0.1	0.270	0.911	1.178
		0.2	0.541	1.833	2.369
		0.3	0.811	2.778	3.589

Table C4. (Continued).

B Mass flow rate (Continued).

C_p	Mach Number	Operating Pressure (atm)	Mass Flow Rate (kg/s)		
			Motive Stream	Propelled Stream	Outlet Stream
31.99	1.1837	0.5	1.352	4.627	5.969
		0.6	1.622	5.558	7.170
		1.0	2.704	9.314	11.988
		3.0	8.112	28.049	36.161
		6.0	16.224	56.165	72.389
		8.0	21.632	73.865	94.697
		10.0	27.040	91.733	117.273
51.28	1.4313	0.01	0.034	0.0854	0.120
		0.03	0.102	0.267	0.369
		0.06	0.205	0.546	0.740
		0.1	0.341	0.907	1.248
		0.3	1.023	2.743	3.766
		0.6	2.046	5.518	7.564
		1.0	3.410	9.203	12.613
		3.0	10.230	27.849	38.079
		6.0	20.461	55.465	75.626
		8.0	27.284	73.365	99.349
		10.0	34.109	90.083	121.091

Table C4. (Continued).

B Mass flow rate (Continued).

C_p	Mach number	Operating Pressure (atm)	Mass Flow Rate (kg/s)		
			Motive Stream	Propelled Stream	Outlet Stream
72.13	1.1677	0.01	0.042	0.086	0.128
		0.03	0.125	0.267	0.392
		0.06	0.251	0.539	0.789
		0.1	0.418	0.901	1.319
		0.3	1.254	2.722	3.976
		0.6	2.508	5.458	7.966
		1.0	4.180	9.169	13.349
		3.0	12.540	27.829	40.169
		6.0	25.081	55.371	79.452
		10.0	41.801	90.600	126.900
101.12	1.9811	0.01	0.052	0.085	0.137
		0.03	0.158	0.261	0.418
		0.06	0.315	0.525	0.840
		0.1	0.525	0.876	1.401
		0.3	1.575	2.638	4.213
		0.6	3.150	5.297	8.447
		1.0	5.250	8.828	14.078
		3.0	15.750	25.180	40.130

Table C4. (Continued).

B Mass flow rate (Continued).

C_p	Mach number	Operating Pressure (atm)	Mass Flow Rate (kg/s)		
			Motive Stream	Propelled Stream	Outlet Stream
101.12	1.9811	6.0	31.500	52.200	83.080
		10.0	52.500	88.282	140.783

C Velocity.

C_p	Mach number	Operating Pressure (atm)	Velocity (m/s)		
			Motive Stream	Propelled Stream	Outlet Stream
4.30	0.7474	0.01	338.90	20.32	26.64
		0.03	339.01	24.03	27.08
		0.06	339.19	24.88	27.83
		0.1	339.41	25.33	28.25
		0.3	340.04	26.07	28.92
		0.6	339.62	26.25	29.06
		1.0	339.74	28.14	31.03
		3.0	339.81	28.03	30.92
		6.0	339.62	28.15	30.56
		10.0	341.19	28.23	30.97
31.99	1.1837	0.01	510.76	25.94	30.94
		0.03	510.76	27.95	32.50

Table C4. (Continued).

C Velocity (Continued).

C_p	Mach Number	Operating Pressure (atm)	Velocity (m/s)		
			Motive Stream	Propelled Stream	Outlet Stream
31.99	1.1837	0.06	510.76	28.44	32.87
		0.1	510.76	28.71	33.07
		0.2	510.76	28.96	33.27
		0.3	510.76	29.15	33.41
		0.5	510.76	29.30	33.53
		0.6	510.76	29.35	33.57
		1.0	510.76	29.49	33.67
		3.0	510.76	29.75	33.85
		6.0	510.76	29.78	33.89
		8.0	510.76	28.94	33.32
		10.0	510.76	28.56	33.04
51.28	1.4313	0.01	595.37	28.02	33.56
		0.03	595.44	29.59	34.57
		0.06	595.50	30.32	35.13
		0.1	595.49	30.31	35.06
		0.3	595.49	30.64	35.26
		0.6	595.50	30.86	35.41
		1.0	595.50	30.92	35.43

Table C4. (Continued).

C Velocity (Continued).

C_p	Mach number	Operating Pressure (atm)	Velocity (m/s)		
			Motive Stream	Propelled Stream	Outlet Stream
51.28	1.4313	3.0	595.50	31.22	35.65
		6.0	595.50	30.86	35.41
		8.0	595.55	30.05	34.96
		10.0	595.58	28.80	34.23
72.13	1.1677	0.01	670.01	30.13	35.93
		0.03	670.01	31.62	36.72
		0.06	670.01	32.06	36.96
		0.1	670.01	32.24	37.05
		0.3	670.01	32.58	37.23
		0.6	670.01	32.73	37.30
		1.0	670.01	33.00	37.50
		3.0	670.01	33.21	37.61
		6.0	670.01	32.43	37.22
		10.0	670.01	29.65	36.08
101.12	1.9811	0.01	750.09	32.87	38.59
		0.03	750.35	34.39	39.16
		0.06	750.35	34.83	39.32
		0.1	750.35	35.00	39.37

Table C4. (Continued).

C Velocity (Continued).

C_p	Mach number	Operating Pressure (atm)	Velocity (m/s)		
			Motive Stream	Propelled Stream	Outlet Stream
101.12	1.9811	0.3	750.35	35.29	39.45
		0.6	750.35	35.50	39.55
		1.0	750.35	35.57	39.55
		3.0	750.35	35.68	40.07
		6.0	750.35	35.72	40.48
		10.0	750.35	35.97	40.95

D Density.

C_p	Mach number	Operating Pressure (atm)	Density (kg/m^3)		
			Motive Stream	Propelled Stream	Outlet Stream
4.30	0.7474	0.01	0.0061	0.0059	0.0059
		0.03	0.0180	0.0176	0.0177
		0.06	0.0358	0.0351	0.0353
		0.1	0.0595	0.0585	0.0588
		0.3	0.1776	0.1752	0.1765
		0.6	0.3545	0.3501	0.3530
		1.0	0.5856	0.5847	0.5883
		3.0	1.7555	1.7531	1.7564

Table C4. (Continued).

D Density (Continued).

C_p	Mach Number	Operating Pressure (atm)	Density (kg/m^3)		
			Motive Stream	Propelled Stream	Outlet Stream
4.30	0.7474	6.0	3.5448	3.5011	3.5299
		10.0	5.8460	5.8321	5.8784
31.99	1.1837	0.01	0.0070	0.0055	0.0059
		0.03	0.0209	0.0165	0.0176
		0.06	0.0417	0.0329	0.0353
		0.1	0.0695	0.0547	0.0588
		0.2	0.1390	0.1093	0.1176
		0.3	0.2085	0.1638	0.1765
31.99	1.1837	0.5	0.3475	0.2728	0.2941
		0.6	0.4170	0.3272	0.3529
		1.0	0.6949	0.5450	0.5882
		3.0	2.0841	1.6329	1.7646
		6.0	4.1700	3.2700	3.5292
		8.0	5.4338	4.3706	4.6989
		10.0	6.6882	5.4695	5.8696
51.28	1.4313	0.01	0.0075	0.0053	0.0059
		0.03	0.0225	0.0156	0.0176
		0.06	0.0454	0.0312	0.0353

Table C4. (Continued).

D Density (Continued).

C_p	Mach number	Operating Pressure (atm)	Density (kg/m^3)		
			Motive Stream	Propelled Stream	Outlet Stream
51.28	1.4313	0.1	0.0749	0.0518	0.0588
		0.3	0.2248	0.1550	0.1764
		0.6	0.4495	0.3096	0.3529
		1.0	0.7491	0.5154	0.5881
		3.0	2.2718	1.5442	1.7645
		6.0	4.5051	3.0952	3.5288
		8.0	5.8856	4.1519	4.6983
		10.0	7.1088	5.2291	5.8600
72.13	1.1677	0.01	0.0081	0.0050	0.0059
		0.03	0.0244	0.0146	0.0176
		0.06	0.0487	0.0291	0.0353
		0.1	0.0812	0.0484	0.0588
		0.3	0.2436	0.1446	0.1764
		0.6	0.4871	0.2887	0.3529
		1.0	0.8117	0.4810	0.5881
		3.0	2.4407	1.4401	1.7643
		6.0	4.8033	2.9024	3.5275
		10.0	7.5006	4.9692	5.8349

Table C4. (Continued).

D Density (Continued).

C_p	Mach number	Operating Pressure (atm)	Density (kg/m^3)		
			Motive Stream	Propelled Stream	Outlet Stream
101.12	1.9811	0.01	0.0091	0.0045	0.0059
		0.03	0.0271	0.0131	0.0176
		0.06	0.0543	0.0261	0.0353
		0.1	0.0904	0.0434	0.0588
		0.3	0.2712	0.1294	0.1764
		0.6	0.5424	0.2583	0.3529
		1.0	0.9039	0.4296	0.5881
		3.0	2.6726	1.2646	1.7644
		6.0	5.5392	2.6169	3.5241
		10.0	9.1494	4.2965	5.8809

Table C4. (Continued).

E Speed of sound and viscosity.

C_p	Mach number	Operating Pressure (atm)	Speed of Sound (m/s)		Viscosity ($\times 10^{-5}$; kg/(m·s))	
			Motive Stream	Propelled Stream	Motive Stream	Propelled Stream
4.30	0.7474	0.01	453.40	472.49	1.4035	1.5173
		0.03	453.61	472.47	1.4036	1.5171
		0.06	453.81	472.47	1.4042	1.5171
		0.1	454.15	472.46	1.4032	1.5171
		0.3	454.99	472.46	1.4028	1.5171
		0.6	454.42	472.46	1.4031	1.5170
		1.0	454.54	472.44	1.4000	1.5169
		3.0	454.67	472.44	1.4008	1.5169
		6.0	454.42	472.46	1.4031	1.5170
		10.0	456.5	472.44	1.3998	1.5169
31.99	1.1837	0.01	431.50	472.45	1.2568	1.5170
		0.03	431.51	472.44	1.2569	1.5169
		0.06	431.52	472.44	1.2570	1.5169
		0.1	431.52	472.43	1.2570	1.5169
		0.2	431.52	472.43	1.2570	1.5169
		0.3	431.51	472.43	1.2570	1.5169
		0.5	431.51	472.43	1.2570	1.5169

Table C4. (Continued).

E Speed of sound and viscosity (Continued).

C_p	Mach Number	Operating Pressure (atm)	Speed of Sound (m/s)		Viscosity ($\times 10^{-5}$; kg/(m·s))	
			Motive Stream	Propelled Stream	Motive Stream	Propelled Stream
31.99	1.1837	0.6	431.51	472.43	1.2570	1.5169
		1.0	431.51	472.43	1.2570	1.5169
		3.0	431.50	472.43	1.2570	1.5168
		6.0	431.50	472.43	1.2570	1.5168
		8.0	431.43	472.43	1.2570	1.5169
		10.0	431.56	472.44	1.2573	1.5169
51.28	1.4313	0.01	415.96	472.43	1.1650	1.5169
		0.03	416.00	472.42	1.1654	1.5168
		0.06	416.00	472.42	1.1654	1.5168
		0.1	416.02	472.42	1.1655	1.5168
		0.3	416.02	472.42	1.1655	1.5168
		0.6	416.02	472.42	1.1655	1.5168
		1.0	416.02	472.42	1.1655	1.5168
		3.0	416.02	472.41	1.1655	1.5168
		6.0	416.03	472.42	1.1656	1.5167
		8.0	416.06	472.42	1.1658	1.5168

Table C4. (Continued).

E Speed of sound and viscosity (Continued).

C_p	Mach number	Operating Pressure (atm)	Speed of Sound (m/s)		Viscosity ($\times 10^{-5}$; kg/(m·s))	
			Motive Stream	Propelled Stream	Motive Stream	Propelled Stream
51.28	1.4313	10.0	416.10	472.43	1.1700	1.5168
72.13	1.1677	0.01	399.65	472.41	1.0722	1.5167
		0.03	399.62	472.41	1.0727	1.5167
		0.06	399.64	472.40	1.0729	1.5167
		0.1	399.65	472.40	1.0730	1.5167
		0.3	399.66	472.40	1.0730	1.5167
		0.6	399.66	472.40	1.0730	1.5166
		1.0	399.66	472.39	1.0730	1.5166
		3.0	399.66	472.39	1.0730	1.5166
		6.0	399.70	472.40	1.0733	1.5167
		10.0	399.66	472.40	1.0737	1.5168
101.12	1.9811	0.01	378.62	472.43	0.9603	1.5166
		0.03	378.75	472.38	0.9607	1.5165
		0.06	378.73	472.38	0.9608	1.5165
		0.1	378.74	472.38	0.9609	1.5165
		0.3	378.75	472.38	0.9610	1.5165

Table C4. (Continued).

E Speed of sound and viscosity (Continued).

C_p	Mach number	Operating Pressure (atm)	Speed of Sound (m/s)		Viscosity ($\times 10^{-5}$; kg/(m·s))	
			Motive Stream	Propelled Stream	Motive Stream	Propelled Stream
101.12	1.9811	0.6	378.75	472.37	0.9610	1.5165
		1.0	378.75	472.37	0.9610	1.5165
		3.0	378.74	472.37	0.9613	1.5166
		6.0	378.76	472.38	0.9614	1.5166
		10.0	378.75	472.37	0.9610	1.5165

APPENDIX D

FLUID PROPERTIES OF OPTIMIZATION CASES

Fluid Static Pressure

Table D1. Static pressure and compression ratio.

$\frac{D_n}{D_p}$	v_m (Mach Number)	Static Pressure (Pa)		
		Motive Stream	Propelled Stream	Outlet Stream
0.03	0.39	101416.0	101279.2	101325.5
	0.78	102406.2	101137.4	101326.1
	1.17	102308.3	100856.1	101327.6
	1.56	102372.8	100369.3	101332.6
	1.95	103647.8	101047.5	101353.7
0.06	0.39	101072.7	101165.9	101325.9
	0.78	99382.1	100689.8	101329.5
	1.17	101972.3	100249.4	101335.5
	1.56	102304	98481.3	101343.6
	1.95	103608.8	95795.5	101376.6
0.11	0.39	99258.9	100964.4	101328
	0.78	94633.8	99263.7	101338.5
	1.17	100828.7	94027.8	101350.6
	1.56	101083.5	83800.7	101364.2
	1.95	101352.2	72539.1	101385.9
0.23	0.39	96298.2	99560.7	101329.5
	0.59	89583.2	97053.2	101339.4
	0.79	85851.6	93553.5	101346.2

Mass Flow Rate and Velocity

Table D2. Fluid mass flow rate and velocity.

$\frac{D_n}{D_p}$	v_m (Mach Number)	Mass Flow Rate (kg/s)			Velocity (m/s)	
		Motive Stream	Propelled Stream	Outlet Stream	Propelled Stream	Outlet Stream
0.03	0.39	0.003	0.0723	0.0753	3.50	3.81
	0.78	0.006	0.1578	0.1641	7.65	7.66
	1.17	0.011	0.2572	0.2678	12.50	12.01
	1.56	0.017	0.3741	0.3909	18.27	17.54
	1.95	0.028	0.7404	0.7684	35.84	36.99
0.06	0.39	0.012	0.1361	0.1479	6.61	6.63
	0.78	0.025	0.2894	0.3146	14.70	15.27
	1.17	0.042	0.6163	0.6585	30.01	29.52
	1.56	0.067	0.7010	0.7682	34.93	34.56
	1.95	0.112	0.9938	1.106	50.42	44.35
0.11	0.39	0.047	0.2185	0.2659	10.74	13.44
	0.78	0.101	0.4735	0.5743	23.63	26.82
	1.17	0.169	0.5880	0.7570	28.62	33.00
	1.56	0.269	0.5850	0.8540	34.90	41.07
	1.95	0.448	0.5846	1.0327	37.20	46.33
0.23	0.39	0.190	0.1653	0.3553	8.58	18.72
	0.59	0.292	0.2790	0.5706	14.88	28.84
	0.79	0.350	0.3350	0.6850	17.86	33.26

Fluid Density

Table D3. Fluid density.

$\frac{D_n}{D_p}$	v_m (Mach number)	Density (kg/m^3)		
		Motive Stream	Propelled Stream	Outlet Stream
0.03	0.39	0.600	0.588	0.589
	0.78	0.639	0.588	0.589
	1.17	0.710	0.586	0.589
	1.56	0.842	0.583	0.589
	1.95	1.108	0.585	0.589
0.06	0.39	0.598	0.588	0.589
	0.78	0.625	0.585	0.589
	1.17	0.707	0.586	0.589
	1.56	0.843	0.572	0.589
	1.95	1.121	0.563	0.589
0.11	0.39	0.589	0.587	0.589
	0.78	0.598	0.578	0.589
	1.17	0.696	0.549	0.589
	1.56	0.821	0.486	0.571
	1.95	1.085	0.453	0.589
0.23	0.39	0.572	0.579	0.589
	0.59	0.555	0.562	0.589
	0.79	0.559	0.541	0.589

Speed of Sound and Viscosity

Table D4. Speed of sound and viscosity.

$\frac{D_n}{D_p}$	v_m (Mach number)	Speed of Sound (m/s)		Viscosity ($\times 10^{-5}$; kg/(m·s))	
		Motive Stream	Propelled Stream	Motive Stream	Propelled Stream
0.03	0.39	468.13	472.56	1.488	1.518
	0.78	455.25	472.56	1.404	1.518
	1.17	431.43	472.54	1.256	1.518
	1.56	396.70	472.51	1.056	1.518
	1.95	347.90	472.36	8.065	1.517
0.06	0.39	468.10	472.56	1.488	1.518
	0.78	453.82	472.53	1.395	1.518
	1.17	430.91	472.47	1.253	1.517
	1.56	395.83	472.37	1.051	1.516
	1.95	345.34	472.16	0.793	1.515
0.11	0.39	467.90	472.55	1.487	1.518
	0.78	452.65	472.48	1.388	1.517
	1.17	431.50	472.43	1.257	1.517
	1.56	397.21	472.38	1.060	1.516
	1.95	347.24	472.32	0.805	1.516
0.23	0.39	467.52	472.55	1.484	1.518
	0.59	459.67	472.53	1.433	1.518
	0.79	453.32	472.52	1.392	1.517

APPENDIX E

RESULTS OF EXTRA STUDY IN CONVERGENT NOZZLE

This study is conducted to understand a convergent nozzle, which is applied to the cascade analysis. (Note: a convergent nozzle can produce an exit velocity less than, or equal to, Mach 1.0) The goal of this study is to understand inlet and outlet velocity for a given nozzle shape. Various mass flow rates are injected through various nozzle shapes. The outlet velocity corresponding to each mass flow rate and shape of convergent nozzle is reported. The efficiency of each case is also evaluated. Steam is used as fluid, and the pressure in the exit space is maintained constant at 101.3 kPa. The simulation model is demonstrated in Figure E1. The simulation result is summarized in Table E1.

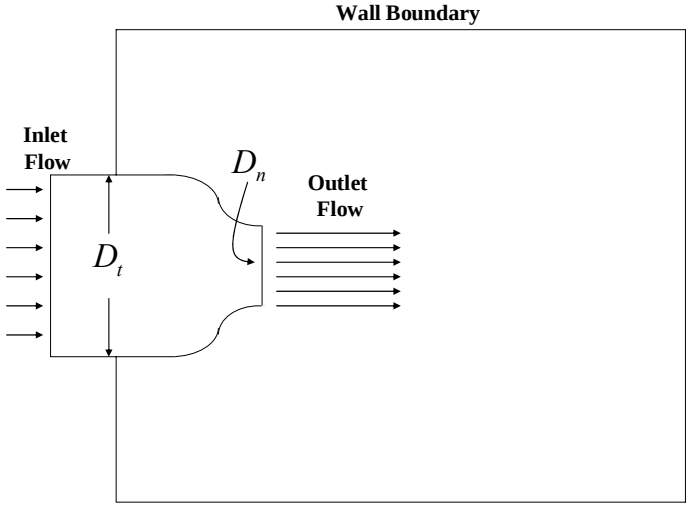

Figure E1. Simulation model of the convergent nozzle study.

Table E1. Simulation result of various nozzle diameter ratio.

$\frac{D_n}{D_t}$	Mass Flow Rate (kg/s)		Velocity (m/s)		Mach Number		Efficiency
	Inlet	Outlet	Inlet	Outlet	Inlet	Outlet	
0.45	0.14	0.14	29.94	110.87	0.06	0.23	0.9983
	0.19	0.19	34.33	144.12	0.07	0.30	0.9980
	0.23	0.23	41.05	176.65	0.09	0.37	0.9971
	0.28	0.28	47.02	208.32	0.10	0.44	0.9960
	0.32	0.32	52.20	238.99	0.11	0.51	0.9949
	0.34	0.34	54.47	253.88	0.12	0.54	0.9944
0.4	0.14	0.14	25.44	171.45	0.05	0.36	0.9959
	0.19	0.19	31.21	220.76	0.07	0.47	0.9935
	0.23	0.23	35.70	267.28	0.08	0.57	0.9909
	0.28	0.28	38.94	310.39	0.08	0.66	0.9888
	0.32	0.32	41.08	348.95	0.09	0.74	0.9899
	0.34	0.34	41.82	365.92	0.09	0.77	0.9880
0.35	0.14	0.14	20.95	287.62	0.04	0.61	0.9849
	0.19	0.19	23.19	354.65	0.05	0.75	0.9817
	0.23	0.23	24.14	401.45	0.05	0.85	0.9844
	0.28	0.28	24.53	429.27	0.05	0.90	0.9899
	0.32	0.32	24.72	445.40	0.05	0.94	0.9943
	0.34	0.34	24.80	450.94	0.05	0.95	0.9957
0.3	0.14	0.14	10.95	448.60	0.02	0.94	0.9775
	0.19	0.19	11.13	469.51	0.02	0.97	0.9901
	0.23	0.23	11.18	478.86	0.02	0.99	0.9930
	0.28	0.28	11.21	483.99	0.02	1.00	0.9943
	0.32	0.32	11.18	487.98	0.02	1.00	0.9983
	0.34	0.34	11.19	489.32	0.02	1.01	0.9991

From the simulation result, the highest outlet velocity of convergent nozzle is about Mach 1.0 with a 0.3 diameter ratio. In the cascade, the motive velocity is Mach 0.95 and 0.99. Mach 0.95 is obtainable with 0.35 nozzle diameter ratio and inlet velocity at 24.80 m/s. The efficiency is 99.57%. Mach 0.99 is obtained with a nozzle diameter ratio equal to 0.3 and inlet velocity at 11.18 m/s. The efficiency is 99.30%. From this experiment, we conclude that if the motive velocity is maintained below Mach 1.0, the shock wave is avoided and the simple convergent nozzle can be applied. Generally, the convergent nozzle has a greater efficiency than a convergent-divergent nozzle; therefore, the overall efficiency of the cascade system with the convergent nozzle will be more than the system with the convergent-divergent nozzle.

APPENDIX F

JET EJECTOR GEOMETRY IN HIGH-EFFICIENCY JET EJECTOR INVENTION DISCLOSURE OF HOLTZAPPLE (2001)

Jet ejector geometry (see Figure F1) presented in this section is used in the proof of the model accuracy, dimensionless analysis, and optimization study. The jet ejector dimension is summarized in Table F1.

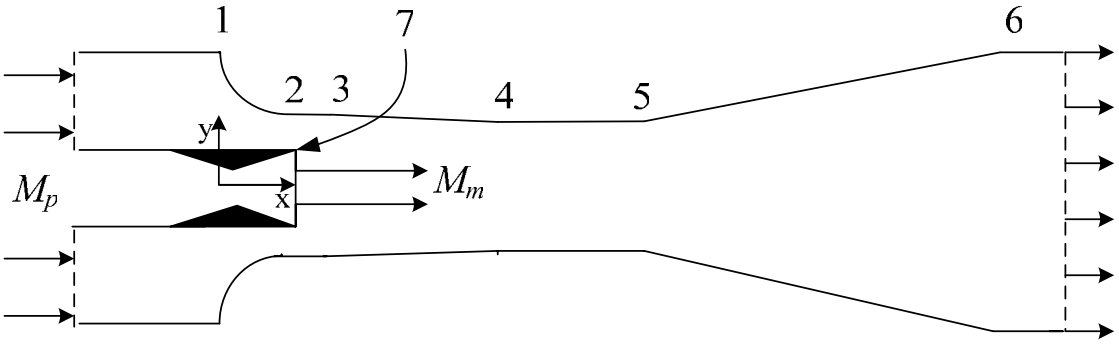

Figure F1. Jet ejector geometry in high-efficiency jet ejector invention disclosure of Holtzapple (2001).

Table F1. Jet ejector dimension according to points in Figure F1 (unit: millimeter).

Point number	x-coordinate	y-coordinate
1	0	105.7783
2	97.79	42.2783
3	182.88	42.2783
4	986.79	39.8653
5	1367.79	39.8653
6	2442.21	105.7783
7	97.79	3.04

VITA

The permanent address for Somsak Watanawanavet is 18 Chalermket 4 Rd, Promprab, Bangkok, Thailand, 10100. Somsak grew up in Bangkok, Thailand. He entered Chulalongkorn University (CU) for his undergraduate study in Bangkok in May 1998. In March 2002, Somsak graduated from the Department of Chemical Engineering with the degree of Bachelor of Engineering and then started his graduate study in the Department of Chemical Engineering at Texas A&M University in College Station, Texas. Somsak completed his Master of Science degree in May 2005.